Optical Fiber Sensor-Embedded Strands for Long-Term Monitoring of Post-Tensioned Tendons in Bridge Elements

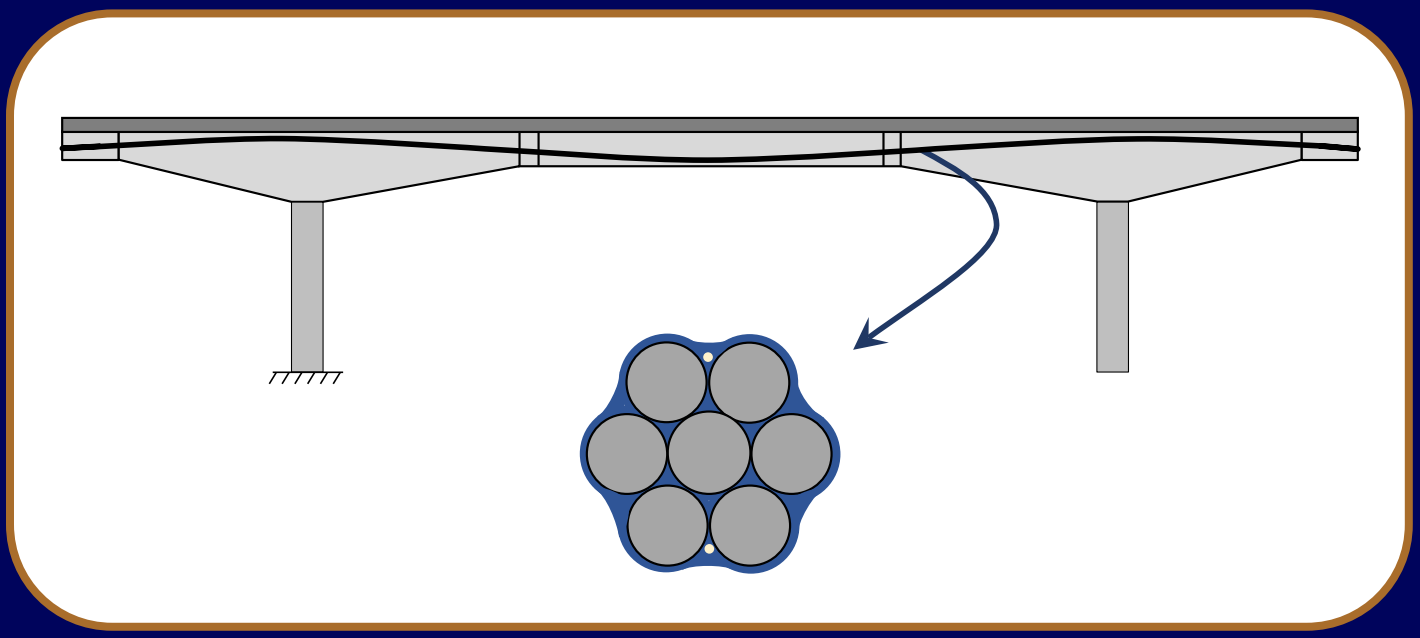

Christopher S. Williams

Pinar Okumus

Manan B. Khatri

Mi Jin Jung

June 2024

Optical Fiber Sensor-Embedded Strands for Long-Term Monitoring of Post-Tensioned Tendons in Bridge Elements

by

Christopher S. Williams
Purdue University

Pinar Okumus
University at Buffalo, The State University of New York

Manan B. Khatri
Purdue University

Mi Jin Jung
University at Buffalo, The State University of New York

Final Report

Research Sponsor:

Federal Highway Administration

Project Partner:

Sumiden Wire Products Corporation

PURDUE UNIVERSITY®

TECHNICAL REPORT DOCUMENTATION PAGE

1. Report No. BOWN-2024-01	2. Government Accession No.	3. Recipient's Catalog No.
4. Title and Subtitle Optical Fiber Sensor-Embedded Strands for Long-Term Monitoring of Post-Tensioned Tendons in Bridge Elements		5. Report Date June 2024 6. Performing Organization Code:
7. Author(s) Christopher S. Williams (ORCID 0000-0001-7512-8939), Pinar Okumus (ORCID 0000-0002-2197-3261), Manan B. Khatri, Mi Jin Jung (ORCID 0009-0004-9667-1649)		8. Performing Organization Report No. BOWN-2024-01
9. Performing Organization Name and Address Purdue University 155 S Grant St West Lafayette, IN 47907		10. Work Unit No. 11. Contract or Grant No. 693JJ321C000034
12. Sponsoring Agency Name and Address Office of Bridges and Structures Federal Highway Administration 1200 New Jersey Ave SE Washington, DC 20590		13. Type of Report and Period Covered 14. Sponsoring Agency Code
15. Supplementary Notes		

16. Abstract

Tendon forces are fundamental to the performance of post-tensioned (PT) bridges. Therefore, monitoring tendon forces is important for understanding the health of PT bridge elements and evaluating the condition of prestressing strands. Implementing a reliable method to monitor PT tendons during the service life of the structure, however, is a challenge. The ideal technology should provide a measurement of prestress (or strain) over the length of the tendon and not be limited to measurement only at discrete locations.

When installed along the length of PT tendons, optical fiber sensors provide a promising means to overcome many of the challenges of tendon force monitoring that currently exist. The technology offers the ability to assess the strain along the length of PT tendons as the bridge is in service.

A research project was conducted to evaluate the use of optical fiber sensors in new PT bridges as a means for long-term monitoring of tendon force and identification of unexpected changes (i.e., losses) in prestress. More specifically, the use of optical fiber sensors embedded within epoxy coating along the length of prestressing strands was assessed. The test program included in the research was aimed at evaluating the accuracy and reliability of data acquired from the optical fiber sensors. The program consisted of tests on optical fiber sensor-embedded prestressing strand specimens in a universal testing machine and installed in a prestressing bed in the laboratory. Then, the strands were used to post-tension beam specimens, allowing the strain data to be evaluated during the post-tensioning procedures and during load tests on the beams. The experimental results from the beam tests were compared to the results from analytical models of the specimens to further assess the strain data from the optical fiber sensors. Overall, the test results indicated the feasibility of using the optical fiber sensor-embedded strands as a reliable means for monitoring PT tendons of in-service bridges.

17. Key Words	18. Distribution Statement
post-tensioning, strands, tendon, optical fiber, epoxy-coated, sensing, monitoring	No restrictions. This document is available to the public through the National Technical Information Service, Springfield, VA 22161. http://www.ntis.gov

19. Security Classif. (of this report)	20. Security Classif. (of this page)	21. No. of Pages	22. Price
Unclassified	Unclassified	93 including appendices	N/A

Form DOT F 1700.7 (8-72) Reproduction of completed page authorized.

SI* (MODERN METRIC) CONVERSION FACTORS

APPROXIMATE CONVERSIONS TO SI UNITS

Symbol	When You Know	Multiply By	To Find	Symbol
		LENGTH		
in	inches	25.4	millimeters	mm
ft	feet	0.305	meters	m
yd	yards	0.914	meters	m
mi	miles	1.61	kilometers	km
		AREA		
in^2	square inches	645.2	square millimeters	mm^2
ft^2	square feet	0.093	square meters	m^2
yd^2	square yard	0.836	square meters	m^2
ac	acres	0.405	hectares	ha
mi^2	square miles	2.59	square kilometers	km^2
		VOLUME		
fl oz	fluid ounces	29.57	milliliters	mL
gal	gallons	3.785	liters	L
ft^3	cubic feet	0.028	cubic meters	m^3
yd^3	cubic yards	0.765	cubic meters	m^3
	NOTE: volumes greater than 1,000 L shall be shown in m^3			
		MASS		
oz	ounces	28.35	grams	g
lb	pounds	0.454	kilograms	kg
T	short tons (2,000 lb)	0.907	megagrams (or "metric ton")	Mg (or "t")
		TEMPERATURE (exact degrees)		
°F	Fahrenheit	5 (F-32)/9 or (F-32)/1.8	Celsius	°C
		ILLUMINATION		
fc	foot-candles	10.76	lux	lx
fl	foot-Lamberts	3.426	$candela/m^2$	cd/m^2
		FORCE and PRESSURE or STRESS		
lbf	poundforce	4.45	newtons	N
lbf/in^2	poundforce per square inch	6.89	kilopascals	kPa

APPROXIMATE CONVERSIONS FROM SI UNITS

Symbol	When You Know	Multiply By	To Find	Symbol
		LENGTH		
mm	millimeters	0.039	inches	in
m	meters	3.28	feet	ft
m	meters	1.09	yards	yd
km	kilometers	0.621	miles	mi
		AREA		
mm^2	square millimeters	0.0016	square inches	in^2
m^2	square meters	10.764	square feet	ft^2
m^2	square meters	1.195	square yards	yd^2
ha	hectares	2.47	acres	ac
km^2	square kilometers	0.386	square miles	mi^2
		VOLUME		
mL	milliliters	0.034	fluid ounces	fl oz
L	liters	0.264	gallons	gal
m^3	cubic meters	35.314	cubic feet	ft^3
m^3	cubic meters	1.307	cubic yards	yd^3
		MASS		
g	grams	0.035	ounces	oz
kg	kilograms	2.202	pounds	lb
Mg (or "t")	megagrams (or "metric ton")	1.103	short tons (2,000 lb)	T
		TEMPERATURE (exact degrees)		
°C	Celsius	1.8C+32	Fahrenheit	°F
		ILLUMINATION		
lx	lux	0.0929	foot-candles	fc
cd/m^2	candela/m2	0.2919	foot-Lamberts	fl
		FORCE and PRESSURE or STRESS		
N	newtons	2.225	poundforce	lbf
kPa	kilopascals	0.145	poundforce per square inch	lbf/in^2

*SI is the symbol for International System of Units. Appropriate rounding should be made to comply with Section 4 of ASTM E380. (Revised March 2003)

Acknowledgments

The authors would like to thank the Federal Highway Administration for sponsoring the research described in this report. Furthermore, the partnership of Sumiden Wire Products Corporation is greatly appreciated. More specifically, the research would not have been possible without the assistance from Luther Saiki, Jon Cornelius, and the team at Sumitomo Electric Industries in Japan. Thanks are also extended to GTI for providing post-tensioning ducts and couplers. The contents of this report reflect the views of the authors, who are responsible for the facts and the accuracy of the data presented herein.

Portions of this document were first published in *Proceedings of the* fib *Symposium 2023 – Volume 2, Building for the Future: Durable, Sustainable, Resilient, Lecture Notes in Civil Engineering 350*, pp. 622-633, 2023, by Springer Nature (see Williams et al. 2023).

Table of Contents

List of Tables

List of Figures

List of Abbreviations and Symbols

Abbreviations

APC	Angled Physical Contact
BOTDR	Brillouin Optical Time Domain Reflectometry
DIC	Digital Image Correlation
SC	Subscriber Connector
SCC	Self-consolidating concrete

Symbols

E_c	Modulus of elasticity of concrete
E_p	Measured modulus of elasticity of prestressing strand
E_{ts}	Tension softening stiffness of concrete
f_c'	Compressive strength of concrete
f_{pe}	Effective stress in prestressing strands at the beginning of the beam test
f_{pu}	Tensile strength of prestressing strand
f_{py}	Stress in prestressing strand corresponding with 1.0% strain
f_t	Tensile strength of concrete
G_c	Crushing energy used to define concrete material model in compression
G_f	Fracture energy used to define concrete material model in tension
L_{IP}	Length of individual integration points in the beam elements of the analytical model
P	Total load applied to beam specimen
Δ	Midspan deflection of beam specimen
ε_{20}	Concrete compressive strain corresponding to 20% of the compressive strength after reaching peak stress
ε_c	Concrete compressive strain corresponding to compressive strength
ε_{pu}	Rupture strain of prestressing strand

Abstract

Tendon forces are fundamental to the performance of post-tensioned (PT) bridges. Therefore, monitoring tendon forces is important for understanding the health of PT bridge elements and evaluating the condition of prestressing strands. Implementing a reliable method to monitor PT tendons during the service life of the structure, however, is a challenge. The ideal technology should provide a measurement of prestress (or strain) over the length of the tendon and not be limited to measurement only at discrete locations.

When installed along the length of PT tendons, optical fiber sensors provide a promising means to overcome many of the challenges of tendon force monitoring that currently exist. The technology offers the ability to assess the strain along the length of PT tendons as the bridge is in service.

A research project was conducted to evaluate the use of optical fiber sensors in new PT bridges as a means for long-term monitoring of tendon force and identification of unexpected changes (i.e., losses) in prestress. More specifically, the use of optical fiber sensors embedded within epoxy coating along the length of prestressing strands was assessed. The test program included in the research was aimed at evaluating the accuracy and reliability of data acquired from the optical fiber sensors. The program consisted of tests on optical fiber sensor-embedded prestressing strand specimens in a universal testing machine and installed in a prestressing bed in the laboratory. Then, the strands were used to post-tension beam specimens, allowing the strain data to be evaluated during the post-tensioning procedures and during load tests on the beams. The experimental results from the beam tests were compared to the results from analytical models of the specimens to further assess the strain data from the optical fiber sensors. Overall, the test results indicated the feasibility of using the optical fiber sensor-embedded strands as a reliable means for monitoring PT tendons of in-service bridges.

1. Introduction

1.1 Overview

Tendon forces are fundamental to the performance of post-tensioned (PT) bridges. Therefore, monitoring tendon forces is important for understanding the health of PT bridge elements and evaluating the condition of prestressing strands. When questions arise regarding the actual tendon force for a bridge element, however, there is currently no simple, reliable method for determining the tendon force that has been widely implemented. Furthermore, the ideal technology should provide a measurement of prestress (or strain) over the length of the tendon and not be limited to measurement only at discrete locations.

When installed along the length of PT tendons, optical fiber sensors provide a promising means to overcome many of the challenges of tendon force measurement that currently exist. The technology offers the ability to assess the strain along the length of PT tendons as the bridge is in service.

A specific optical fiber technology that allows strain to be assessed along PT tendons is Brillouin Optical Time Domain Reflectometry (BOTDR). Unlike optical fiber sensors that incorporate discrete fiber Bragg gratings, BOTDR can be used to measure strain along the entire length of the fiber (Feng et al. 2019). Moreover, the inclusion of optical fiber sensors along the length of the prestressing strands does not impact the structural performance of the tendon.

To further explore the use of BOTDR and optical fiber sensors for monitoring PT tendons, a research project was developed to evaluate optical fiber sensor-embedded prestressing strands, or strands with optical fiber sensors embedded in epoxy coating along their length. In this report, details of the research program and knowledge gained from the study are described.

1.2 Project Objective and Organization

The objective of the test program included in the research was to assess the accuracy and reliability of data acquired from the optical fiber sensors embedded in epoxy coating along the length of prestressing strands and build a knowledge base that could lead to possible future implementation of the technology for the in-service assessment of bridges in the United States. To this end, the research project was divided into three phases. Phase I included tensile tests on the

strands and the determination of correction factors used to acquire accurate strain data from the optical fiber sensors. Phase II was focused on performing tests on strands tensioned in a prestressing bed to evaluate the accuracy and dependability of the strain readings collected from the optical fibers through comparisons with other sensing technologies and by assessing the stability of the strain readings over the time period of one week. Phase III consisted of the evaluation of the optical fiber sensor-embedded strands through flexural load tests on two post-tensioned concrete beam specimens. Furthermore, results from analytical models were compared to measurements from the optical fiber sensor-embedded strands over the entire length of the beam specimens.

1.3 Organization of Report

Prior to describing the research program, background information regarding BOTDR and the optical fiber sensor-embedded prestressing strands is first provided in Chapter 2. The steps taken to prepare the strands for strain measurements are also presented in this chapter. Phases I, II, and III of the research program are then detailed in Chapters 3, 4, and 5, respectively. Comparison of the results for the analytical models with measurements collected from the beam specimens is included in Chapter 5. Important considerations related to the use of the optical fiber technology for monitoring the strain in prestressing strands are discussed in Chapter 6. Finally, a summary of the research along with concluding remarks is provided in Chapter 7.

2. Background and Overview of Strain Measurement Technology

2.1 Overview of BOTDR

BOTDR is a technique used to measure the strain along an optical fiber. While the technology is most often used in the telecommunications industry, the ability of BOTDR to provide accurate strain measurements lends to the potential for its widespread implementation for the monitoring of civil infrastructure.

A BOTDR system consists of optical fiber sensors that are connected to a BOTDR module, as illustrated in Figure 2.1. The module injects pulses of light into the optical fiber sensor. A portion of the light backscatters due to inherent impurities in the optical fiber. The backscattered light that returns to the BOTDR module is analyzed. Light that returns with a frequency that is either slightly less than or greater than the incident light is called Brillouin backscattered light (Corning Incorporated 2015; Soto 2019; VIAVI 2019; Zou et al. 2015).

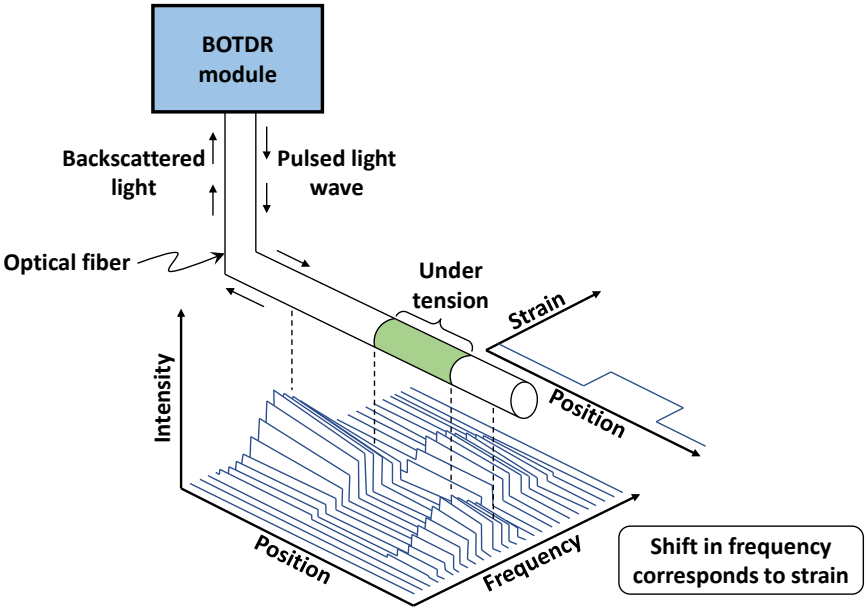

Figure 2.1: Brillouin frequency shift within portion of an optical fiber experiencing strain (adapted from Imai et al. 2019).

When an optical fiber is exposed to strain, the frequency of Brillouin backscattered light experiences a small change (Figure 2.1). This change in frequency is known as a Brillouin frequency shift. A BOTDR module is able to provide strain values along the length of a fiber by

detecting Brillouin frequency shifts at points along the fiber (Corning Incorporated 2015; Imai et al. 2019; VIAVI 2019). The velocity of light within the optical fiber and the time needed for the backscattered light to return to the BOTDR module are used to determine distance, or location, along the fiber corresponding to each measurement (Imai et al. 2019). The minimum spatial resolution of BOTDR is approximately 3.28 ft (1 m) (Feng et al. 2019; Imai et al. 2019; Okubo et al. 2019; VIAVI 2022). In other words, each strain measurement is a weighted average over a minimum distance of 3.28 ft (1 m) (Klar et al. 2006, 2010).

The BOTDR module used during the experimental program described in this report is capable of providing strain values at points spaced at a minimum of 3.15 in. (80 mm) along the length of an optical fiber. This distance between data points is known as the spatial step and can be adjusted by the operator. The BOTDR module includes four ports with measurements along optical fibers acquired from one port at a time (VIAVI 2022). The measurement duration varies based on several test parameters and settings. Approximate measurement times for tests conducted as part of the research program are reported in later sections. The coefficient relating strain to frequency shift used as an input into the BOTDR module throughout the research program was 0.0494 MHz/με.

2.2 Optical Fiber Sensor-Embedded Prestressing Strands

The seven-wire prestressing strand used for the research program is manufactured by Sumitomo Electric Industries, Ltd. (SEI). The strand is epoxy-coated and contains two 0.9-mm diameter optical fiber cables that are embedded within the epoxy and extend along the length of the strand. The epoxy coating provides bond between the fiber cable and the steel strand. A cross section of the strand is illustrated in Figure 2.2. As indicated, the fiber cables are located opposite one another, and each cable is positioned between two of the outer wires of the strand and follow the helical shape of the outer wires.

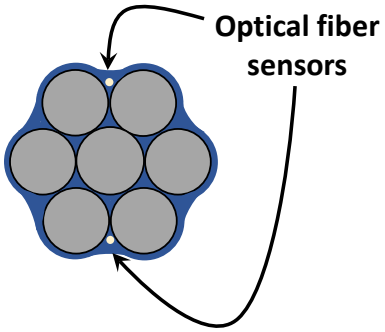

Figure 2.2: Cross section of optical fiber sensor-embedded prestressing strand.

The strand has a nominal diameter of 0.6 in. (15.2 mm) and a nominal area of 0.217 in.^{2} (140 mm^2). The epoxy coating either has a smooth finish for unbonded applications or grit is impregnated in the epoxy for bonded applications (Sumiden Wire 2015). Strand with both coating types were used during the research program described in this report. Because the same bare strand was used for both finish types, no notable differences in material properties were observed between strand with different coatings.

In any application, specialized anchorage hardware (i.e., chucks/wedges) are used for epoxy-coated strands. The wedges have larger teeth compared to conventional wedges to penetrate through the epoxy coating and grip the steel strand.

During the research program, four samples of the optical fiber sensor-embedded strand were tested to rupture using a universal testing machine. The results from the four tests are summarized in Table 2.1, where f_{pu} is the maximum stress resisted by the strand and f_{py} is the stress measured at 1.0% strain. The strain at rupture of the strand specimens is also included in Table 2.1. The reported values assume a nominal strand area of 0.217 in.^{2} (140 mm^2). A representative stress-strain response captured using a digital image correlation (DIC) system is presented in Figure 2.3. The average value of the measured ultimate tensile strength for the strand samples was 280.0 ksi (1931 MPa). During the tests, the samples were anchored at both ends with one-time-use post-tensioning chucks designed for epoxy-coated strand. For this reason, each specimen ruptured at one of the chucks. Therefore, failure likely occurred prematurely during these tests. Nevertheless, the stress-strain response provides the information needed for the research program.

Table 2.1: Measured properties of strand.

Specimen	f_{pu}, ksi (MPa)	f_{py} (Stress at 1.0% Strain), ksi (MPa)	Strain at Rupture
1	279.2 (1925)	237.3 (1636)	0.057
2	279.5 (1927)	239.7 (1653)	0.053
3	280.9 (1937)	239.8 (1653)	0.060
4	280.4 (1933)	238.2 (1642)	0.061
Average	280.0 (1931)	238.8 (1646)	0.058

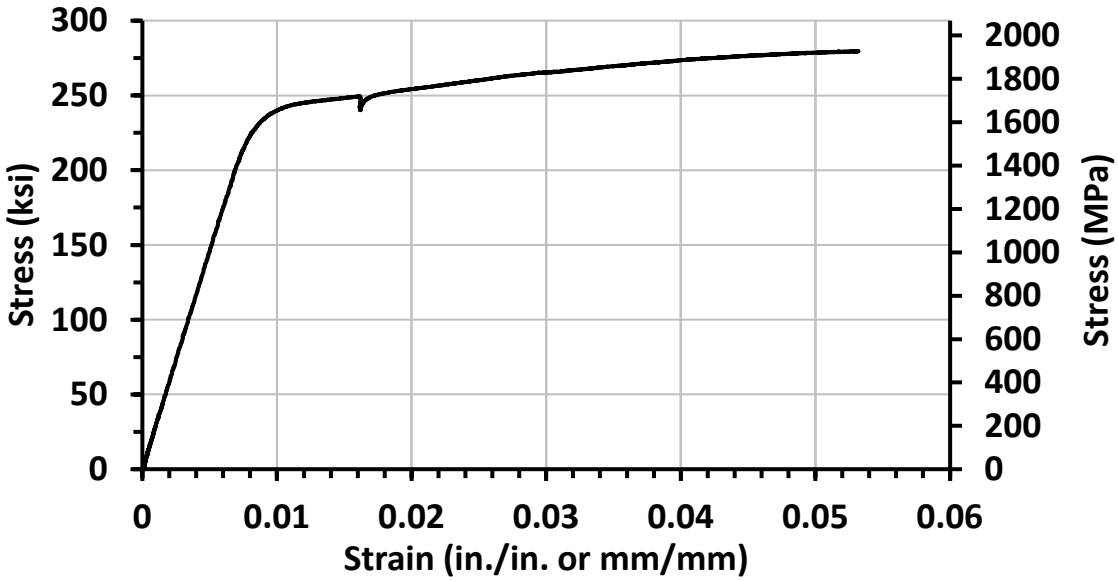

Figure 2.3: Representative stress-strain response of optical fiber sensor-embedded strand.

The strands used for the research were manufactured in Japan to meet the applicable Japanese Industrial Standard (JIS G 3536)[1], and therefore, the stress at 1.0% strain for the strand samples (average of 238.8 ksi [1646 MPa]) is less than the value typical of strand manufactured to meet ASTM A416[2].

The average 1000-hour relaxation loss considering epoxy-coated strand samples with both smooth and grit-impregnated finishes at a stress level of $0.7f_{pu}$, where f_{pu} is the specified tensile strength of the strand (270 ksi [1860 MPa]), was 5.36%.

[1] JIS G 3536, *Steel wires and strands for prestressed concrete*, is not a Federal requirement.
[2] ASTM A416, *Standard Specification for Low-Relaxation, Seven-Wire Steel Strand for Prestressed Concrete*, is not a Federal requirement.

2.3 Preparing the Strands

Before taking measurements along the optical fiber sensor-embedded prestressing strand using the BOTDR module, a short length of each optical fiber cable is first extracted from the epoxy-coated strand and then spliced with an external optical fiber cable. These procedures are described in the following subsections. The fiber extraction and splicing procedures are performed at each end of the prestressing strand for both optical fiber cables that are embedded in the epoxy coating.

2.3.1 Optical Fiber Cable Extraction

The equipment used for the extraction procedure includes a custom electric heater system (Figure 2.4(a)), an electric chisel (Figure 2.4(b)), and a pair of needle-nose pliers. The electric heater system consists of a heater through which the strand can be inserted and a temperature control unit. The cylindrical portion of the heater used during the research project (Figure 2.4(a)) contained a heating element and had a length of approximately 13 in. (330 mm). The electric chisel is equipped with a rounded chisel blade (i.e., sweep gouge blade) that fits within the space between the outer wires of the prestressing strand where the optical fiber cables are embedded.

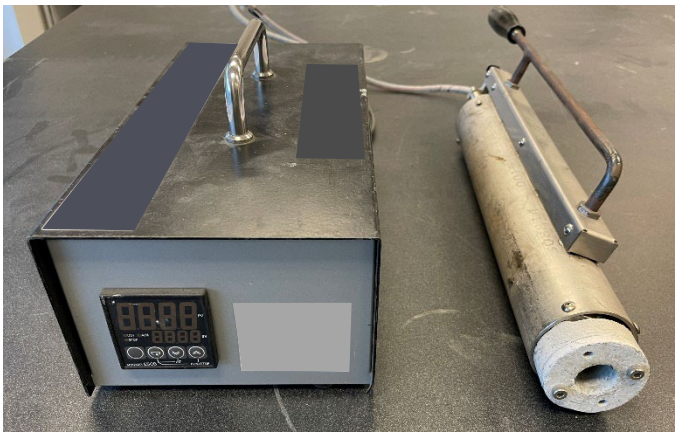

(a) Custom heating system

(b) Electric chisel

Figure 2.4: Equipment for extracting cable from epoxy-coated strand.

The typical process for extracting a fiber cable from the epoxy-coated strand consists of the following steps:

1. The heater is started and the internal temperature is increased to 392°F (200°C).
2. After the heater temperature stabilizes at 392°F (200°C), the heater is placed on the end of the strand for approximately 10 minutes (Figure 2.5(a)). This allows the epoxy coating to soften and become more easily removed from the strand.
3. The optical fiber cable embedded in the epoxy coating is located by examining the end of the strand. The electric chisel is used to remove the coating along the cable between the two wires of the strand (Figure 2.5(b)) over a length of approximately 1 ft (305 mm), resulting in the condition shown in Figure 2.5(c).
4. Steps 1 through 3 are repeated farther along the length of the strand until epoxy is removed along the desired length of cable.
5. Starting at the end of the strand, the cable is extracted from the epoxy coating using the needle-nose pliers (Figure 2.5(d)). If the cable cannot be readily extracted using the pliers, the end of the strand may be reheated for up to 10 minutes at 392°F (200°C) to ease cable extraction and reduce the risk of breaking the cable during this process.

(a) Heating strand

(b) Removing epoxy with electric chisel

(c) Epoxy coating removed

(d) Partially extracted cable

Figure 2.5: Procedure for extracting optical fiber cable from epoxy-coated strand.

External protection to the extracted portion of the cable is provided to prevent the fiber from fracturing when bent. During the research project, heat shrink tubing with a diameter of 1⁄16 in. (1.6 mm) was used, as shown in Figure 2.6. Alternatively, corrugated metal tubing may be used.

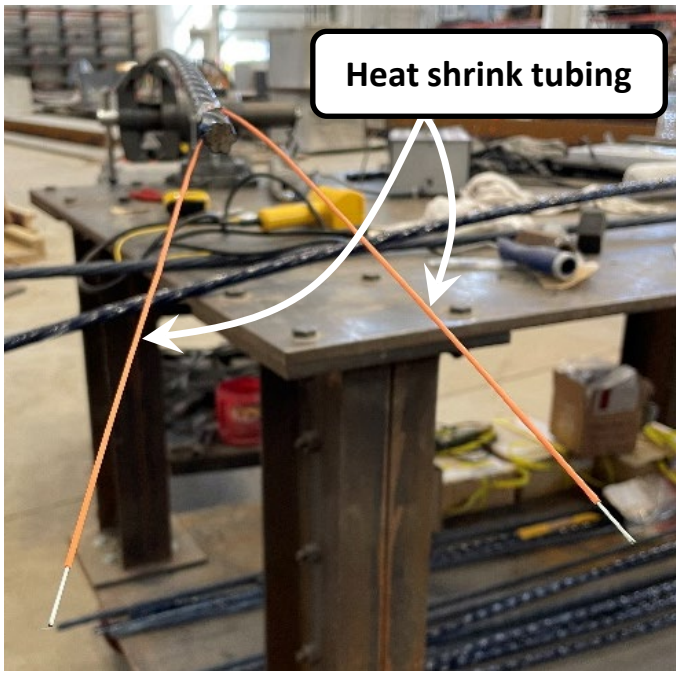

Figure 2.6: Protection installed on extracted optical fiber cables.

The fiber cable extraction procedure is performed at each end of the strand for both cables embedded in the epoxy coating. The strand can then be cut to remove the portion of the strand over which the cables have been extracted, as shown in Figure 2.6.

2.3.2 Splicing Fiber

A fusion splice is provided between the end of each optical fiber cable extracted from the epoxy-coated strand and another cable. Providing a fusion splice reduces the signal loss caused by other connection types. Creating fusion splices is a routine procedure in the optical fiber industry. The splicing procedure followed during the research program involved the use of a fusion splicer (Figure 2.7(a)), a cleaver (Figure 2.7(b)), fiber holders (Figure 2.7(c)), splice protection sleeves (Figure 2.7(d)), a wire stripper, and optical fiber cleaning fluid and disposable wipes. Due to the low bending tolerance of the optical fiber cables extracted from the prestressing strand, extra care can help to ensure the fibers are not broken as they are handled. The procedure used to splice the fiber cables from the strands during the research consisted of the following steps:

1. Using the wire stripper, the heat shrink coating was removed from the end of the optical fiber cable extracted for the strand over a length of approximately 4 in. (102 mm). Similarly,

the outer jacket of the cable was removed over a length of approximately 4 in. (102 mm) from its end.

2. A splice protection sleeve was slipped onto one of the cables. The ends of the cables to be spliced were each placed in a fiber holder. The wire stripper was then used to remove the inner coating at the end of each cable over a length of approximately 1.5 in. (38 mm).
3. While still in the fiber holders, the cleaver was used to cut each fiber. The cleaver left 0.39 in. (10 mm) of optical fiber extending from the end of each cable.
4. The optical fiber was cleaned with the fiber cleaning fluid and disposable wipes.
5. While still in the fiber holders, the two fiber ends were placed into the fusion splicer (Figure 2.8(a)), and the splice was created. The spliced fiber was then removed from the fiber holders, and the splice protection sleeve was moved along the cable so that it was centered over the splice. The cable with the protective sleeve was placed within the heater located on the fusion splicer to cause the sleeve to shrink and provide appropriate protection to the splice (Figure 2.8(b)).

(a) Fusion splicer

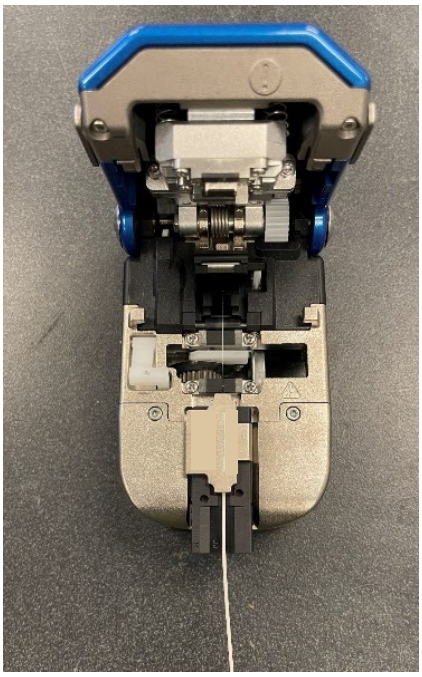

(b) Fiber cleaver

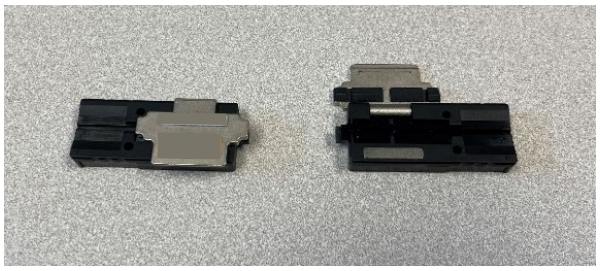

(c) Fiber holders

(d) Splice protection sleeve

Figure 2.7: Equipment for fusion splicing optical fibers.

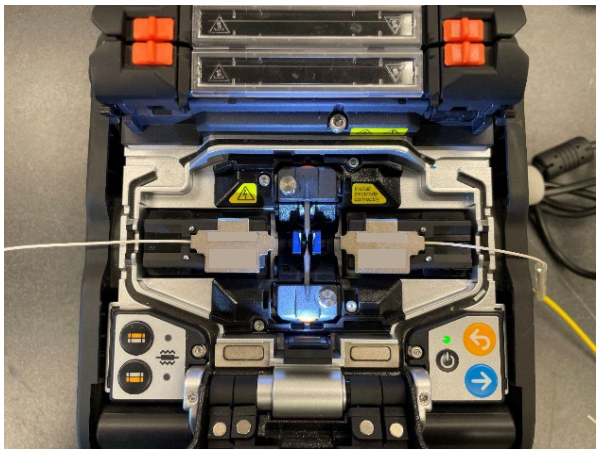

(a) Fiber ends placed in fusion splicer

(b) Heating splice protection sleeve

Figure 2.8: Splicing procedure.

To collect strain measurements from the strands, the splicing procedure is performed at each end of both optical fiber cables embedded in the epoxy coating of the prestressing strand. Once the strand and extracted fibers are prepared, the appropriate connections can be made to develop the full setup for strain measurements, as described in Section 2.4.

2.4 General Setup for Strain Measurements

A general setup used during the research project for collecting measurements from the optical fibers is illustrated in Figure 2.9. At each end of the prestressing strand, the fibers were spliced to an optical fiber pigtail, or a cable with a connector only provided at one end, with a length of approximately 39 ft (~12 m). This cable was sufficiently long to prevent back reflection that occurs at the connector located at the end of the pigtail from interfering with the measurements taken along the length of the strand. As shown in Figure 2.9, a 16.4-ft (5-m) long fiber patch cable, or a cable with connectors at both ends, was installed between the BOTDR module and one of the pigtail cables.

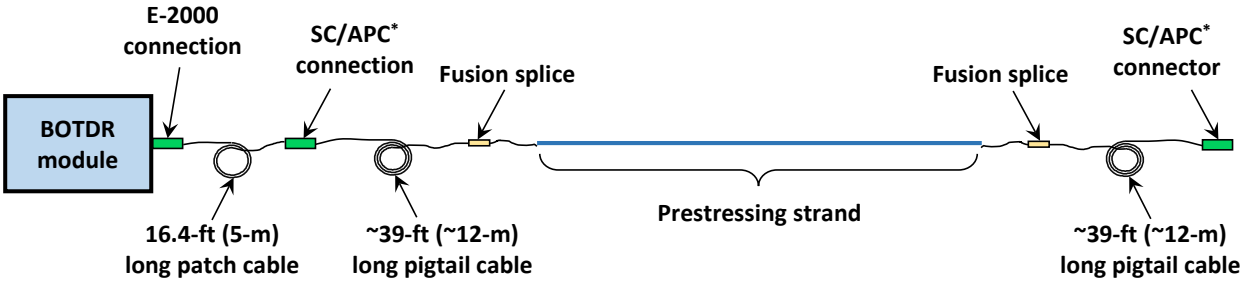

Figure 2.9: General setup for strain measurements.

Depending on the setup needed for the particular measurements performed during the research project, the optical fiber cables embedded within the prestressing strands were often connected in series as illustrated in Figure 2.10. This allowed the full length of optical fiber cable to be connected to a single port on the BOTDR module. Because measurements along the optical fibers could only be acquired from one port at a time, using a single port on the BOTDR module reduced the time needed to collect strain data; only one port was scanned in order to collect data for all of the strand specimens.

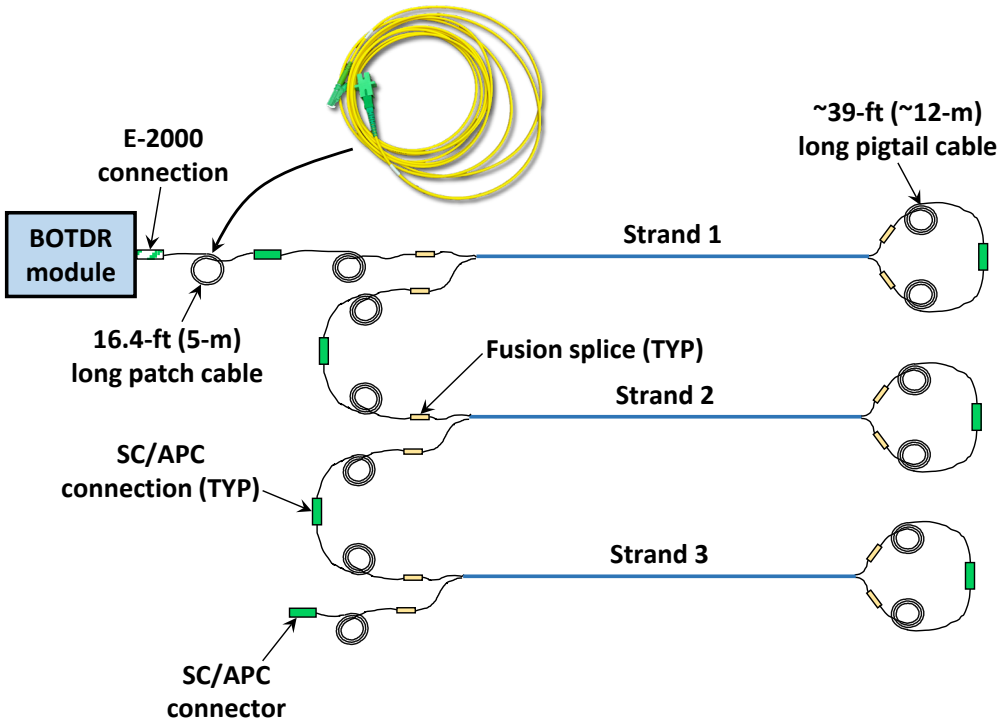

Figure 2.10: Setup with strands connected in series.

In Figure 2.9 and Figure 2.10, the connector types used in the setups are labeled and are all common connector types used in the optical fiber industry. As indicated, intermediate connectors along the length of the setup as well as the connector located at the end of the setup were placed approximately 39 ft (~12 m) from the strand specimens to avoid the effects of back reflection on strain measurements.

3. Elastic Modulus Tests on Optical Fiber Sensor-Embedded Strands

3.1 Introduction

During Phase I of the research program, tensile tests were conducted on the optical fiber sensor-embedded strands to calculate the correction factor used to convert the strain measured by the optical fiber sensors using BOTDR to the axial strain along the length of the strand. Because of the helical shape of the optical fiber embedded in the epoxy coating of the strand, the strain measured by the fiber is different than the axial strain measured along the longitudinal axis of the strand. For this reason, the appropriate correction factor needs to be found experimentally.

3.2 Elastic Modulus Test Details

Four strand specimens were stressed within the linear-elastic range in a universal testing machine to measure the modulus of elasticity of the strand and compare it with the modulus of elasticity indicated by the strain measurements from the optical fibers. A strand specimen installed in the machine for an elastic modulus test is shown in Figure 3.1, and an illustration of the test setup is provided in Figure 3.2. The strands were anchored at both platens with reusable chucks designed for epoxy-coated strand. The length of the specimen measured between the chucks was approximately 5 ft (1.52 m).

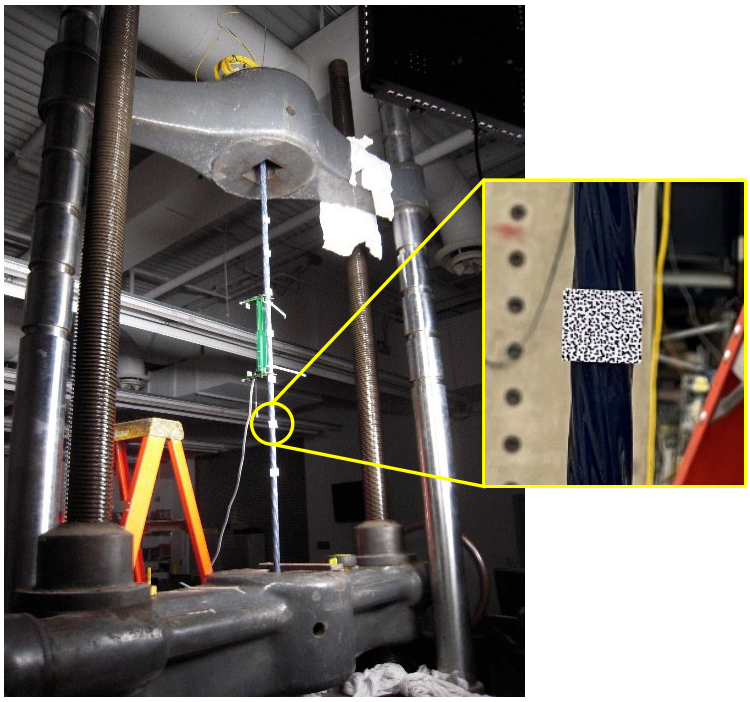

Figure 3.1: Strand specimen installed in universal testing machine for elastic modulus test.

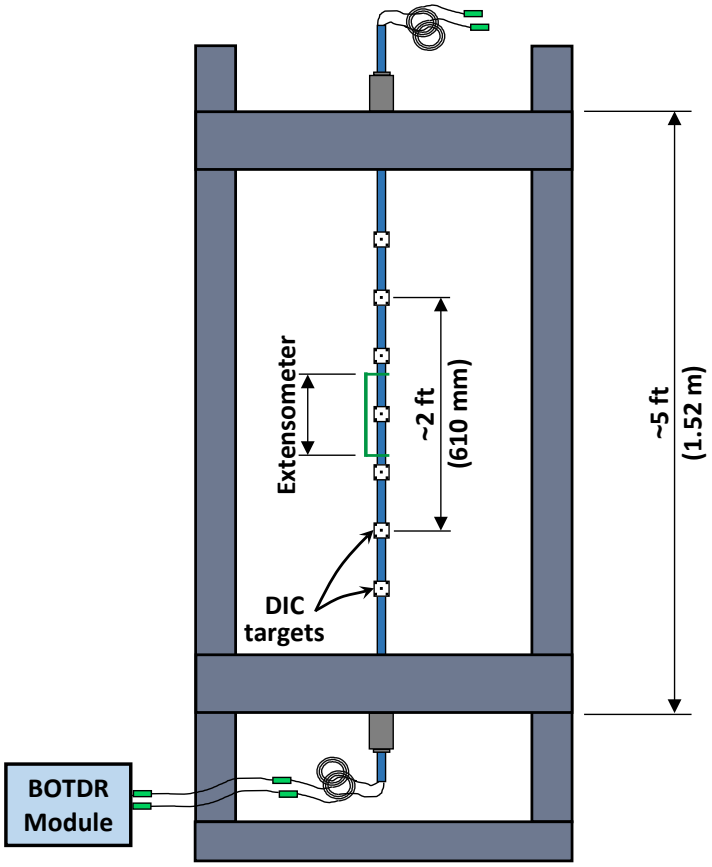

Figure 3.2: Setup for elastic modulus tests.

The optical fibers were connected to the BOTDR module and set up in a manner consistent with Figure 2.9. To measure axial strain along the strand, a digital image correlation (DIC) system was used. Square-shaped paper targets with a speckle pattern were adhered to the strand as indicated in Figure 3.1 and Figure 3.2. Movement of the targets was captured by a set of cameras, and the engineering strain between targets was able to be calculated. The two targets indicated in Figure 3.2 with a spacing of approximately 2 ft (610 mm) were used to determine the elastic modulus of the strand. The other targets were provided for redundancy. An extensometer was also attached to the strand and used for verification of the strain data from the DIC system.

Strain was measured with a spatial step of 9.84 in. (250 mm). In other words, the module provided strain values every 9.84 in. (250 mm) along the length of the optical fiber. Considering the spatial step of the data points and the 3.28-ft (1-m) spatial resolution, the average of the two data points near the center of the strand specimen (i.e., near the midpoint along the length of the specimen) was taken as the strain experienced by the optical fiber cable. Strain readings corresponding with points farther from the center of the specimen may have been affected by the unstrained portion of the fiber located beyond the ends of the specimen. The measurement time for the BOTDR module to capture strain and temperature data along the length of the specimen was approximately 8 to 8.5 minutes for each of the two fibers embedded in the epoxy coating. The acquisition of temperature data from the optical fibers will be discussed in Section 6.2.

For each test, load was applied with increments of 5 kip (22.2 kN), corresponding to a strand stress of 23.0 ksi (159 MPa), assuming a nominal strand area of 0.217 in.^{2} (140 mm^2). Between each loading increment, the load applied to the strand was held constant while the BOTDR module measured the strain in each of the two fibers. The DIC system captured strain data while load was increased during each 5-kip (22.2-kN) increment. The incremental loading continued up to a load of 45 kip (200 kN), corresponding to a strand stress of 207.4 ksi (1430 MPa).

3.3 Elastic Modulus Test Results

Consistent with the elastic modulus extrapolation method of ASTM A1061[3], stress-strain data between 20% and 65% of the specified tensile strength of the strand (270 ksi [1860 MPa]) were used to determine the least-squares linear regression fit line. The slope of the fit line was

[3] ASTM A1061, *Standard Test Methods for Testing Multi-Wire Steel Prestressing Strand*, is not a Federal requirement.

taken as the elastic modulus E_p. The resulting values for the four strand specimens are provided in Table 3.1. Values assume a nominal strand area of 0.217 in.^{2} (140 mm^2). For the specimens listed in Table 3.1, the values of E_p based on the DIC data and an effective E_p indicated by the BOTDR data from both optical fibers along the length of the strand are provided. No data were collected from one fiber of Specimen 4 due to inadvertent damage that occurred to the fiber that extended from the specimen.

Table 3.1: Measured modulus of elasticity and correction factors from Phase I tests.

Specimen	E_p from DIC, ksi (GPa)	E_p from BOTDR, ksi (GPa)		Correction Factor	
		Fiber 1	Fiber 2	Fiber 1	Fiber 2
1	28,550 (196.8)	30,330 (209.1)	29,700 (204.8)	1.06	1.04
2	28,510 (196.6)	30,440 (209.9)	30,770 (212.2)	1.07	1.08
3	28,160 (194.2)	29,360 (202.4)	29,960 (206.6)	1.04	1.06
4	28,610 (197.3)	-	30,040 (207.1)	-	1.05
Average	28,460 (196.2)	30,090 (207.5)		1.06	

The correction factors calculated for the BOTDR data in the linear-elastic range of the strand are provided in Table 3.1 for each specimen and are taken as the ratio of the effective E_p based on BOTDR data to the E_p based on DIC data. The correction factors range from 1.04 to 1.08 with an average value of 1.06.

As an example, the test results for Specimen 2 are presented in Figure 3.3. The solid portion of each line represents the range of data used to determine the E_p value. The lines for the BOTDR data for Fiber 1 and Fiber 2 overlap one another.

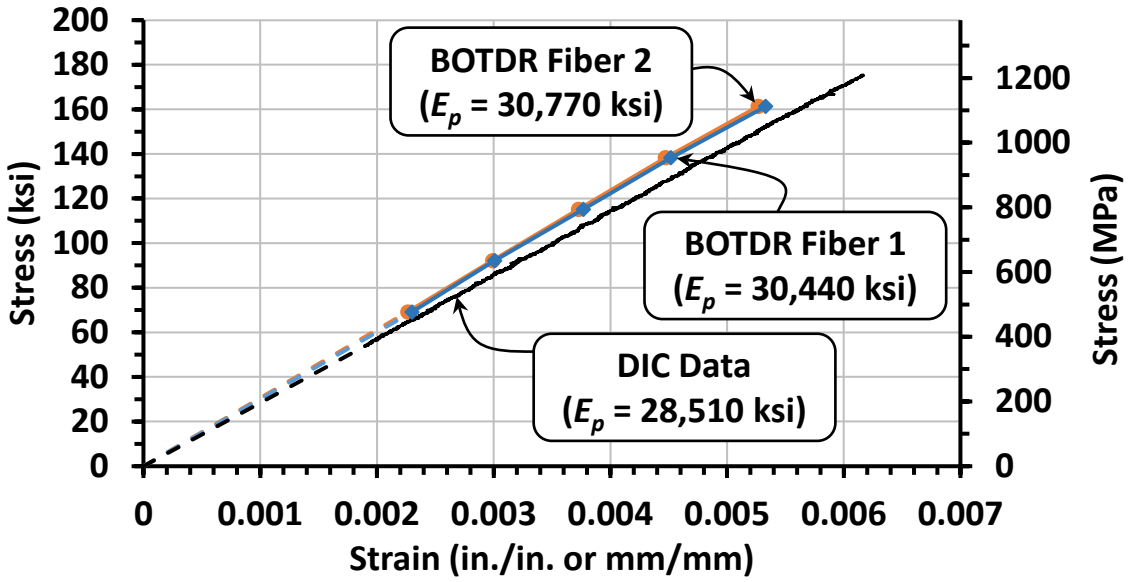

Figure 3.3: Stress-strain response of strand in linear range – DIC and BOTDR data for Specimen 2 (1 ksi = 0.006895 GPa).

4. Monitoring of Strands in Prestressing Bed

4.1 Introduction

During the second phase of the research, optical fiber sensor-embedded strands were stressed within a prestressing bed in the laboratory. The prestressing bed allowed straight strands to be stressed "in air" with lengths significantly greater than what could be tested in a universal testing machine. Specifically, three strand specimens with lengths of approximately 48.4 ft (14.8 m) measured between anchorage chucks were stressed and held in a prestressing bed over the period of one week. The optical fiber sensors, a DIC system, and load cells were used to collect data from the strand specimens. Furthermore, a thermocouple was used to continuously monitored the temperature experienced by the strand specimens. Because the strands were not subjected to any friction losses between the prestressing abutments, the uniformity of the strain measurements along the strand length was assessed. Moreover, the stability of the strain readings was evaluated over the week-long period.

4.2 Prestressing Bed Test Details

The prestressing bed used for the experimental program consisted of two steel abutments that were each post-tensioned to the strong floor of the laboratory to prevent slip of the abutments relative to the floor. The abutments are shown in Figure 4.1. An illustration of the prestressing bed with the strand specimens is presented in Figure 4.2. Each of the three strands was stressed from one end (live end) of the prestressing bed.

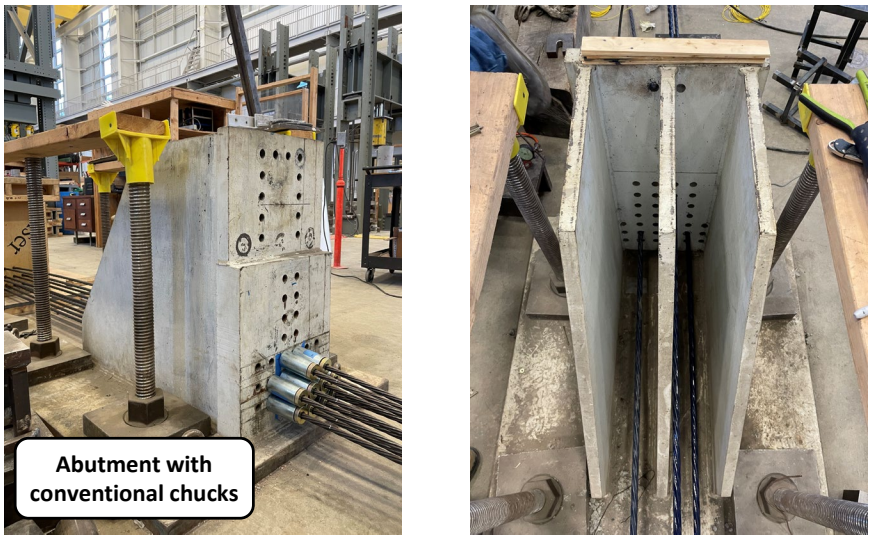

Figure 4.1: Steel abutments of prestressing bed.

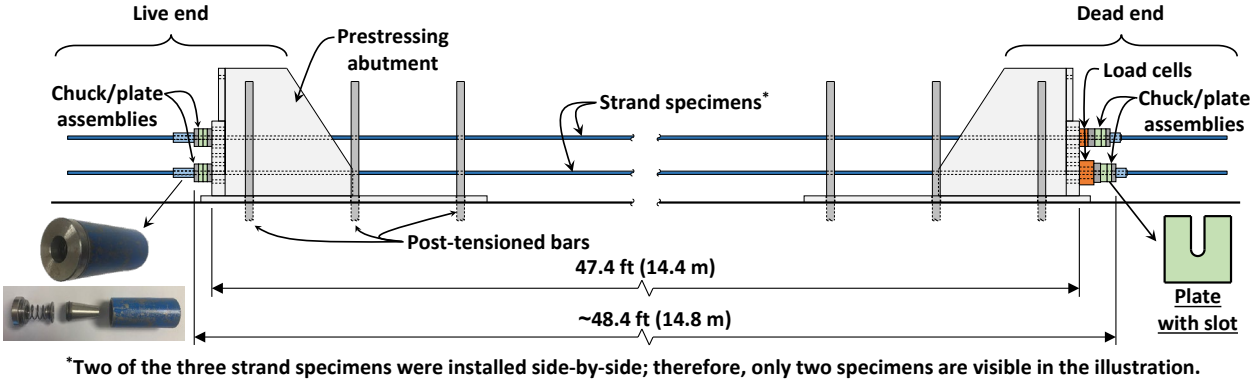

Figure 4.2: Strand specimens in prestressing bed.

The strands were anchored at each abutment with reusable prestressing chucks for epoxy-coated strand, resulting in approximately 48.4 ft (14.8 m) of each strand specimen being held under stress. Each chuck consisted of a three-piece wedge contained in a cylindrical barrel. A prestressing chuck with a cap and spring was provided at the live end, while a prestressing chuck without a cap and spring was used at the other end (dead end). Each chuck type is shown in Figure 4.3.

(a) Chuck with cap and spring (used at live end)

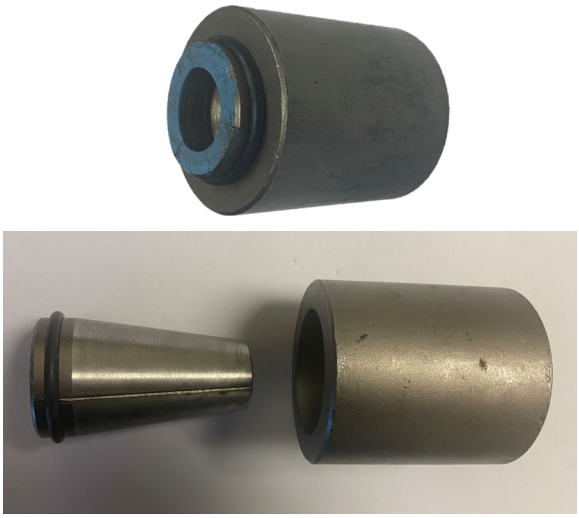

(b) Chuck without cap and spring (used at dead end)

Figure 4.3: Prestressing chucks used for strand specimens in Phase II.

A series of steel plates was installed at each end of the strand. Steel shim plates with slots were used to allow for detensioning of the strands after the strands were evaluated over a week-long period. The plate/chuck assemblies are shown in Figure 4.4(a) and (b) for the live and dead ends, respectively. A hollow load cell was installed on each strand at the dead end of the prestressing bed (Figure 4.4(b)) and directly measured the force in each strand.

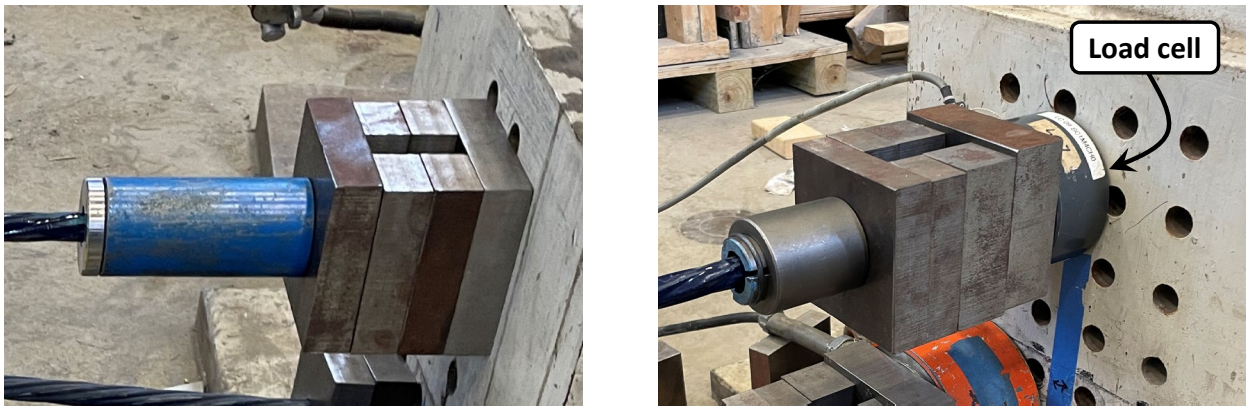

(a) Assembly at live end

(b) Assembly at dead end

Figure 4.4: Plate/chuck assemblies at each abutment.

The equipment used to stress the epoxy-coated strands in the prestressing bed is shown in Figure 4.5. The force from the hydraulic cylinder was applied to the chuck shown in Figure 4.4(a) through a steel plate during the stressing operations.

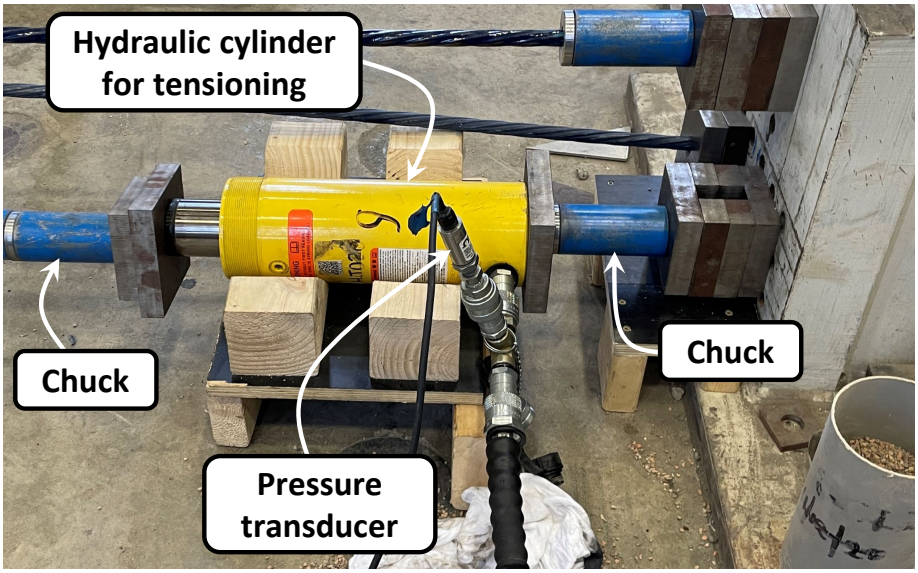

Figure 4.5: Equipment for stressing epoxy-coated strands in Phase II.

To measure axial strain along the strand specimens, the same DIC system used for the elastic modulus tests was again used. Square-shaped paper targets with a speckle pattern were adhered to each strand specimen at a spacing of 6 in. (152 mm) over a length of 5 ft (1.52 m) as indicated in Figure 4.6. Movement of the targets was captured by cameras and the engineering strain between two targets was able to be calculated. Because the strand rotated as it was tensioned, targets needed to be placed at various orientations on the strand. The targets initially in view of the

DIC cameras would rotate out of view as tension was applied to the strand. Therefore, targets at a different orientation that could be captured by the cameras as the strand was tensioned further were needed.

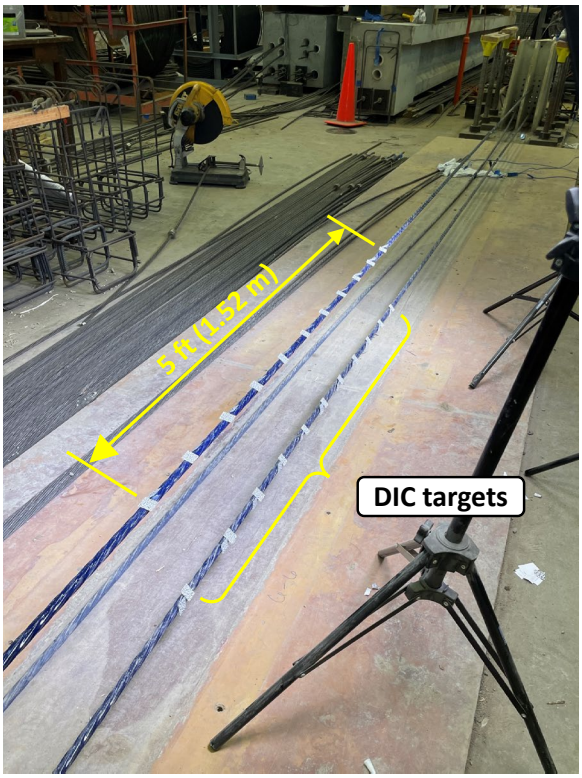

Figure 4.6: DIC targets installed on strand.

The setup of the optical fiber measurement system is illustrated in Figure 2.10. Based on their placement within the setup, the three strand specimens are herein referred to as Strand 1, Strand 2, and Strand 3 as labeled in Figure 2.10. All of the fibers (that is, both fibers in each of the three strands) were connected in series so that only one port on the BOTDR module needed to be scanned in order to collect data for all of the strand specimens. Strain was measured with a spatial step of 3.15 in. (80 mm). The measurement time for the BOTDR module to capture strain and temperature data along the full length of the optical fiber cable was approximately 12 minutes. The acquisition of temperature data from the optical fibers will be discussed in Section 6.2.

As during the Phase I tests, the strands were stressed in increments to allow for strain using the optical fibers to be measured by the BOTDR module between load steps while the applied load was held on the strand. For each strand, load was applied in increments corresponding to a strand stress of approximately 40 ksi (276 MPa), assuming a nominal strand area of 0.217 in.^{2} (140 mm^2).

For the last load step of Strand 1 and Strand 2, instead of stopping when 200 ksi (1379 MPa) was applied to the strand, the strand stress was increased to 202.5 ksi (1396 MPa), corresponding to $0.75f_{pu}$, where f_{pu} is the specified tensile strength of the prestressing strand (270 ksi [1860 MPa]). For Strand 3, the stroke limit of the hydraulic cylinder was unexpectedly reached prior to applying a stress of 202.5 ksi (1396 MPa). Therefore, the maximum stress applied to Strand 3 prior to anchorage set was 194.4 ksi (1340 MPa).

During the week-long evaluation period for each strand, data from the load cells were continuously recorded, and the BOTDR module was programmed to conduct a scan every 60 minutes. Furthermore, a thermocouple was placed near the prestressing bed and was used to continuously record the air temperature over the evaluation period.

4.3 Prestressing Bed Test Results

4.3.1 BOTDR Strain Results

To describe the procedure for collecting strain data for the two optical fiber sensors embedded in the epoxy-coating of each strand specimen, an example from Phase II of the measured strain values along the optical fiber using BOTDR is presented in Figure 4.7(a). The strains represented in Figure 4.7 were collected after all three strands had been stressed. The location of each fiber embedded in the three strand specimens is labeled in the figure. A close-up view of the strain measured over the length of Fiber 1 of Strand 2 is provided in Figure 4.7(b). For the BOTDR strain values used for the analysis presented in this section, the average value of the strains measured along the relatively flat portion of the strain data is used as indicated in the figure.

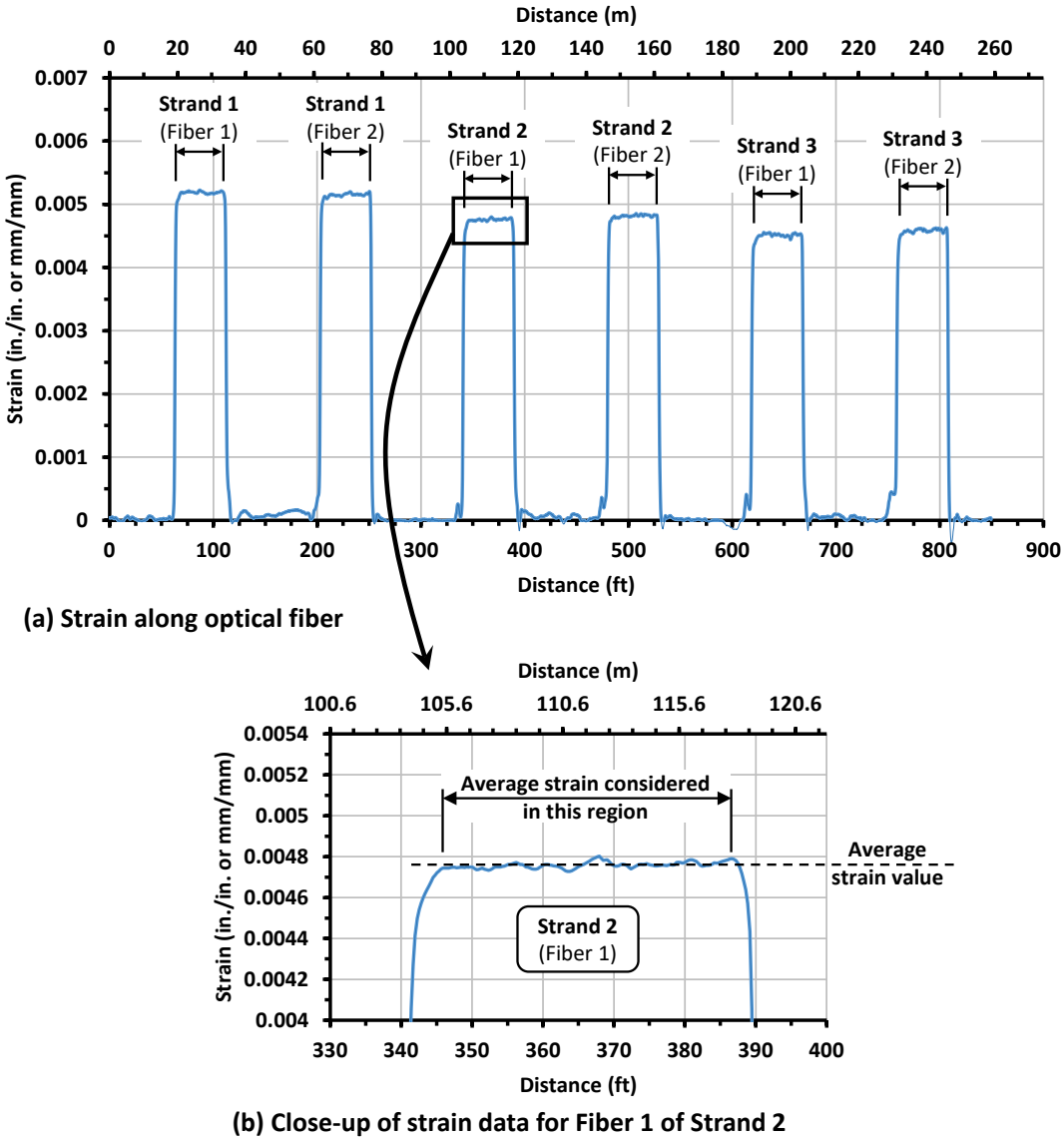

Figure 4.7: Example of measured strain values along optical fiber using BOTDR.

As evident in Figure 4.7(b), some scatter, or unevenness, in the strain readings is present over the length of the strand despite the strand being under uniform strain between the prestressing abutments. To quantify this scatter, the relatively flat portion of the strain data, such as the region indicated in Figure 4.7(b), was evaluated for a sample of 34 measurements along the Phase II strand specimens at various levels of applied load. The largest difference between the maximum and minimum strain values for any particular sample (i.e., along a particular fiber embedded along the length of a strand specimen) was $117(10^{-6})$. The standard deviation of the strain data along a strand varied from $8.45(10^{-6})$ to $24.7(10^{-6})$.

4.3.2 During Stressing Operations

Each strand was stressed in increments as described in Section 4.2. Due to the measurement time of the BOTDR module (approximately 12 minutes), strain readings along the optical fibers could not be collected while the force applied to the strand was increased. Therefore, a scan using the BOTDR module was run between each load step. Even though the hydraulic system was set to maintain pressure in the hydraulic cylinder during this time, due to the nature of the hydraulic system, a small decrease in load occurred over the measurement period of the BOTDR scan. Data from the load cell were continuously recorded during stressing and between each load step. Therefore, to determine a single load value corresponding to the strain measured by the BOTDR module, load cell readings that were collected for the strand between the load steps were averaged.

The DIC system captured the position of the targets adhered to the strand while load was increased during each loading increment and while the BOTDR readings were taken. However, only select photographs that corresponded with the times of the BOTDR scans were considered in order to provide a direct comparison to the BOTDR results.

For each of the three strand specimens, strain data collected from the optical fibers and the DIC system during the stressing operation were compared in a manner similar to the data from the elastic modulus tests of Phase I. The results are provided in Figure 4.8 in the form of stress-strain diagrams. In each plot, the strain values measured between each load step using BOTDR are plotted for each of the optical fibers (Fiber 1 and Fiber 2) embedded in the epoxy coating of the strand specimen. The corresponding strain value measured along the longitudinal axis of the strand using DIC is also plotted. The stress values along the *y*-axis are calculated as the readings from the load cell divided by the nominal area of the strand (0.217 in.^{2} [140 mm^2]). The strain values from the DIC system were derived by considering the relative movement of targets spaced 6-in. (152-mm) apart located near the center of the field of view of the cameras as these targets provided the most accurate results. The dashed portions of the DIC plots near the origin in Figure 4.8 were extrapolated from the DIC data as inaccurate readings would otherwise be shown in this region due to slack in the strands. Furthermore, the additional dashed portion of the DIC plot in Figure 4.8(b) represents a period during which the DIC targets rotated outside the view of the cameras. The increase in strain was estimated within this region of the plot. The DIC data for Strand 3 was unfortunately lost and is therefore not included in Figure 4.8(c). Nevertheless, the elongation behavior of this specimen is expected to be similar to that of the other two strands. It should be

noted that the lines for the BOTDR data for Fiber 1 and Fiber 2 overlap one another in each of the three plots.

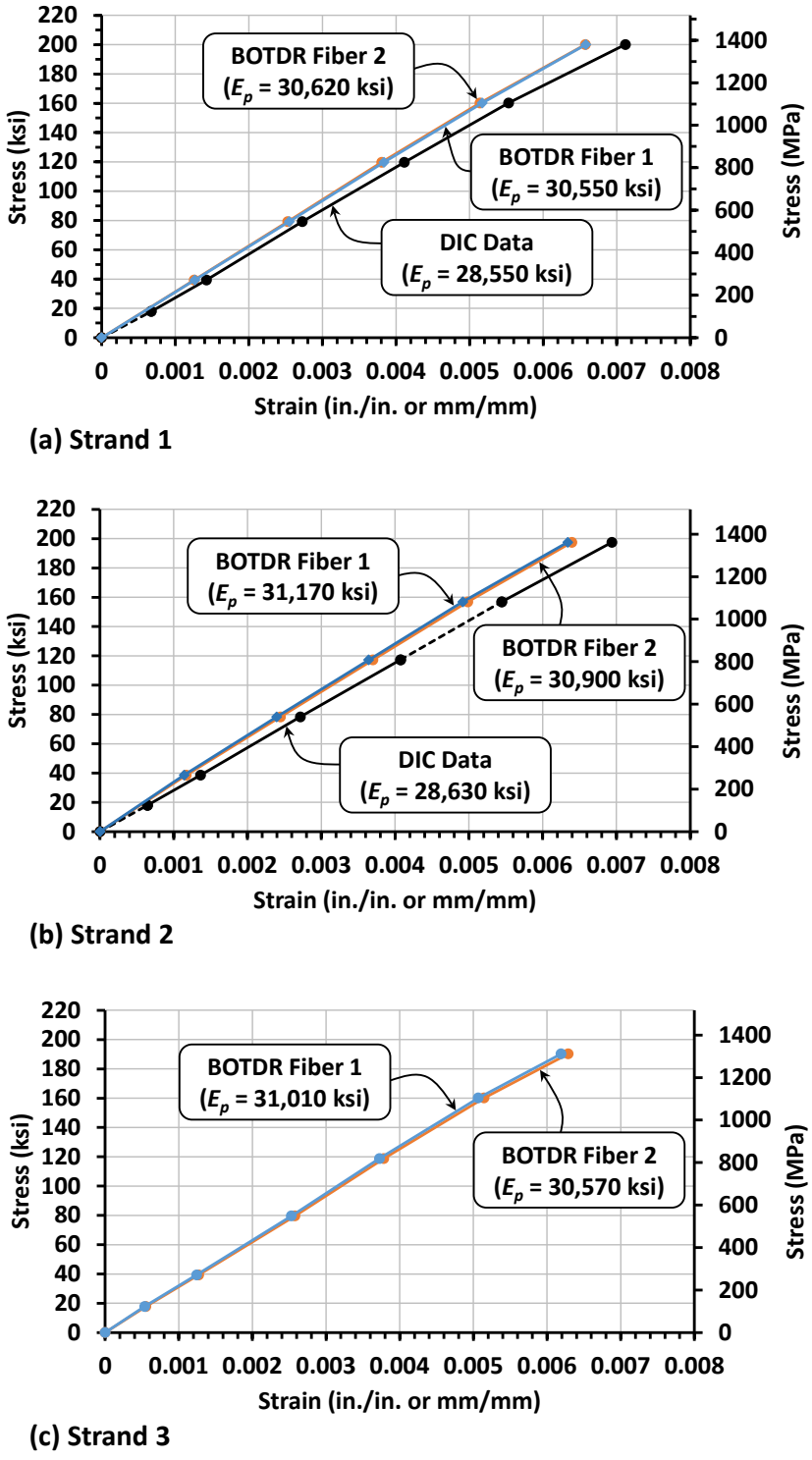

Figure 4.8: Stress-strain response during stressing operations of Phase II – DIC and BOTDR data (1 ksi = 0.006895 GPa).

Each value for the modulus of elasticity E_p provided in Figure 4.8 is the slope of the least-squares linear regression fit line considering all of the plotted data points. These values of E_p are summarized in Table 4.1. The modulus of elasticity values from both DIC and BOTDR are similar to the values found during the Phase I tension tests (Table 3.1). Furthermore, the average correction factor defined as the ratio of the effective E_p based on BOTDR data to the E_p based on DIC data is 1.08, relatively similar to the average value of 1.06 found during Phase I.

Table 4.1: Measured modulus of elasticity and correction factors from Phase II stressing operations.

Specimen	E_p from DIC, ksi (GPa)	E_p from BOTDR, ksi (GPa)		Correction Factor	
		Fiber 1	Fiber 2	Fiber 1	Fiber 2
Strand 1	28,550 (196.8)	30,550 (210.6)	30,620 (211.1)	1.07	1.07
Strand 2	28,630 (197.4)	31,170 (214.9)	30,900 (213.0)	1.09	1.08
Strand 3	-	31,010 (213.8)	30,570 (210.8)	-	-
Average	28,590 (197.1)	30,800 (212.4)		1.08	

After the maximum jacking stress for a strand specimen was reached and a BOTDR scan was performed, pressure was released from the hydraulic system, and stress on the strand was transferred to the prestressing chuck located near the abutment at the live end (Figure 4.5). This chuck was equipped with a cap and spring as shown in Figure 4.3(a). The anchorage set due to the seating of the wedge in the prestressing chuck was estimated to be approximately 1 in. (25 mm), resulting in relatively large set losses. These large set losses were mitigated during Phase III by implementing a power-seating procedure for the wedges.

4.3.3 During Week-Long Monitoring Period

After anchorage set, each strand specimen was evaluated over a week-long period as strain on the specimen was maintained. Change in stress was expected only due to small temperature variations in the laboratory, relaxation, and possible disturbances due to the stressing or detensioning of adjacent strand specimens.

Stress values based on readings from the optical fibers and load cells for the three strand specimens are presented in Figure 4.9. Data points are plotted in increments of approximately 12 hours. The stress values based on the BOTDR data for each fiber are equal to the strain in the fiber acquired from the BOTDR module multiplied by the corresponding value of E_p reported in Table

4.1 for that fiber. The stress values from the load cell data are taken as the force value indicated by the load cell divided by the nominal area of the prestressing strand (0.217 in.^{2} [140 mm^2]).

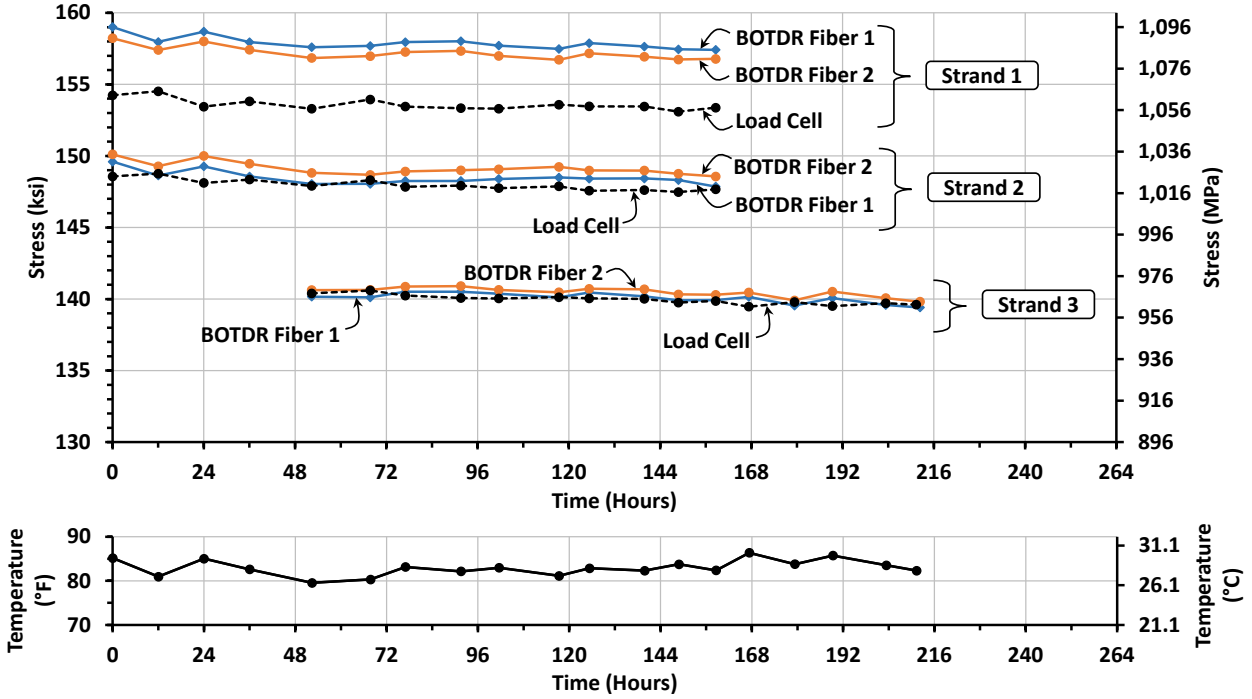

Figure 4.9: Stress values from sensing techniques over week-long evaluation period for each strand specimen (E_p *values from Table 4.1 applied to BOTDR data).*

As indicated by the data in Figure 4.9, Strand 1 and Strand 2 were both stressed on the same day (Day 1). Strand 3 was later stressed on Day 3. Following the week-long evaluation period of Strand 1 and Strand 2, the two strands were detensioned on Day 8. Finally, Strand 3 was detensioned on Day 10.

The stress in the strands at the beginning of the evaluation periods according to the load cell data was 154.2 ksi, 148.6 ksi, and 140.4 ksi (1063 MPa, 1025 MPa, and 968.0 MPa) for Strand 1, Strand 2, and Strand 3, respectively. Over the evaluation periods, the stress values based on the BOTDR and load cell data remain relatively constant for all three strand specimens. In general, the stress values from both sources present a slight downward trend over the week-long period for reasons that are unclear.

The temperatures measured by the thermocouple at the times corresponding to the plotted stress data are presented at the bottom of Figure 4.9. The temperature varied between 80°F and 86°F (26°C and 30°C) during the evaluation period. A relationship between the stress values based

on BOTDR and temperature is evident. The effects of temperature are further discussed in Section 6.2.

With the BOTDR strain value from each optical fiber embedded in the strand multiplied by its specific E_p value obtained during the stressing operation (Table 4.1), the resulting stress values are nearly equal to the stresses based on the load cells for Strand 2 and Strand 3. However, a discrepancy exists in the stress values for Strand 1. Because this discrepancy appeared after anchorage set for this strand and was not present during the stressing operation, the cause may be due to unexpected friction loss developing at the abutment located at the dead end of the prestressing bed, possibly because of rubbing of the strand against the abutment or the steel plates. Localized loss at the abutment would cause the load cell to measure a lower force than what was carried by the strand between the abutments. The largest discrepancy between the stress values from the BOTDR data and the load cell for Strand 1 occurs at 24 hours into the evaluation period. The ratio between the stress value from Fiber 1 and the corresponding value from the load cell at this time is 1.034.

In the field, it may be desired that an average value for E_p be applied to the BOTDR strain values rather than collecting data during the stressing of each strand to derive a specific E_p value for each optical fiber sensor. Therefore, Figure 4.9 has been recreated with the stress values from the BOTDR data calculated by multiplying the strain values from the optical fiber sensors by the average effective modulus of elasticity E_p for the strands determined through the elastic modulus tests of the Phase I experimental program. As reported in Table 3.1, the average value of E_p based on the BOTDR data is 30,090 ksi (207.5 GPa). The resulting plot is provided in Figure 4.10.

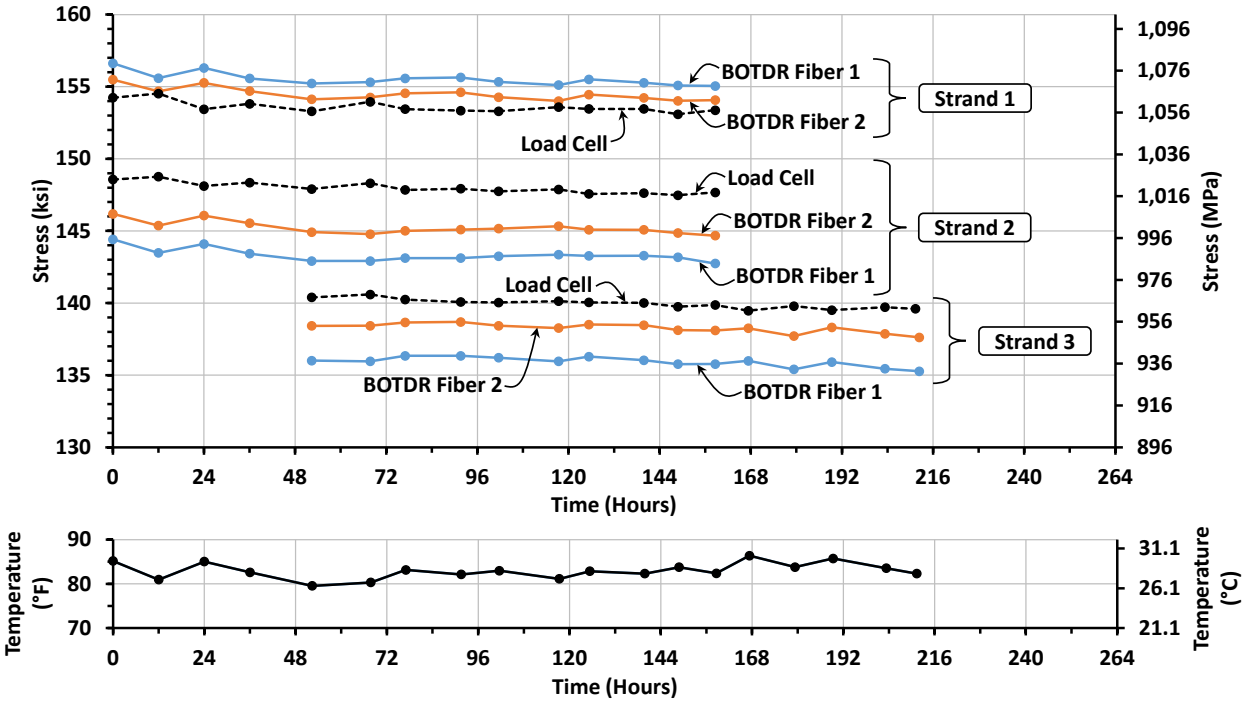

Figure 4.10: Stress values from sensing techniques over week-long evaluation period for each strand specimen (average E_p *value from Phase I applied to BOTDR data).*

In this case, the discrepancy between the stress values based on BOTDR and the load cells increases for Strand 2 and Strand 3 while it improves for Strand 1. The largest discrepancy between the stress values from the load cell for Strand 2 and the values from Fiber 1 of that specimen occurs at approximately 68 hours. The ratio between the stress value from Fiber 1 and the value from the load cell is 0.964 at this time. Similarly, the largest discrepancy between the stress values from Fiber 1 of Strand 3 and the corresponding load cell, which also occurs at approximately 68 hours, gives a ratio of 0.967. These values may provide an idea of the error expected during field implementation if elastic modulus values based on tensile tests performed on small strand samples are used.

5. Beam Tests

5.1 Introduction

During Phase III of the research project, flexural load tests were conducted on two post-tensioned beam specimens containing the optical fiber sensor-embedded strands for further verification of the strain data obtained through BOTDR. The details of the beam specimens, fabrication procedure, test setup, and test results are provided in this chapter. Key observations regarding strain data from the optical fibers are noted for both the post-tensioning operations and load tests. Strain measurements from the optical fibers obtained during the tests are compared to strains measured using conventional strain gauges. Furthermore, analytical models were developed in order to compare strain values output from the models over the length of the beams with those measured by the optical fibers.

5.2 Details of Beam Specimens

The details of the two beam specimens are presented in Figure 5.1 and Figure 5.2. Both beams had a length of 28 ft (8.53 m). One specimen had a box-shaped cross section, and the other beam was shaped as an I-beam. All strands in the specimens had a nominal diameter of 0.6 in. (15.2 mm).

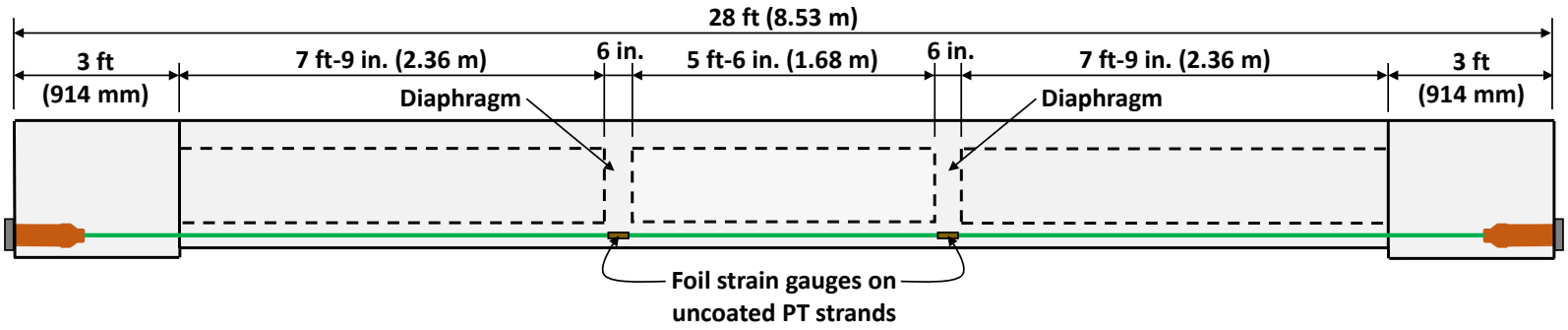

(a) Box beam elevation

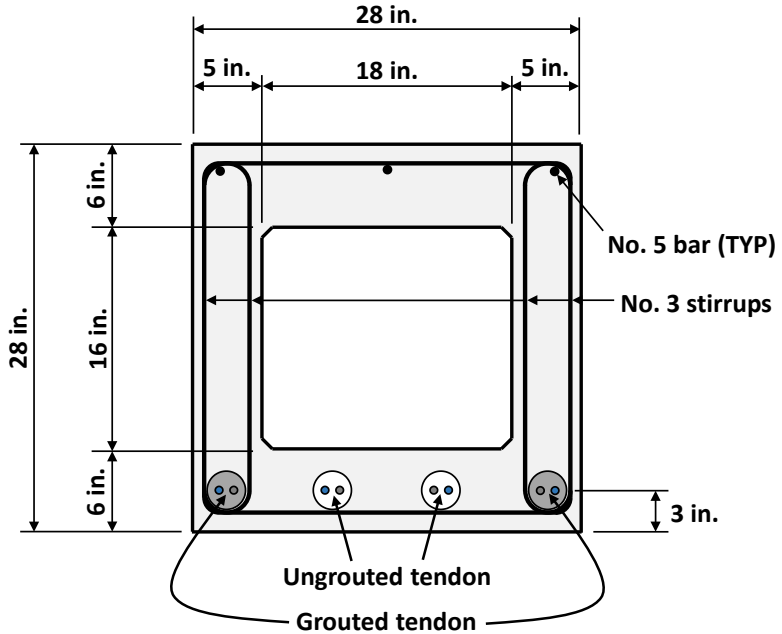

Note: Each tendon contains one epoxy-coated strand
and one uncoated strand

(b) Box beam cross section

Figure 5.1: Details of box-beam specimen (1 in. = 25.4 mm).

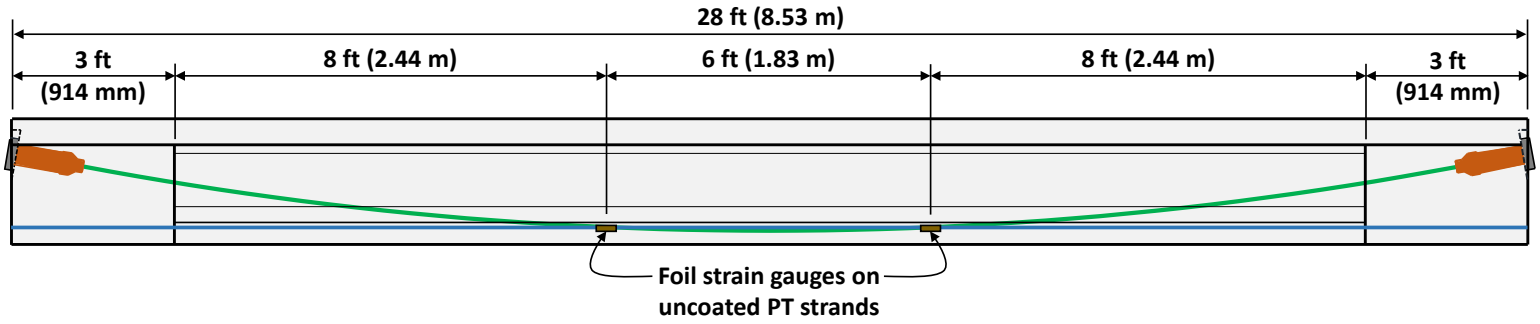

(a) I-beam elevation

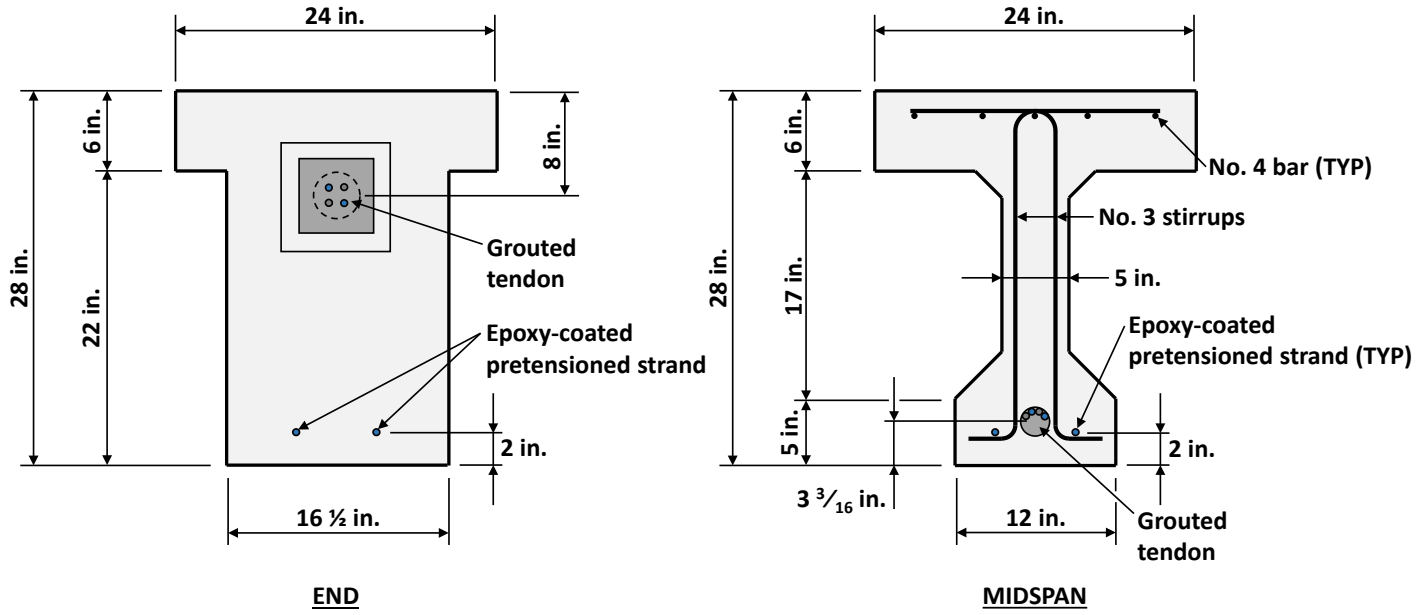

Note: Tendon contains two epoxy-coated strands and two uncoated strands

(b) I-beam cross sections

Figure 5.2: Details of I-beam specimen (1 in. = 25.4 mm).

The box-beam specimen contained four straight post-tensioned tendons in its bottom flange. Each tendon consisted of one optical fiber sensor-embedded strand and one uncoated strand (i.e., typical strand meeting ASTM A416[2]). The two outermost tendons were grouted, creating a bonded condition, while the two innermost tendons were unbonded. The epoxy coating of the sensor-embedded strands in the bonded tendons was grit-impregnated.

The I-beam specimen was pretensioned with two straight optical fiber sensor-embedded strands located in the bottom flange. The specimen also contained one draped post-tensioned tendon consisting of two optical fiber sensor-embedded strands and two uncoated strands. The tendon was grouted (bonded). The drape of the tendon (i.e., change in elevation from beam end to midspan) was approximately 16.75 in. (425 mm). The epoxy-coating of all sensor-embedded strands in the I-beam specimen was grit-impregnated.

Each post-tensioned tendon in the test specimens included at least one uncoated strand and one epoxy-coated strand with optical fibers. This combination represents situations in the field for which the desire may exist to include one or two sensor-embedded strands in conventional grouted tendons with uncoated strands.

Each beam included thickened end blocks with lengths of 3 ft (914 mm). Expanded polystyrene foam was used to form the voids of the box-beam specimen. Two diaphragms (Figure 5.1(a)) were provided along the length of the box beam at locations corresponding with the load points of the test setup, described in Section 5.5. To prevent shear failure, the box-beam specimen was reinforced with No. 3 (10-mm diameter) stirrups with four legs spaced at 5 in. (127 mm), and the I-beam specimen contained two-legged No. 3 (10-mm diameter) stirrups spaced at 4 in. (102 mm).

As indicated in Figure 5.1 and Figure 5.2, two foil strain gauges (i.e., electrical resistance strain gauges) were installed on each uncoated strand in both beam specimens. Their placement corresponded with the load points of the test setup.

5.3 Beam Specimen Fabrication

The beam specimens were fabricated in the laboratory. The formwork and reinforcing cages for the I-beam and box-beam specimens prior to casting are shown in Figure 5.3. All mild

reinforcing steel was Grade 60 (ASTM A615[4]). The ducts for bonded tendons were corrugated plastic, while the ducts for unbonded tendons were smooth plastic.

(a) I-beam specimen

(b) Box-beam specimen

Figure 5.3: Formwork and reinforcing cages of beam specimens prior to casting.

The concrete used for the specimens was a self-consolidating concrete (SCC) with a target compressive strength of 8 ksi (55.2 MPa). Casting of the beams is shown in Figure 5.4. The box beam was cast over a two-day period. On the first day, the concrete for the bottom flange was cast. The remainder of the concrete was cast the following day. This procedure was followed to prevent the expanded polystyrene foam from floating upwards, which may have occurred if the beam was fabricated with a single cast.

[4] ASTM A615, *Standard Specification for Deformed and Plain Carbon-Steel Bars for Concrete Reinforcement*, is not a Federal requirement.

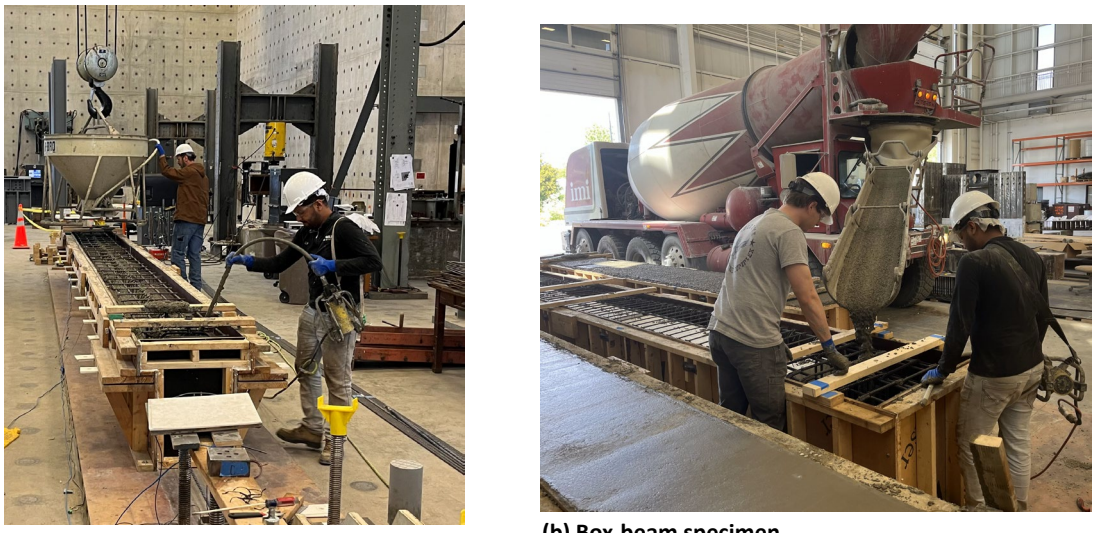

(a) I-beam specimen

(b) Box-beam specimen

Figure 5.4: Casting beam specimens.

Before preparing the reinforcement and casting the concrete for the I-beam specimen, the two pretensioned strands were tensioned using the same prestressing bed described in Section 4.2 (Figure 4.2). The equipment used to individually stress the pretensioned epoxy-coated strands in Phase III is shown in Figure 5.5. The same equipment and setup were also used to stress all of the post-tensioned epoxy-coated strands in the beam specimens. As indicated in Figure 5.5, a small hydraulic cylinder was used to power seat the wedges prior to anchorage set to mitigate the set losses observed during Phase II.

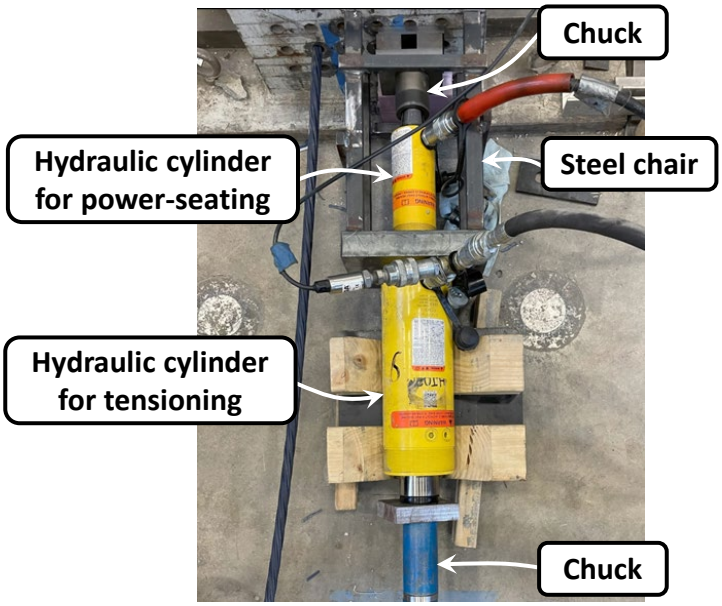

Figure 5.5: Equipment for stressing epoxy-coated strands in Phase III.

The post-tensioned strands in both beams were individually stressed prior to the beam tests. A commercially available monostrand post-tensioning jack was used for all of the uncoated strands, as shown in Figure 5.6(a). Figure 5.6(b) and (c) present the post-tensioning of an epoxy-coated strand in the I-beam and box-beam specimens, respectively.

(a) Stressing uncoated strand in box-beam specimen

(b) Stressing epoxy-coated strand in I-beam specimen

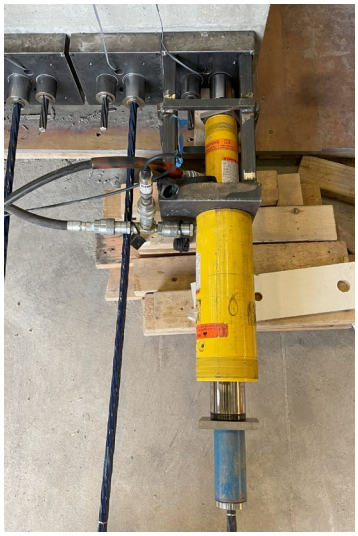

(c) Stressing epoxy-coated strand in box-beam specimen

Figure 5.6: Post-tensioning beam specimens.

The jacking stress for uncoated strands in the beam specimens was approximately 210 ksi (1448 MPa). For the post-tensioned epoxy-coated strands, the jacking stress was approximately 205 ksi (1413 MPa). The stroke on the hydraulic cylinder was reached while tensioning the

pretensioned epoxy-coated strands in the I-beam. Therefore, the jacking stresses for these two strands were 173 ksi (1193 MPa) and 186 ksi (1282 MPa).

Each optical fiber sensor-embedded strand in the beam specimens was stressed in increments in order to collect strain readings using BOTDR during the stressing operation. Using the collected BOTDR strain data, the effective modulus of elasticity E_p for each fiber was determined in a similar manner as shown for the E_p values based on BOTDR in Figure 3.3 and Figure 4.8. For the strands in the I-beam that experienced large friction losses (discussed in Section 5.4), the strain readings near the live end were used to determine an effective E_p value. A correction factor for each fiber was then calculated as the ratio of the effective E_p based on BOTDR to an E_p of 28,600 ksi (197 GPa). The value of 28,600 ksi (197 GPa) is the average value for the modulus of elasticity of the epoxy-coated strands based on previous tests performed during the experimental program. The resulting correction factors for the strands in the beam specimens ranged from 1.03 to 1.10 with an average value of 1.07. All strains from the optical fiber sensors along the strands of the beam specimens reported herein have had the corresponding correction factor applied.

Following post-tensioning, the bonded tendons were grouted. Custom grout caps were used at the ends of the beams to accommodate the optical fiber sensor-embedded strands. To reduce the risk of damage to the fibers and to provide the opportunity for repairs if any fibers were broken, the strands extended through holes provided in the grout caps as shown in Figure 5.7. The ends of both beams during the grouting procedure are shown in Figure 5.8.

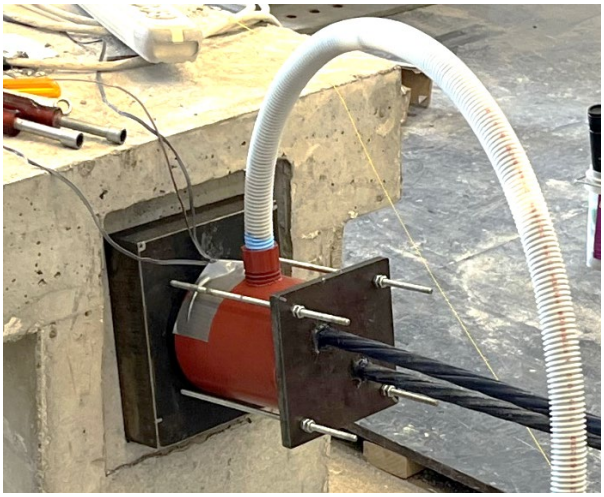

Figure 5.7: Custom grout cap used at ends of bonded tendons.

(a) I-beam specimen (b) Box-beam specimen

Figure 5.8: Grouting of tendons in beam specimens.

5.4 Observations from Post-Tensioning

Important observations can be made from the BOTDR strain data collected during the post-tensioning operations that were not possible during previous phases of the research when strands were stressed outside of beam specimens.

First, significant friction losses were observed during the stressing of strands within the draped tendon of the I-beam. The nominal inner diameter of the duct was 1.89 in. (48 mm). Each of the four strands were tensioned individually, which likely increased the friction losses experienced by the strands as they interacted inside the duct. Strain based on the BOTDR data along both of the post-tensioned epoxy-coated strands in the I-beam is presented in Figure 5.9. The figure shows the strains both before and after anchorage set, and the data from both optical fibers along the strands are shown. In each plot, the extents of the horizontal axis exceed the length of the beam specimen and include a portion of the optical fibers that extended beyond the ends of the beam.

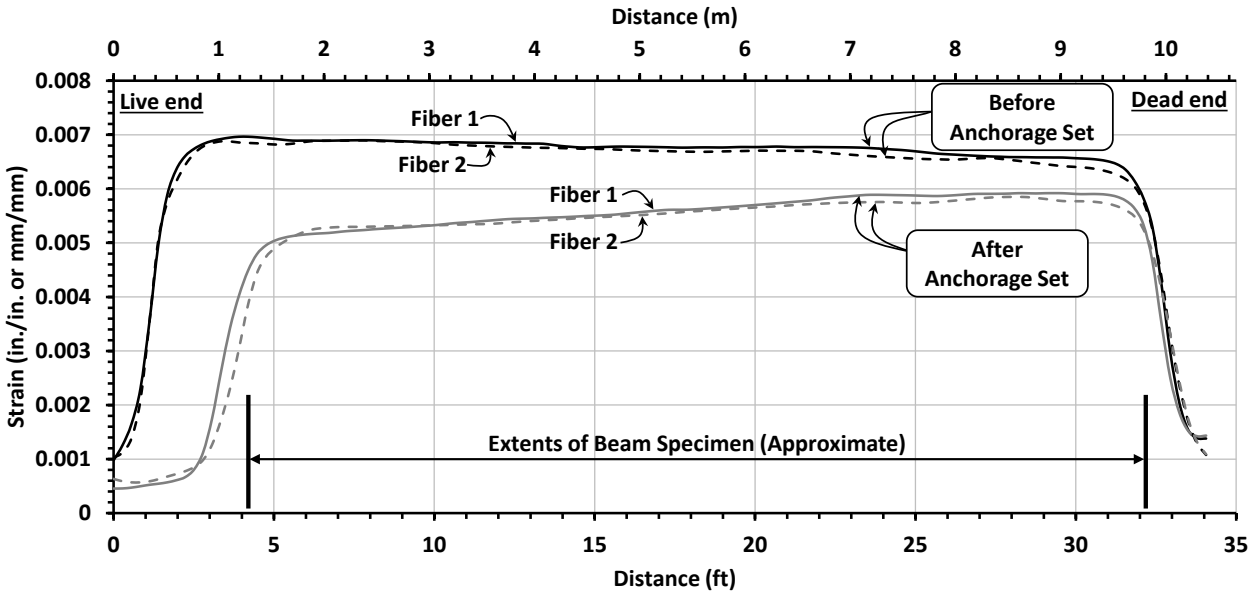

(a) First epoxy-coated strand to be stressed

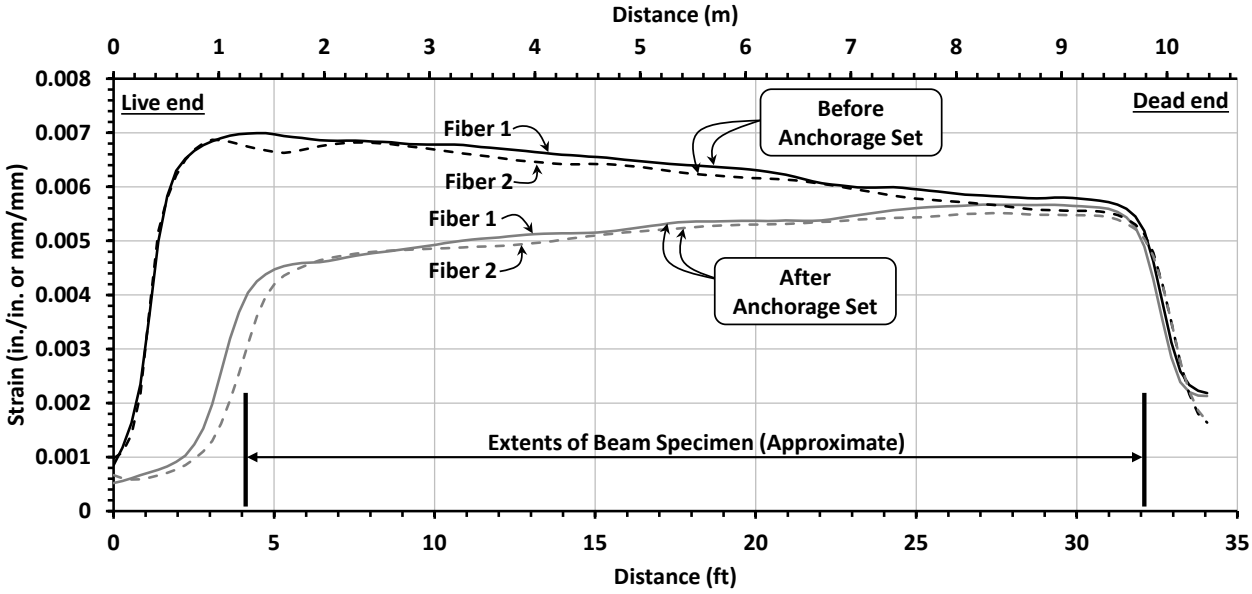

(b) Second epoxy-coated strand to be stressed

Figure 5.9: Strain before and after anchorage set of post-tensioned strands in I-beam.

The strand represented in Figure 5.9(b) was the last strand in the I-beam that was post-tensioned and presented greater friction losses than the other epoxy-coated strand in the same duct (Figure 5.9(a)). The last strand to be tensioned was likely constrained by the three other tensioned strands in the draped tendon, resulting in larger friction losses. Before anchorage set of this strand, the difference in strain values between the dead end and live end was approximately 0.0012,

corresponding to an estimated friction loss of (0.0012)(28,600 ksi) = 34.3 ksi ([0.0012][197 GPa] = 236 MPa). The 3.28-ft (1-m) spatial resolution of the BOTDR data should be kept in mind when considering the strain values. Another observation from Figure 5.9 is that the strain in the strands after anchorage set is less at the live end than at the dead end due to the effects of friction losses.

A similar plot is shown in Figure 5.10 for a post-tensioned strand in the box-beam specimen. Here, any friction losses along the straight tendon are insignificant.

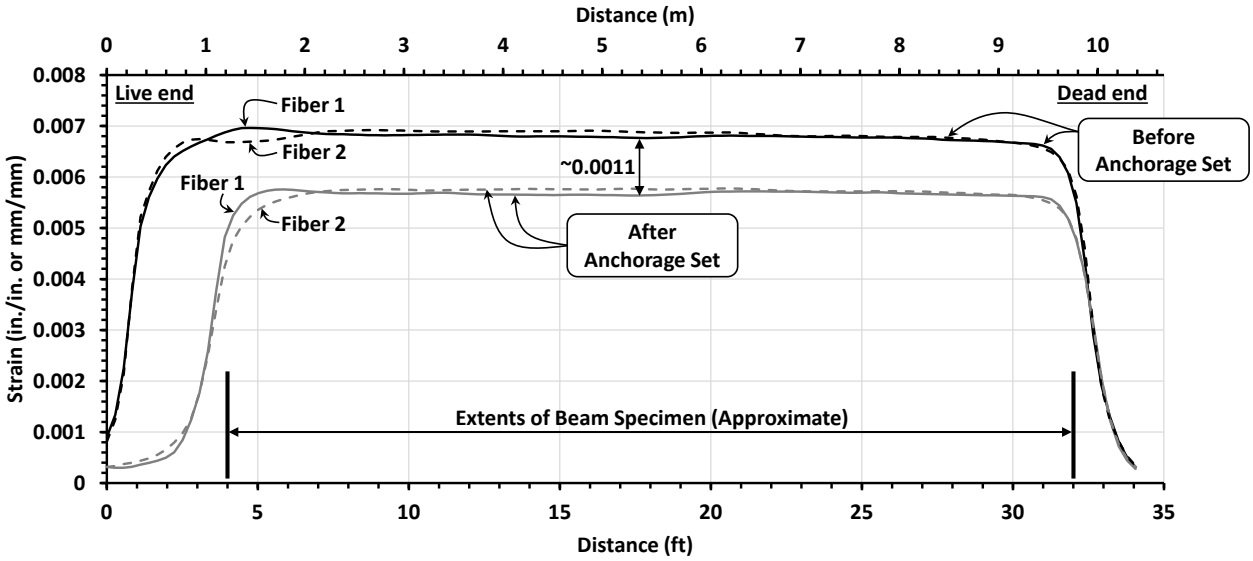

Figure 5.10: Strain before and after anchorage set of post-tensioned strand in box beam.

The data in Figure 5.9 and Figure 5.10 can be used to estimate the value of the set distance Δ_{set} at the live end at anchorage set of the strand (i.e., the movement of the strand prior to seating). As an example, the strand in the box beam represented in Figure 5.10 and the last strand to be tensioned in the I-beam (Figure 5.9(b)) will be considered. For the strand in the box beam, the loss in strain at anchorage set is approximately 0.0011 as labeled in Figure 5.10. Multiplying this value by the beam length (28 ft [8.53 m]) gives a value for Δ_{set} of 0.37 in. (9.4 mm). For the strand in the I-beam, the area between the curves before and after anchorage set is equal to the estimated value of Δ_{set}. Approximating the area as a triangle with a depth of 0.0023 and a length of 25.5 ft (7.77 m) as shown in Figure 5.11, the calculated value of Δ_{set} is 0.35 in. (8.9 mm). The estimated values of Δ_{set} are not unreasonable considering the use of epoxy-coated strands.

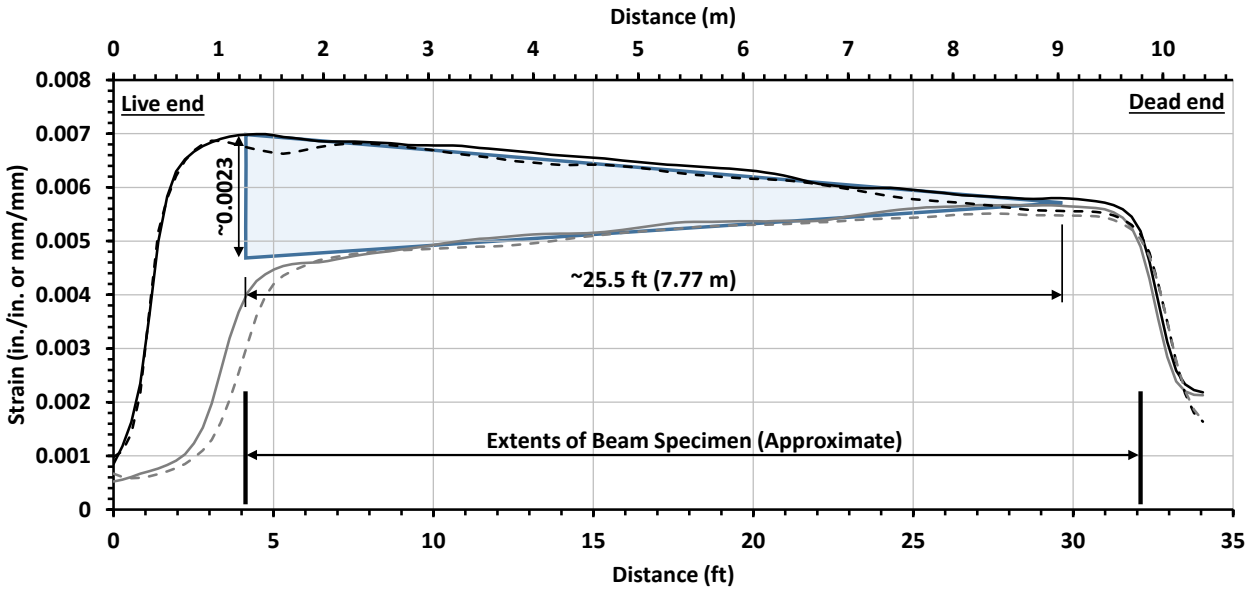

Figure 5.11: Estimating area between curves before and after anchorage set of post-tensioned strand in I-beam.

Another observation from the post-tensioning operations is the strain reduction due to elastic shortening that was experienced by one strand in a beam specimen while another strand in the same beam was being tensioned. The fracturing of a strand in a tendon of a post-tensioned beam can be assumed to cause the reverse effect on an optical fiber sensor-embedded strand in the same member if the strands are in unbonded tendons, which may provide valuable information if only select strands in the beam have embedded sensors.

The strain measured by one of the optical fibers along a post-tensioned strand in the box-beam specimen that had previously been tensioned is shown in Figure 5.12. The two curves represent the strain distribution along the strand (Strand 1) before and after the post-tensioning of another strand (Strand 2). More specifically, Strand 2 in Figure 5.12 was the last strand in the box beam to be tensioned and was located in one of the tendons of the specimen that was later grouted. Strand 1 was located in the tendon that was immediately adjacent to the tendon containing Strand 2. Only one other strand was tensioned after tensioning Strand 1 and prior to tensioning Strand 2. It should be noted that the range of the strain values along the vertical axis in Figure 5.12 is only 0.001. Furthermore, the distance along the horizontal axis extends beyond the ends of the beam. The difference in strain between the two curves is noticeable, but small. Of course, the elastic gain experienced by a strand in a bridge beam due to the fracturing of another strand is dependent on the cross-sectional properties of the member and tendon placement. Moreover, distinguishing any

small changes in strain measurements due to a fractured strand from other possible causes, such as service loads, temperature fluctuations, or long-term effects, could potentially be a challenge. For the box-beam specimen, other cases examined for the loss in strain of one strand during the tensioning of a strand in another tendon showed less change than the loss presented in Figure 5.12, and changes in the state of strain were nearly imperceptible in some cases.

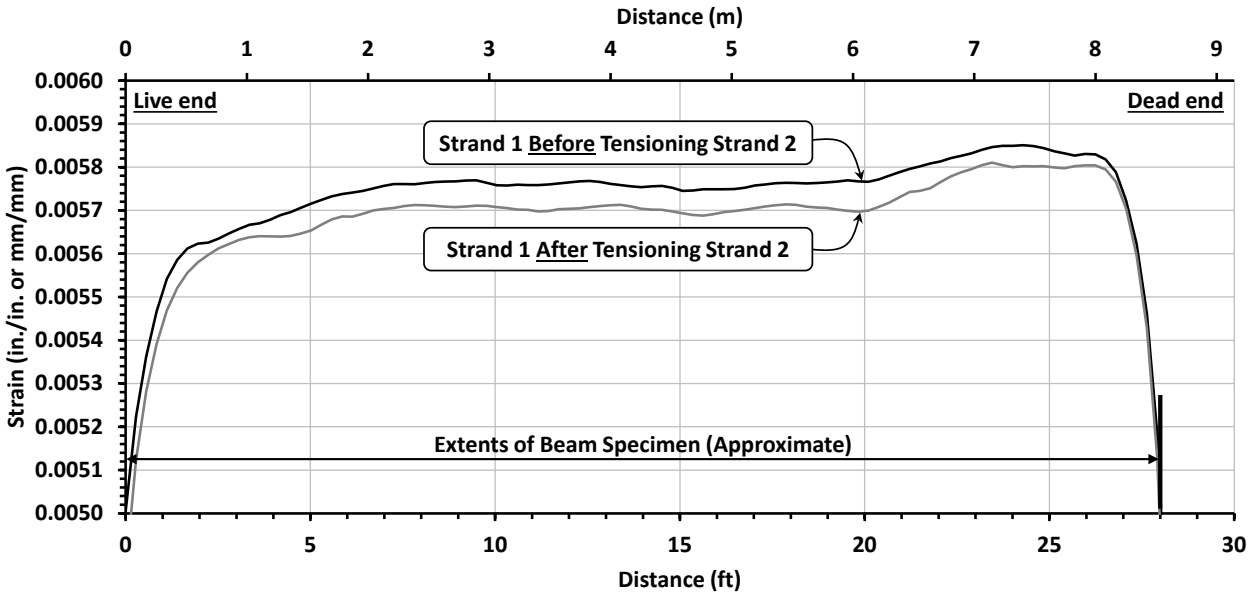

Figure 5.12: Change of strain in one strand in box beam due to post-tensioning of a strand in an adjacent tendon.

In a similar manner, the change in the state of strain indicated by an optical fiber along the first epoxy-coated strand to be stressed (Strand 1) in the post-tensioned tendon of the I-beam specimen as the second epoxy-coated strand (Strand 2) was post-tensioned is presented in Figure 5.13. In this case, both strands were located within the same duct. The change in strain is approximately 0.0001 over a portion of the strand length. Of course, changes in strain for a tendon of a bridge beam that consists of a greater number of strands may be different. Nevertheless, the data from the measurements in the laboratory are informative.

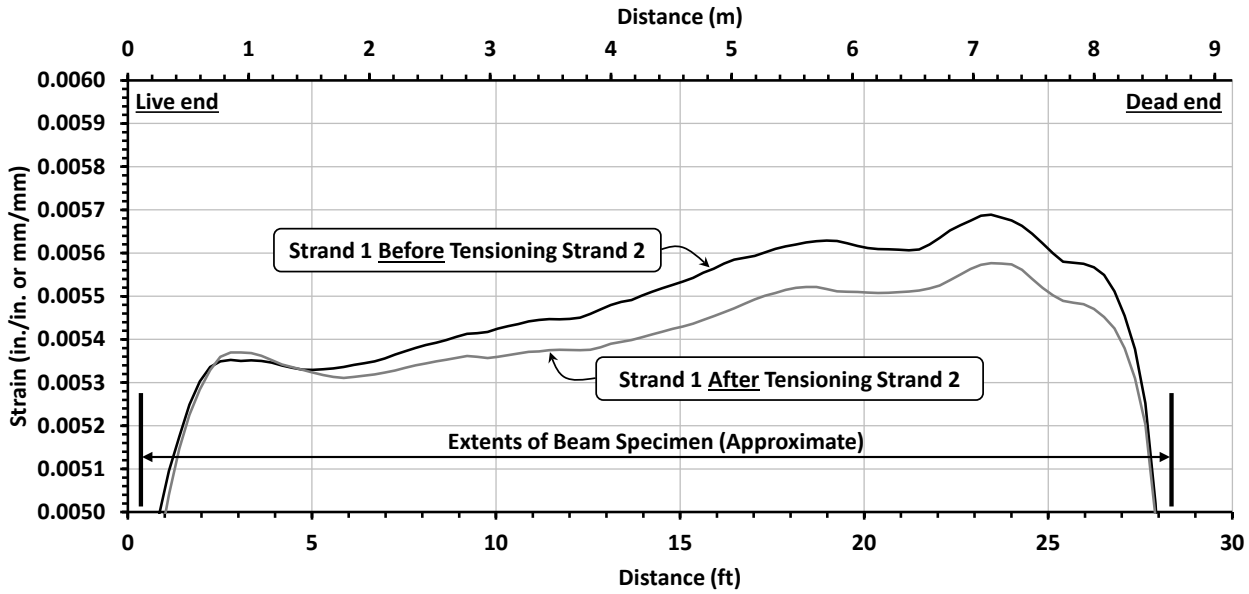

Figure 5.13: Change of strain in one strand in I-beam due to post-tensioning of a strand in the same tendon.

5.5 Beam Test Setup and Procedure

The setup for the beam tests is illustrated in Figure 5.14. A hydraulic cylinder was used at each load point to apply load to the beam specimen. A load cell measured the applied force at each load point. Furthermore, linear potentiometers were used to measure the displacement of the beam at midspan and at the two load points. Load was increased in increments, and the BOTDR module measured the strain in the strands between each load step.

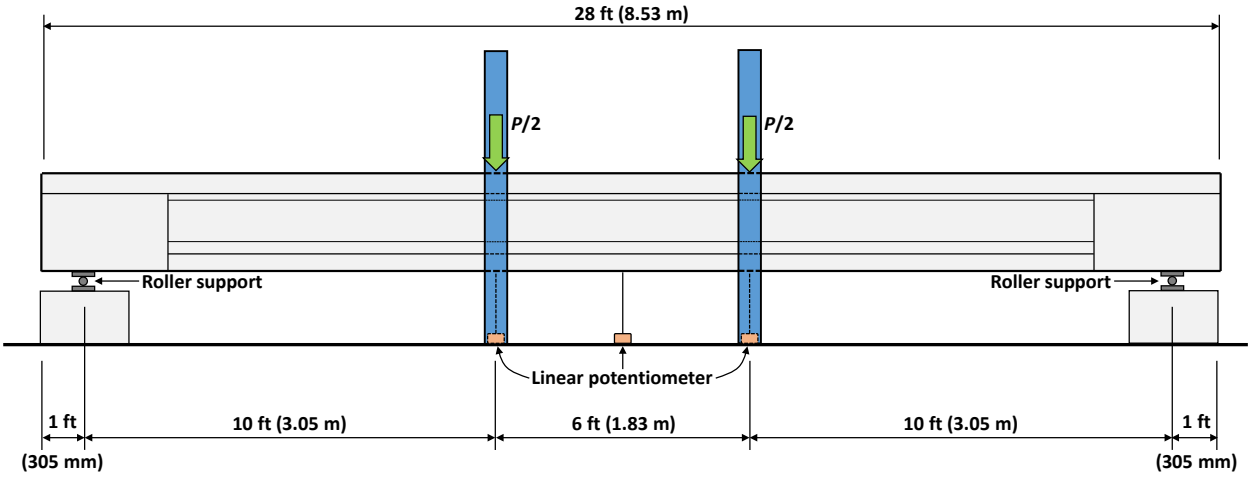

Figure 5.14: Setup for beam tests.

Each specimen contained a total of four optical fiber sensor-embedded prestressing strands. The optical fibers in all four strands were connected in series, allowing the full length of optical fiber cable to be connected to a single port on the BOTDR module. Strain was measured with a spatial step of 3.15 in. (80 mm). For each measurement, the time for the BOTDR module to capture strain and temperature data along the full length of the optical fiber cable was approximately 23 to 27 minutes. The acquisition of temperature data from the optical fibers will be discussed in Section 6.2.

5.6 Beam Test Results and Discussion

On the test day for the I-beam specimen, the strength of the concrete was 11.40 ksi (78.60 MPa). On the test day for the box-beam specimen, the strength of the concrete in the bottom flange was 10.30 ksi (71.02 MPa), and the strength of the concrete in the rest of the beam was 11.23 ksi (77.43 MPa). Concrete strengths are based on tests performed on 4-in. by 8-in. (100-mm by 200-mm) cylinders. Effective stresses in the optical fiber sensor-embedded strands on test day were calculated using the BOTDR strain data. Most of the strain gauges installed on the uncoated strands were no longer functioning after being damaged during the post-tensioning and grouting procedures. Therefore, effective stresses in the uncoated strands were estimated based on losses indicated by available strain gauge data and losses of the epoxy-coated strands indicated by the BOTDR data. The resulting average estimated stress in the strands of the I-beam was 151 ksi (1041 MPa) at midspan, and the average estimate stress in the strands of the box beam was 156 ksi (1076 MPa).

The load-displacement plots for both beam specimens are presented in Figure 5.15. The load along the vertical axis is the total load P applied to the beam, and the displacement along the horizontal axis is the beam deflection at midspan Δ. The maximum load P resisted by the I-beam and box-beam specimens was 133.2 kip (592.5 kN) and 177.5 kip (789.5 kN), respectively.

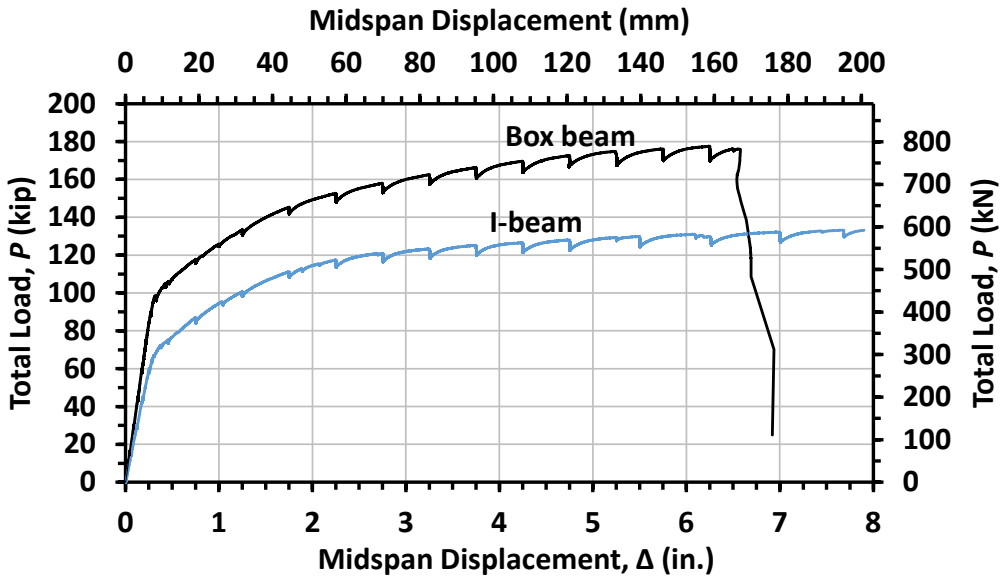

Figure 5.15: Load-displacement relationships for beam specimens.

Photographs of the I-beam and box-beam specimens during the load tests are presented in Figure 5.16 and Figure 5.17, respectively. The beams in the test setup are shown in Figure 5.16(a) and Figure 5.17(a). As load was increased during the tests, the beams exhibited flexural cracking that was distributed within the constant moment region between the load points, as presented in Figure 5.16(b) and Figure 5.17(b) for a midspan deflection of 1.25 in. (31.8 mm). The I-beam specimen reached large midspan deflections of nearly 8 in. (203 mm) during the test. Due to safety concerns and reaching the limit of the linear potentiometer at midspan, the test was stopped prior to ultimate failure of the beam. The I-beam under large deflections is shown in Figure 5.16(c). Concrete crushing, however, had initiated at the top of the member at the location of one of the load points (Figure 5.16(d)). The box-beam specimen reached its ultimate failure condition and experienced a flexural failure due to concrete crushing. The box beam after failure is shown in Figure 5.17(c).

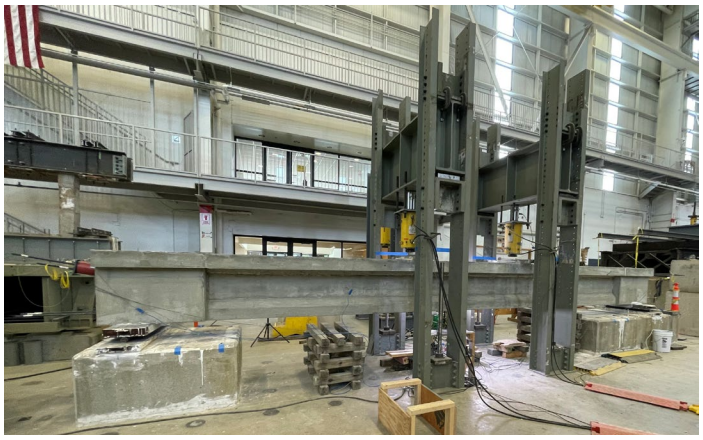

(a) Beam in test setup

(b) Beam under load (Δ = 1.25 in. [31.8 mm], *P* = 101 kip [449 kN])

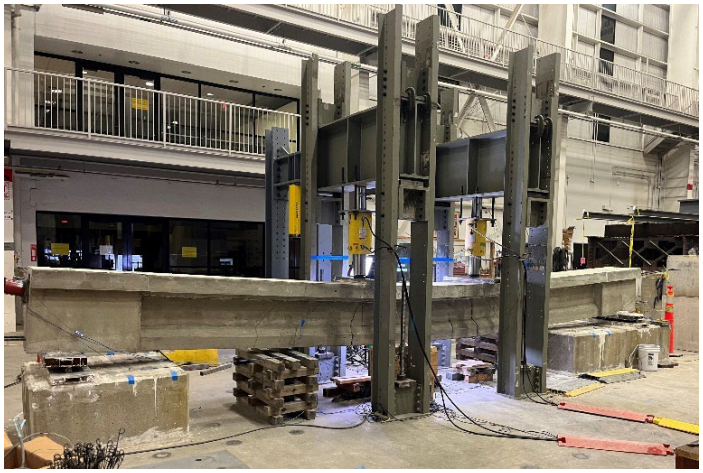

(c) Beam with large deflections

(d) Initiation of concrete crushing

Figure 5.16: Load test on I-beam specimen.

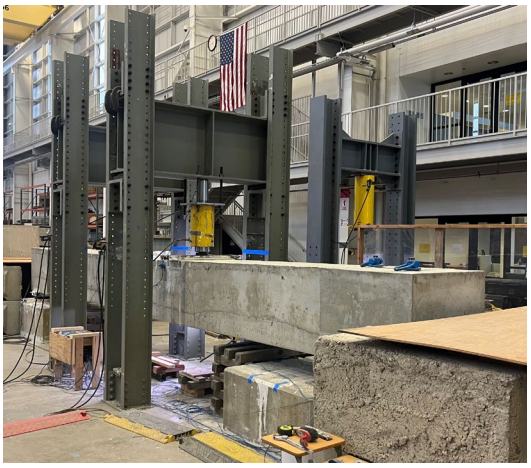

(a) Beam in test setup

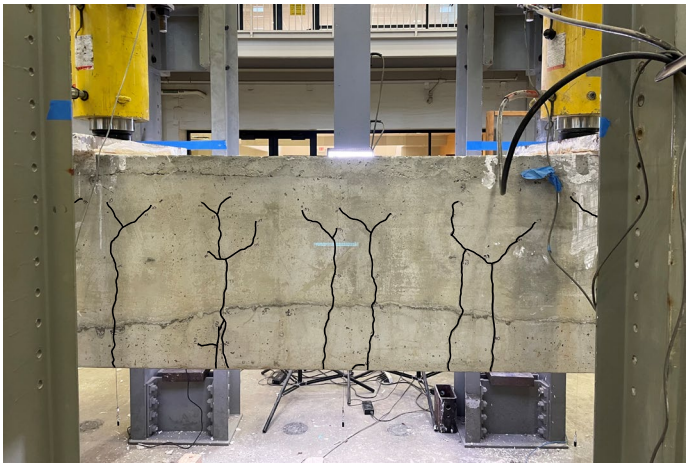

(b) Beam under load (Δ = 1.25 in. [31.8 mm], *P* = 133 kip [592 kN])

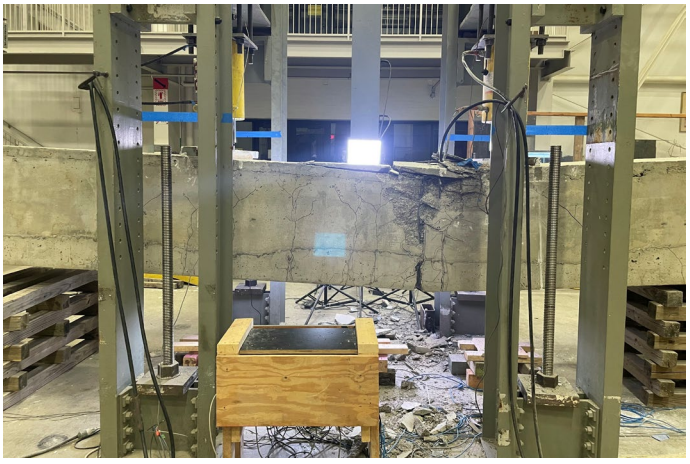

(c) Beam after failure

Figure 5.17: Load test on box-beam specimen.

The strain along the length of each epoxy-coated strand was acquired between every load step. Representative examples of the resulting strain plots are provided in Figure 5.18 and Figure

5.19. Similar plots for all optical fiber sensors along the epoxy-coated strands in the beam specimens are provided in Appendix A. In these plots, each curve is labeled with a total applied load P (for loading increments early in the test) or midspan displacement Δ that corresponds with the BOTDR strain data being presented. Curves for only select values of P and Δ are shown to avoid clutter. As indicated by the plots, the optical fiber sensors continued to provide data up to the end of the test (for the I-beam) or failure of the specimen (for the box beam).

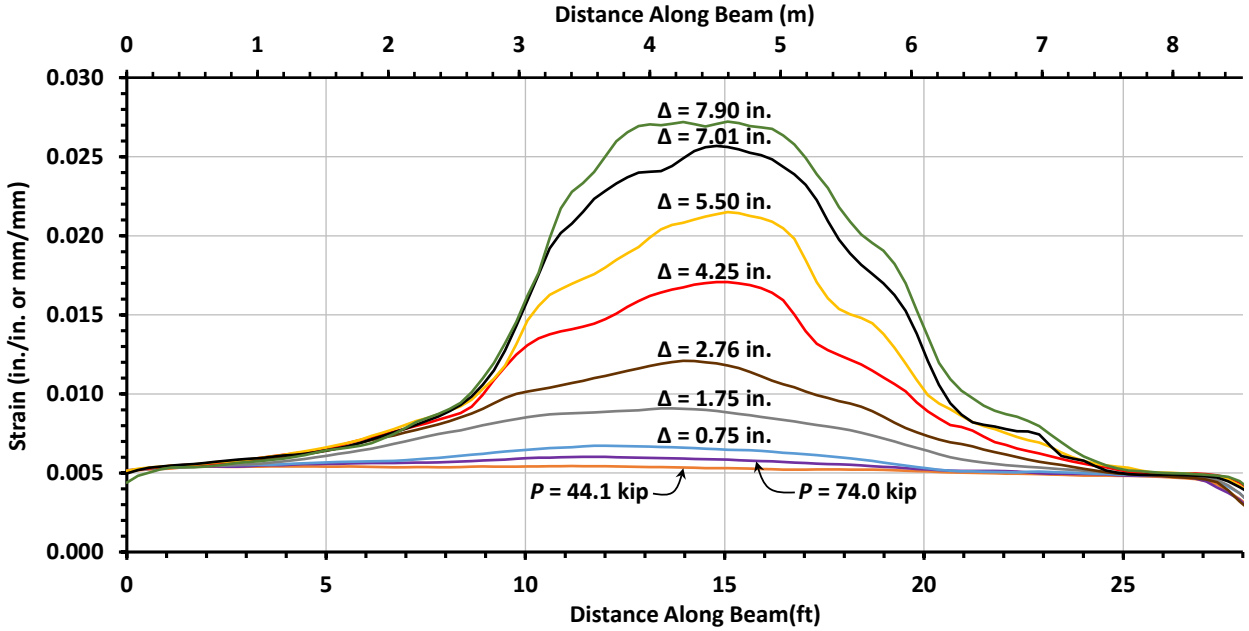

Figure 5.18: Strain along bonded post-tensioned strand in I-beam (1 in. = 25.4 mm, 1 kip = 4.448 kN).

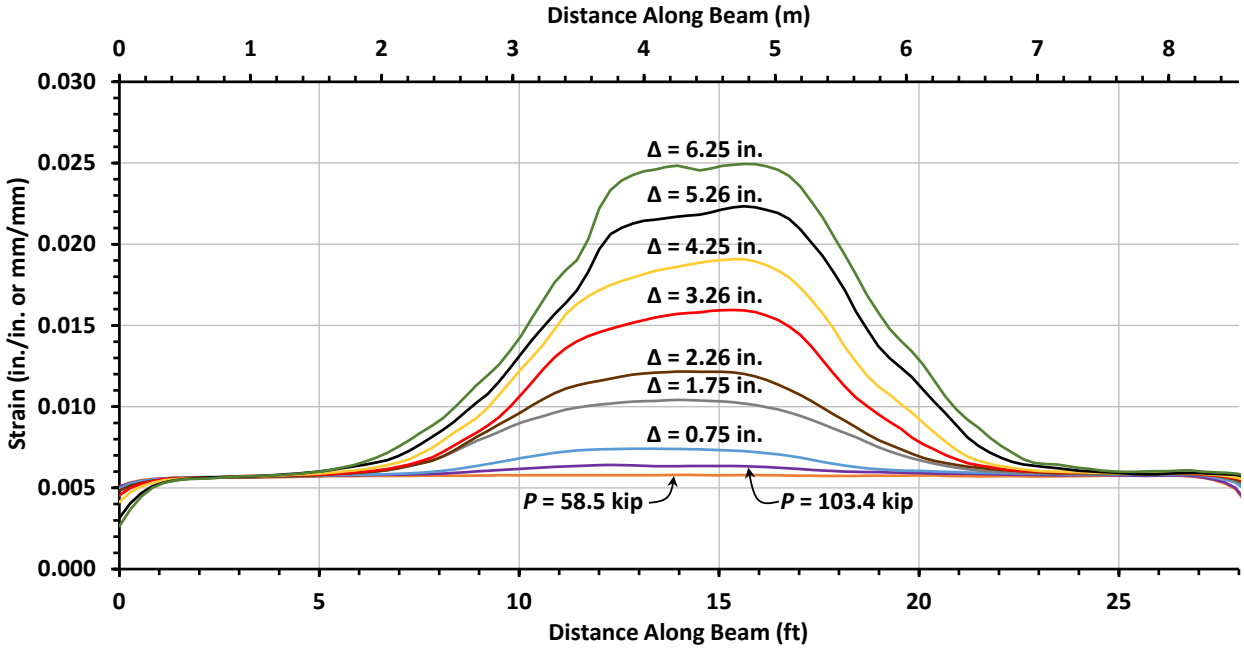

(a) Bonded strand

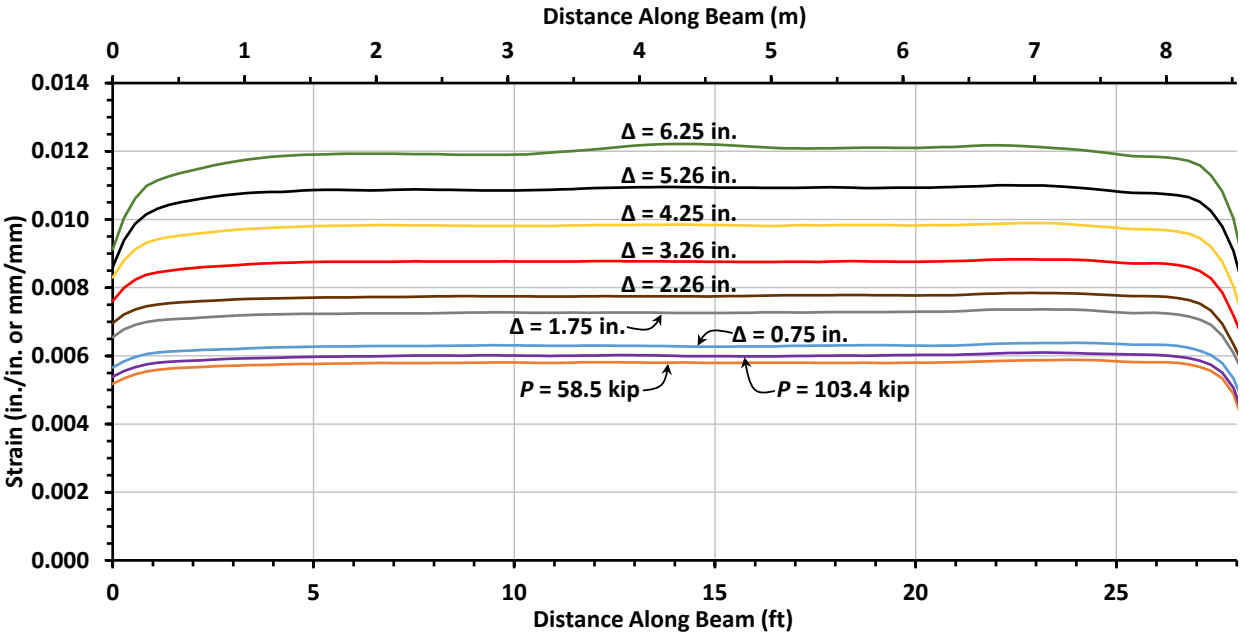

(b) Unbonded strand

Figure 5.19: Strain along bonded and unbonded post-tensioned strands in box beam (1 in. = 25.4 mm, 1 kip = 4.448 kN).

The strain along the length of one of the bonded post-tensioned strands in the draped tendon of the I-beam specimen is presented in Figure 5.18. Early in the test, relatively small increases in the strand strain were observed within the constant moment region. Upon further loading,

extensive flexural cracking and yielding of the strands resulted in large strains in the strand. Due to the spatial resolution of the BOTDR technology, localized increases in strains at the locations of individual cracks were not captured. Therefore, locations of strains greater than those indicated in the plot would be expected along the strand.

A similar behavior is shown in Figure 5.19(a) for a strand in a bonded tendon of the box beam. A different response, however, is presented in Figure 5.19(b) for a strand located in an unbonded tendon of the beam. As expected, the strain remained relatively uniform along the length of the strand throughout the test. At a midspan deflection Δ of 6.25 in. (158.8 mm) prior to the load step that resulted in failure of the beam, the strain in the strand based on BOTDR was approximately 0.012.

Considering data from the foil strain gauges installed on the uncoated strands in the same tendons as the epoxy-coated strands allows the BOTDR strain data to be compared to data from more traditional sensors. Although most of the foil strain gauges were damaged during post-tensioning and grouting, one gauge installed on the uncoated strand located in each of the two unbonded tendons of the box beam was still functioning. The strains indicated by these two gauges can therefore be compared to the strains from the optical fiber sensor-embedded strands located in the same two tendons.

Due to strain values output from the foil strain gauges at the beginning of the beam tests being lower than expected, the gauge readings were suspected to have drifted over time since their installation on the strands. Therefore, the strain values were offset to correspond with the estimated effective prestress in the uncoated strands on the test day. Furthermore, similar to the correction factor applied to the strain values from the optical fiber sensors due to their helical shape along the strand, a similar correction was applied to the foil strain gauges because they were installed on a single outer wire of the strand.

The strain in the epoxy-coated strands in the unbonded tendons of the box beam based on the optical fiber data from one of the fibers in each strand is compared with the strain values from the foil strain gauges in Figure 5.20. The strains from both sensor types that were collected between every load step during the beam test are plotted. The BOTDR strains in Figure 5.20 are the average of the strain values over the middle 14-ft (4.27-m) of the beam. The strain data are plotted against the midspan displacement Δ of the specimen. In the figure, the strands referred to as “Epoxy-

Coated Strand 1" and "Uncoated Strand 1" were both in one of the unbonded tendons, while "Epoxy-Coated Strand 2" and "Uncoated Strand 2" were in the other unbonded tendon.

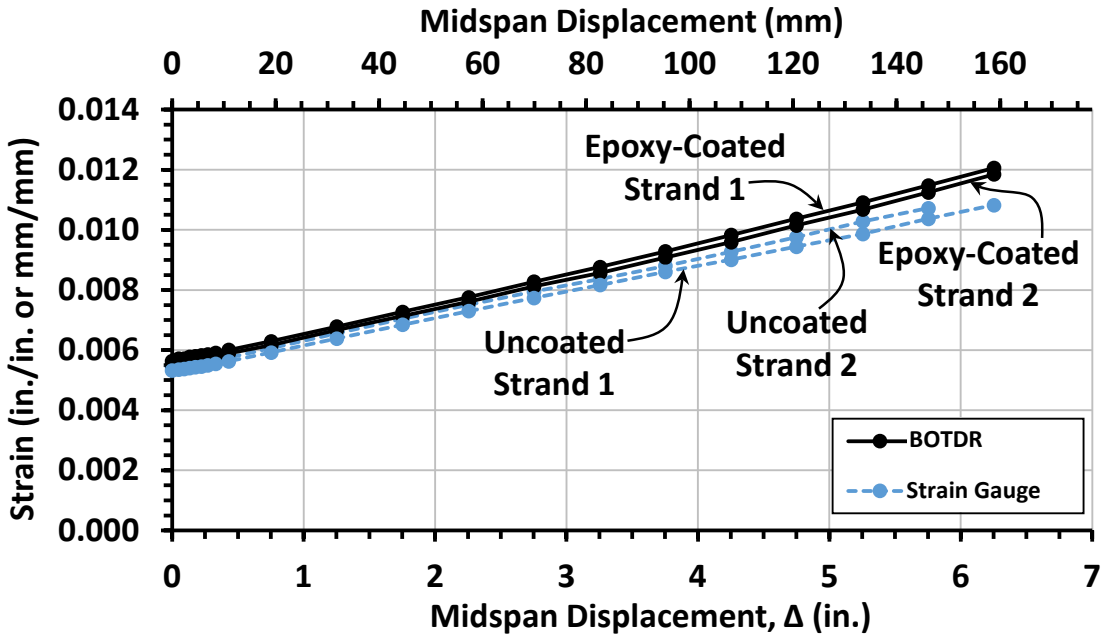

Figure 5.20: Comparison of strains from BOTDR and foil strain gauges.

The data from all four sensors in Figure 5.20 present a nearly linear increase in strain with increasing deflection of the beam. Although the slopes of the lines are different, the BOTDR and foil strain gauge results show a similar trend. Considering the relative unreliability of more conventional sensors for measuring strand strain, such as foil strain gauges, and the limitation of only gathering strain data at discrete locations, optical fiber sensors and BOTDR technology are a potential solution.

5.7 Comparison to Analytical Models

Computational models of the two beam specimens were created and analyzed to provide an additional point of comparison to the optical fiber strain values along the lengths of the strands. As no other sensor was used during the experimental program that allowed strain to be measured along the entire length of the beams, the results of the computational analysis provide another means of validation, especially in the range of service-level loads within which flexural behavior is essentially linear and the analysis is most reliable.

5.7.1 Details of Analysis

Sectional analysis was used to perform a flexural analysis of the post-tensioned specimens. The analysis method can provide the load-displacement relationship of the beam models along with strand stresses and strains during loading.

The sectional analysis was performed using an open-source analysis software, OpenSees (McKenna 2011). A schematic of the modeling technique is shown in Figure 5.21. As indicated, force-based beam-column elements were defined to represent the beam specimens. These elements consisted of several cross sections which were each discretized into fibers. The fibers were assigned material properties for concrete, high-strength steel used for strands, and mild steel used for nonprestressed reinforcement. Bonded strands and mild reinforcement were modeled within the cross sections. Unbonded strands, however, were modeled by defining truss elements that were rigidly connected to the beam-column elements only at anchorage points, indicated by the rigid elements at the ends of the beam in Figure 5.21. Nodes of the beam-column elements denoted by black dots in Figure 5.21 were vertically constrained to the truss elements (i.e., unbonded strands) to ensure the strands and beam displace together. For the I-beam specimen, multiple beam cross sections and beam-column elements were defined along the beam length to properly capture the draped profile of the bonded tendon.

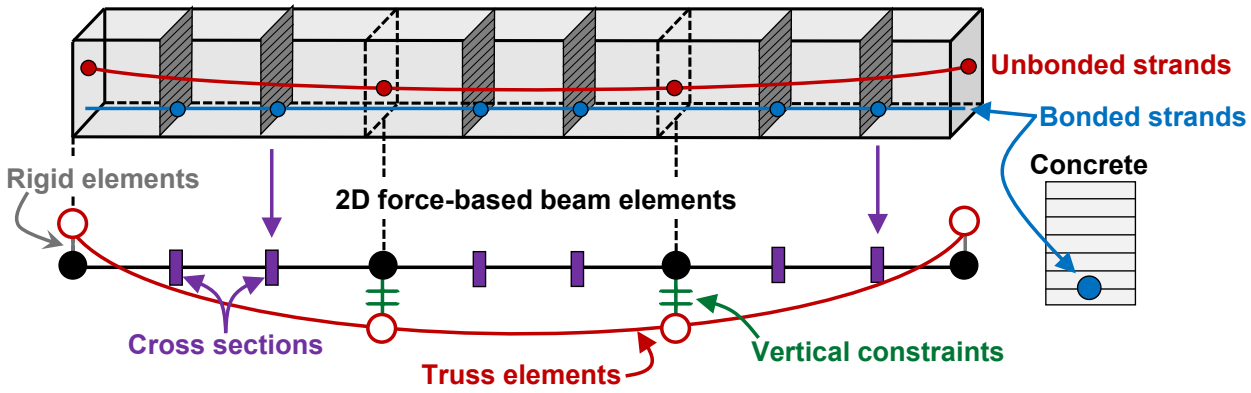

Figure 5.21: Schematic of sectional analysis modeling technique for beam with bonded and unbonded tendons.

The uniaxial stress-strain relationship for concrete in compression and tension used in the analysis is shown in Figure 5.22 and is based on the concrete02IS material model in OpenSees (McKenna 2011). Corresponding numerical inputs are provided in Table 5.1. Concrete compressive strength f_c' was based on material testing from the experimental program. The pre-

peak stress-strain curve in compression was based on the Popovics concrete model (Popovics 1973). The modulus of elasticity E_c and concrete compressive strain corresponding to the compressive strength ε_c were assumed to be $57{,}000\sqrt{f_c'}$ (in psi units) and $1.1f_c'/E_c$, respectively. The post-peak response in compression was calibrated based on crushing energy and assuming a bi-linear stress-strain relationship (Pugh et al. 2015). Concrete compressive strain corresponding to 20% of the compressive strength after the peak stress ε_{20} was selected based on crushing energy G_c and the length of individual integration points in the beam elements L_{IP} to ensure constant crushing energy release (Pugh, et al. 2015). For concrete in tension, the tensile strength of concrete f_t was assumed to be $7.5\sqrt{f_c'}$ (in psi units), and the modulus of elasticity in tension was assumed to be the same as the modulus of elasticity in compression. Furthermore, the tension softening stiffness E_{ts} was selected based on fracture energy G_f and the length of individual integration points in the beam elements L_{IP} to ensure constant fracture energy release.

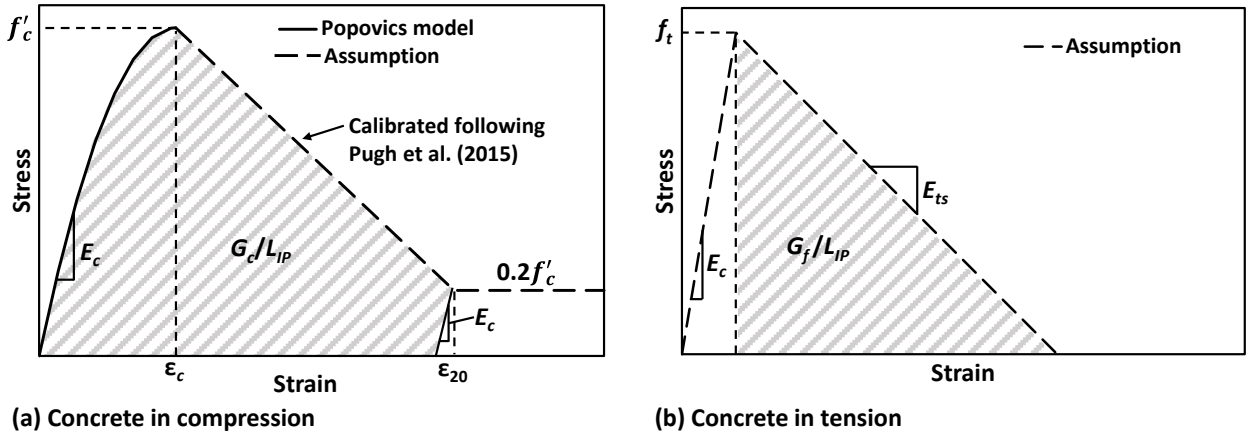

Figure 5.22: Concrete material model used in analysis.

Table 5.1: Concrete properties input into analytical models.

Model	Concrete			
	f_c', ksi (MPa)	E_c, ksi (GPa)	ε_c, %	f_t, ksi (MPa)
I-Beam	11.40 (78.60)	6087 (41.97)	0.2	0.801 (5.52)
Box Beam – Bottom Flange	10.30 (71.02)	5785 (39.89)	0.2	0.761 (5.25)
Box Beam – Webs and Top Flange	11.23 (77.43)	6040 (41.64)	0.2	0.795 (5.48)

The high-strength steel stress-strain relationship for the prestressing strand is represented in Figure 5.23 with inputs based on material tests of the strands used in the beam specimens. The stress-strain behavior from tests on both the epoxy-coated and uncoated strands were used to create unique models for each strand type. The numerical values input into the models for uncoated and epoxy-coated strand are given in Table 5.2 and Table 5.3, respectively. The Steel4 material model in OpenSees (McKenna 2011) was used for the nonlinear strain-hardening behavior. The value of the rupture strain ε_{pu} for the epoxy-coated strand given in Table 5.3 is based on test results on the epoxy-coated strand reported by the strand manufacturer because the strands tested in the universal testing machine as described in Section 2.2 are expected to have ruptured prematurely. Prestressing was introduced to the models as a predefined stress field and was constant along the length of the beam models. Therefore, friction losses were not included in the analysis. The values for f_{pe} presented in Table 5.2 and Table 5.3 are the effective stress in the strands at the beginning of the beam tests, determined as described in Section 5.6.

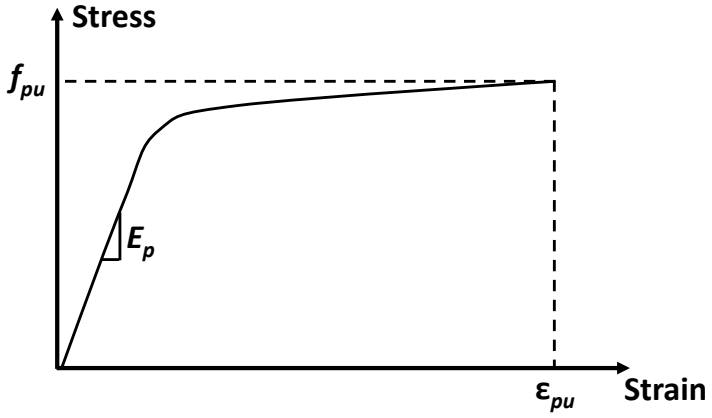

Figure 5.23: Steel material model for prestressing strand used in analysis.

Table 5.2: Uncoated strand properties input into analytical models.

Model	Uncoated Strand				
	f_{pe} for Bonded PT, ksi (MPa)	f_{pe} for Unbonded PT, ksi (MPa)	f_{pu}, ksi (MPa)	E_p, ksi (GPa)	ε_{pu}, %
I-Beam	164 (1131)	-	280 (1931)	28,300 (195)	4.6
Box Beam	153 (1055)	153 (1055)	280 (1931)	28,300 (195)	4.6

PT = Post-Tensioned

Table 5.3: Epoxy-coated strand properties input into analytical models.

Model	Epoxy-Coated Strand					
	f_{pe} for Pretensioned, ksi (MPa)	f_{pe} for Bonded PT, ksi (MPa)	f_{pe} for Unbonded PT, ksi (MPa)	f_{pu}, ksi (MPa)	E_p, ksi (GPa)	ε_{pu}, %
I-Beam	136 (938)	149 (1027)	-	280 (1931)	28,600 (197)	6.6
Box Beam	-	159 (1096)	158 (1089)	280 (1931)	28,600 (197)	6.6

PT = Post-Tensioned

5.7.2 Comparison of Results

The load-displacement relationships from the beam tests are compared to the results from the sectional analysis models in Figure 5.24. As shown in the figure, the initial stiffness, post-yielding stiffness, and maximum load were predicted well by the models.

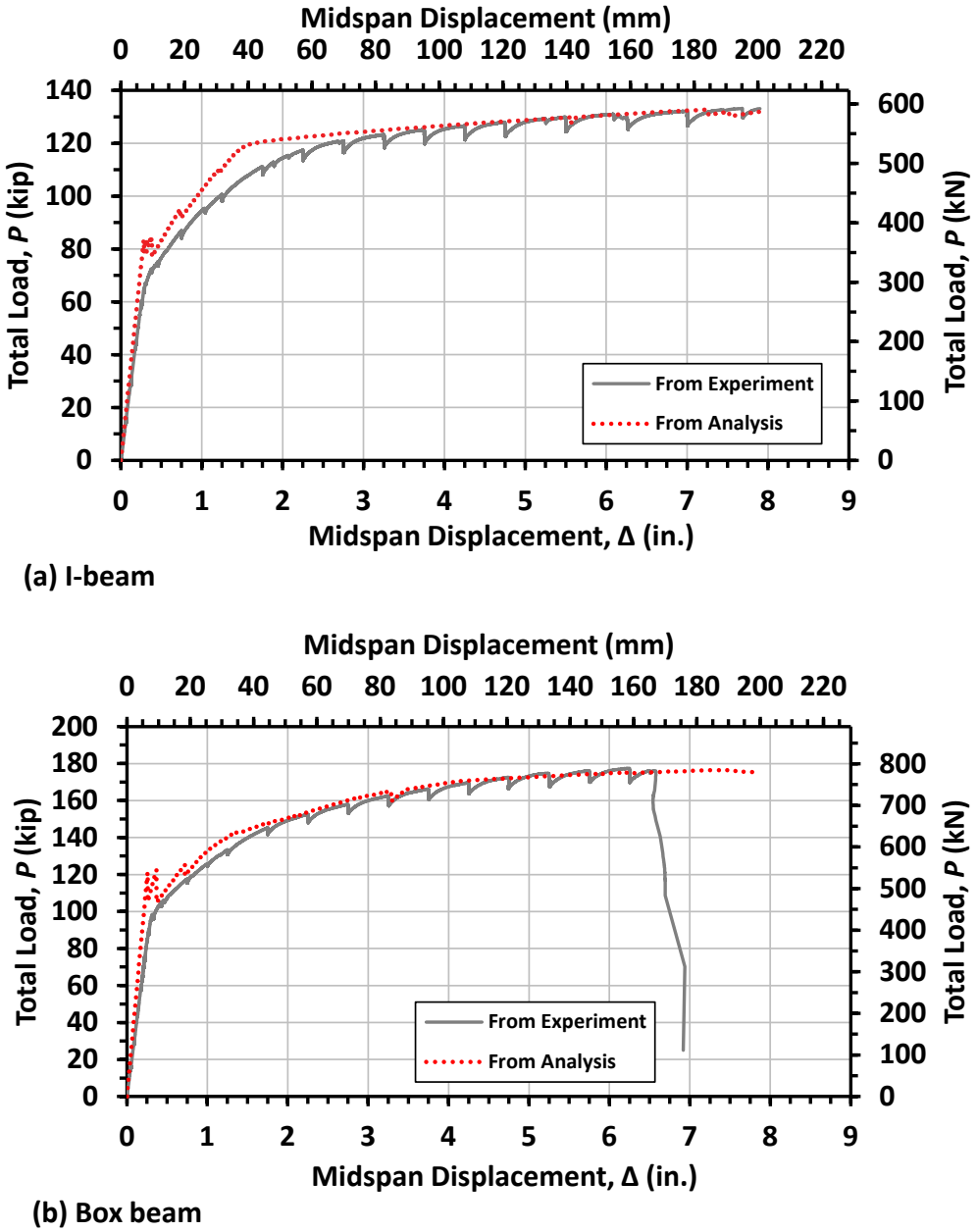

Figure 5.24: Comparison of load-displacement relationships from experiment and analysis.

In Figure 5.25 and Figure 5.26, the results provided by the sectional analysis models for the strand strain along the beam length are compared to the corresponding experimental results for select strands with optical fiber sensors. To avoid clutter, the strain data are only shown for select values of the total applied load P and midspan displacement Δ of the beam specimens.

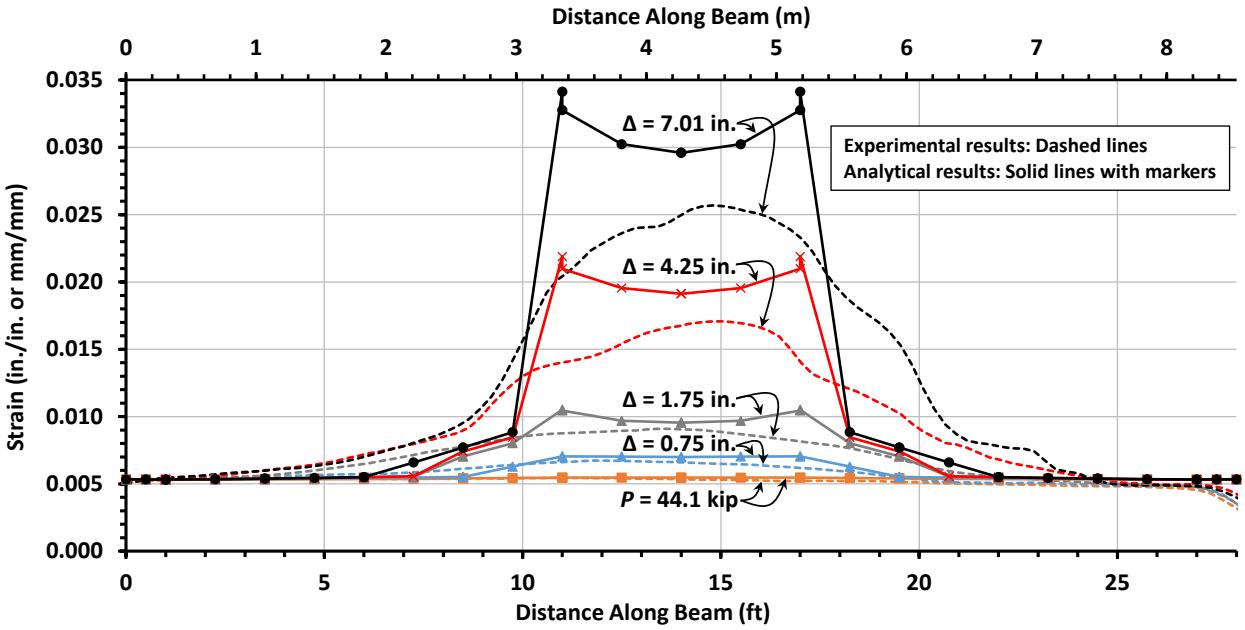

Figure 5.25: Comparison of experimental and analytical strain results along bonded post-tensioned strand in I-beam (1 in. = 25.4 mm, 1 kip = 4.448 kN).

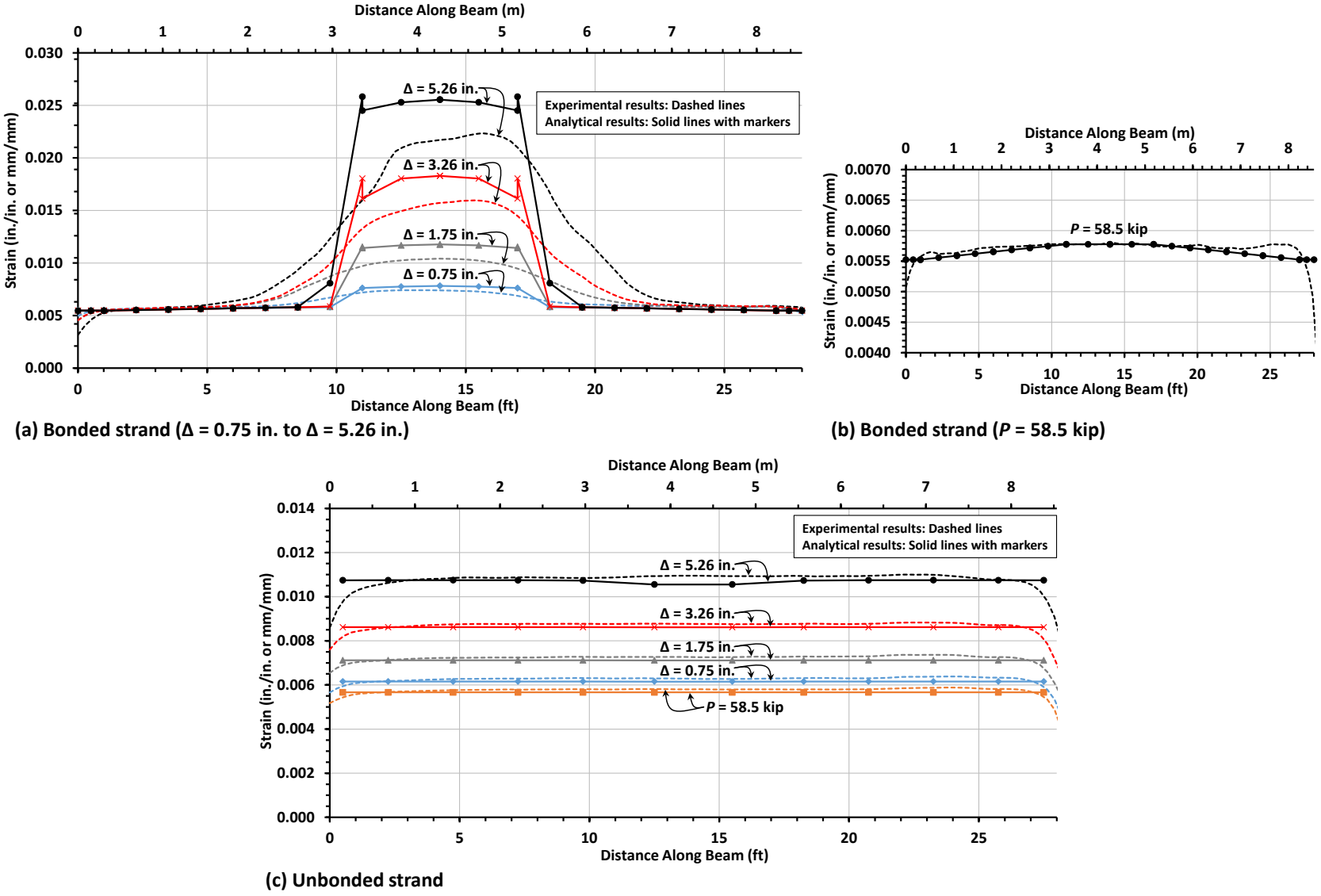

Figure 5.26: Comparison of experimental and analytical strain results along bonded and unbonded post-tensioned strands in box beam (1 in. = 25.4 mm, 1 kip = 4.448 kN).

Considering only the sectional analysis results, the strain distribution near the center of the beam (i.e., along the region of the beam between the load points of the test setup) for the bonded post-tensioned strand in the I-beam (Figure 5.25) exhibits a different pattern than the distribution along this region for the bonded post-tensioned strand in the box beam (Figure 5.26(a)). This difference is due to the post-tensioned strands of the I-beam being draped, which creates a parabolic moment distribution caused by the prestressing. The straight post-tensioned strands of the box beam, however, result in a constant moment distribution.

Comparing the experimental and analytical results for strains along the bonded post-tensioned strand in the I-beam (Figure 5.25), the results are relatively similar prior to extensive yielding of the strands. For larger beam displacements, however, significant differences between the results are observed. The strains obtained from the optical fiber sensors are distributed over a longer region with smaller maximum strains than the strains obtained from the sectional analysis. One potential reason for the differences between the results is the 3.28-ft (1-m) spatial resolution of the BOTDR strain data, which causes the experimental data to represent a more averaged state of strain along the strand. The strain values obtained from the sectional analysis, however, represent strains at individual integration points in the beam elements. Another reason for the differences between the experimental and analytical results is the localized slip of the strands near cracks and the region of bond development on each side of a crack in the beam specimens. These effects of bond are not captured by the analytical model. For these reasons, when cracks begin to develop and propagate in the beams, the data from the optical fiber sensors tend to present less abrupt changes along the beam length and provide lower strain values for cracked regions of the member compared to the results of the analytical model which provides strains associated with cracked concrete at the integration points without capturing localized slip.

The comparison between the experimental and analytical results for the bonded post-tensioned strand in the box beam shown in Figure 5.26(a) is similar to the strand in the I-beam. To present the results more clearly for a small applied load, the results are compared separately for an applied load of P = 58.5 kip (260.2 kN) in Figure 5.26(b). In this plot, the range of the strain values along the vertical axis is 0.003. The analytical results compare very well to the experimental data. It should be noted that the experimental data in this plot is from the bonded strand in the box beam with the largest effective stress value at the beginning of the test. The comparison of the analytical data to other bonded post-tensioned strain data from the beam test would present small differences

in strain values instead of the nearly exact match shown in Figure 5.26(b). The sectional analysis model only considers an average effective prestress of the bonded epoxy-coated strands.

Unlike the bonded strands, the experimental and analytical strain results compare well through the full range of beam displacements for the unbonded strand in the box beam shown in Figure 5.26(c).

The relatively close comparison between the experimental and analytical results for the unbonded strand through all beam loadings and for the bonded strands prior to extensive strand yielding helps to add confidence to the suitability of using the optical fiber sensor-embedded strands to monitor the post-tensioned tendons of bridges under service loads. At the same time, the accuracy of strains from bonded tendons may have limitations, especially after extensive cracking and strand yielding. This is at least partially due to the spatial resolution of BOTDR. For field implementation, however, the absolute accuracy of the strain values is likely less important than identifying relative changes over time.

6. Other Considerations

6.1 Introduction

During the research project described in this report, additional considerations regarding the use of BOTDR technology for monitoring post-tensioning tendon forces were noted. Two considerations are discussed in this chapter that may warrant further investigation during a future project.

6.2 Measurement of Temperature

In addition to the changes in the frequency of Brillouin backscattered light due to strain, small changes in frequency are also caused by changes in temperature of the optical fiber (VIAVI 2019). For the data presented in this report, Brillouin frequency shifts were considered as being due to changes in strain alone with any error due to temperature changes in the laboratory being neglected. For optical fiber alone, the error in measured strain with changes in temperature is expected to be approximately $20(10^{-6})$ per 1.8°F (1°C). This error is estimated to be greater for the optical fiber embedded in the epoxy-coated strand and bonded to concrete (V. Lecoeuche, personal communication, January 26, 2024). Approximate temperature data that was collected indicate that the change in temperature of the strand in the laboratory between the post-tensioning operation and the beam test was likely as much as 10.8°F (6°C). In the field where temperatures throughout the year exhibit more extreme fluctuations than in the laboratory, temperature is a more significant factor.

BOTDR technology can be used to measure both strain and temperature along an optical fiber. However, compared to strain, obtaining accurate temperature measurements is more sensitive to the setup of the optical fiber sensor system and measurement parameters. This is because temperature data depend on measuring the intensity, or power, of the backscattered light (VIAVI 2019), which is more sensitive to the setup and acquisition parameters than measuring the Brillouin frequency shift.

Many of the optical fiber setups used during the experimental program were not conducive to accurate temperature measurements, primarily due to the use of several connectors along the setup (Figure 2.10) and the fibers embedded in the epoxy coating of the strands being different

from the external fibers used between strands. Nevertheless, the scan times mentioned in this document include the time needed to collect data for both strain and temperature despite the temperature data being considered unreliable in most cases. Collecting data for only strain reduces the scan durations.

To obtain reliable temperature values along with strain, practices that will aid with collecting dependable data include using fusion splices in place of connectors, using the same fiber from the same manufacturer along the length of the setup, avoiding transitions between multiple short sections of fiber, and referencing an unstrained portion of optical fiber at a known temperature to obtain accurate temperature values (D. Costantini, personal communication, December 22, 2023). Furthermore, correct calibration coefficients are needed to relate the Brillouin frequency shift and intensity measurements to temperature. Attaining these correct coefficients is explained by Lecoeuche (2023).

6.3 Accuracy in Non-Linear Range

In the research program, obtaining accurate strain values from the optical fiber sensor-embedded prestressing strands was primarily focused on the linear range of the prestressing steel. Direct comparisons between the measured stress in a strand to measured strains using BOTDR in the nonlinear range of the steel were not included in the study. Therefore, the accuracy of the strain measurements in the nonlinear range of the strands cannot be quantified.

As discussed in previous sections and illustrated in Figure 3.3 and Figure 4.8, an effective modulus of elasticity E_p was obtained for each fiber along the prestressing strands. Using this effective modulus, a correction factor was calculated to convert the strain measured by the optical fiber sensor using BOTDR to the axial strain along the length of the strand. For the beam tests, this correction factor was applied to all strain readings from the optical fibers, including within the nonlinear range of the prestressing steel. The accuracy of this correction factor outside of the linear range of the material, however, still needs to be verified.

These uncertainties, however, do not have a significant impact on the intended use of the strands for long-term monitoring of post-tensioned tendons in bridge structures under service loads and the ability to detect unexpected changes in strain over time.

7. Summary and Concluding Remarks

7.1 Summary

Research investigating the use of optical fiber sensor-embedded prestressing strands for monitoring post-tensioned tendons was described in this report. The strands include two optical fibers embedded in the epoxy coating that follow the helical shape of the outer wires of the strand. Before using the strands, the optical fiber sensors are extracted from each end and the appropriate connections are made to a BOTDR module that measures strain along the entire length of the optical fiber.

During the first phase of the experimental program of the research, tensile tests were conducted to determine the correction factor needed to convert the strain measured using the optical fibers that wrap around the strand to axial strain along the length of the strand. From the tensile tests, the factor was determined to be approximately 1.06. Correction factors were also obtained for the fibers of the strands in the other phases of the research program by taking a series of strain readings during the tensioning operations and relating the measured strain to the known stress applied to the strand.

The second phase included the monitoring of the sensor-embedded strands in a prestressing bed over a period of one week. The strand stress values based on the optical fiber strain measurements were generally consistent with the strand stress values based on load cell data with small fluctuations corresponding with minor temperature changes in the laboratory.

The final phase of the research program focused on the fabrication and load testing of two post-tensioned beam specimens. Important observations from the post-tensioning of the beams included the capture of friction losses along a draped tendon by the optical fiber sensors. Additionally, the changes in strain along the strand at anchorage set were used to estimate the set distance at the live end.

During the load tests, the optical fibers continued to provide strain reading through all stages of loading as the applied load on the specimen was increased. The experimental results were then compared to the results from analytical models of the beam specimens. The experimental and analytical results matched well for strains for an unbonded strand, but significant differences existed for bonded tendons after yielding of the strands. Nevertheless, based on the overall results

and observations from the beam tests, the optical fiber sensor-embedded prestressing strands were shown to be a powerful tool for prestress strain measurements.

7.2 Concluding Remarks

Data collected from the optical fiber sensors can provide valuable insight into the strain, and therefore the force, in post-tensioned tendons. Nevertheless, the limitations of the technology must be kept in mind. For example, an important reminder for users of the technology is the 3.28-ft (1-m) minimum spatial resolution provided by BOTDR. At locations of abrupt increases in strain, the strain data will not capture a sharp peak but will provide a more averaged state of strain.

Overall, the optical fiber sensor-embedded prestressing strands combined with BOTDR are a promising technology for monitoring post-tensioned tendons in the field with potential widespread impact toward helping to ensure the safety and longevity of post-tensioned bridge structures.

Appendix A. Strain Data from Optical Fiber Sensors During Beam Tests

This appendix includes strains measured along each optical fiber sensor-embedded strand in the beam specimens described in Chapter 5. The correction factors that account for the effective modulus of elasticity E_p for each fiber along the length of each strand have been applied to all presented data, as described in Section 5.3. Each beam contained four optical fiber sensor-embedded strands. Because two optical fiber sensors ran the length of each strand, a total of eight plots are provided for each beam specimen. The plots present strains for several load steps with each curve labeled with a total applied load P (for loading increments early in the test) or midspan displacement Δ that corresponds with the strain data being presented.

A.1 I-Beam Specimen

The I-beam specimen contained two pretensioned and two post-tensioned optical fiber sensor-embedded strands. During the load test on the I-beam, the optical fibers along the sensor-embedded strands were connected in series using the arrangement illustrated in Figure A.1. The strain data output by the BOTDR module, therefore, show the strain values along the continuous optical fiber extending from the BOTDR module to the end of the last strand. The measured strains plotted in Figure A.2 to Figure A.9 were extracted directly from these data, with only the correction factors accounting for the effective modulus of elasticity E_p for each fiber applied. The length along the horizonal axis of the strain plots correspond approximately to the 28-ft (8.53-m) length of the beam.

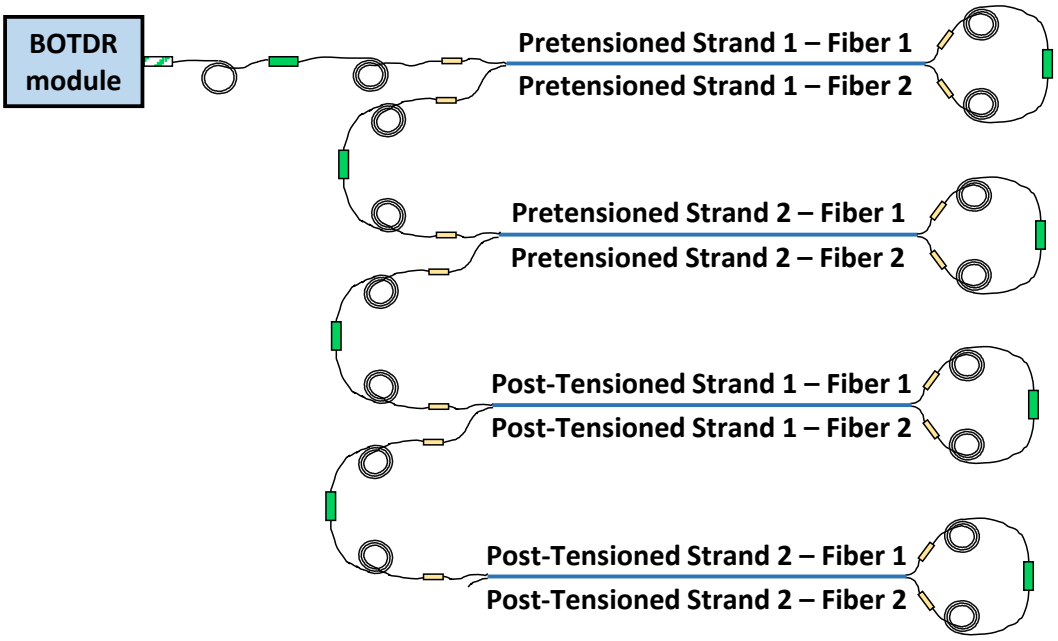

Figure A.1: Optical fiber setup for I-beam specimen.

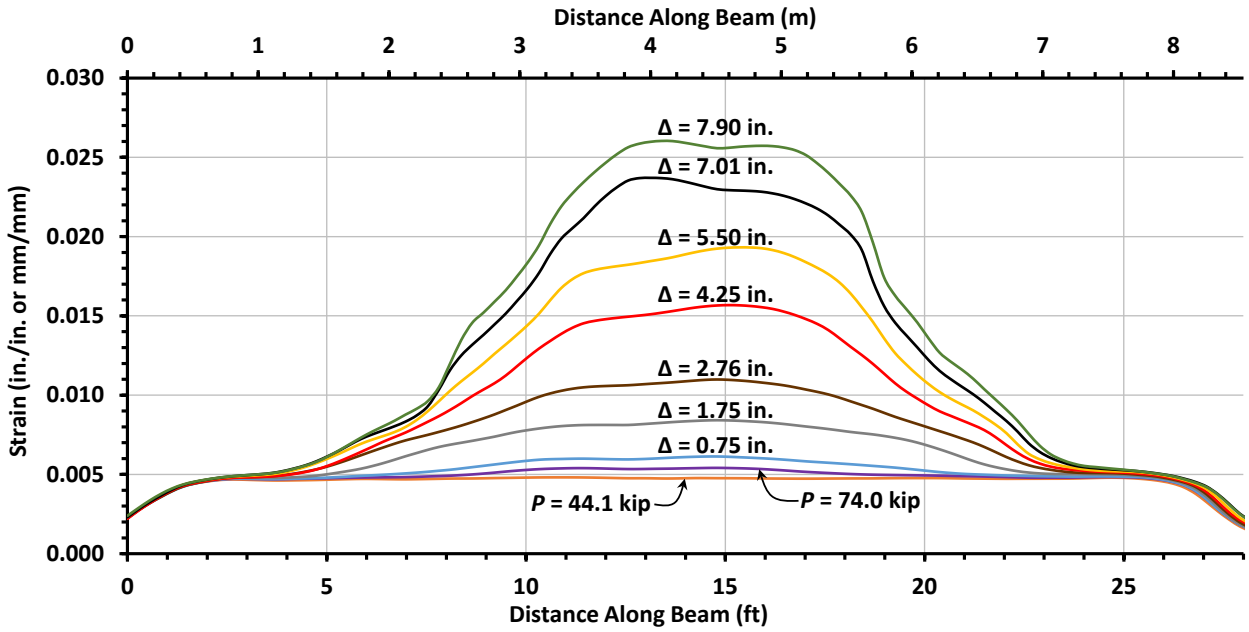

Figure A.2: Pretensioned Strand 1 – Fiber 1 (1 in. = 25.4 mm, 1 kip = 4.448 kN).

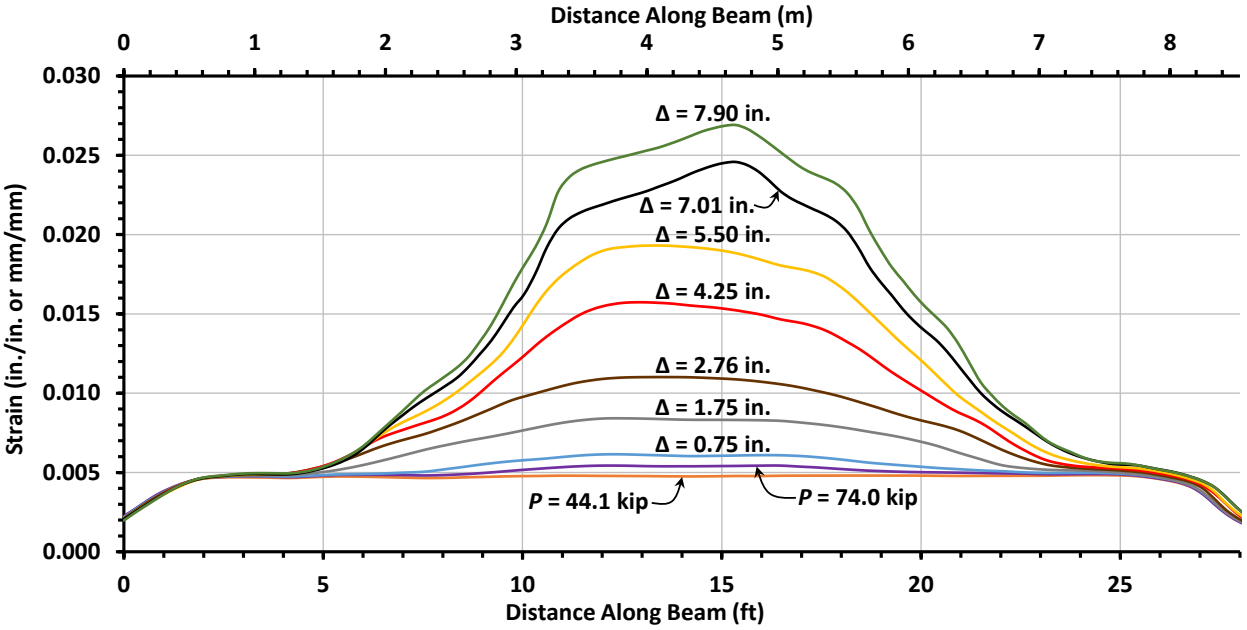

Figure A.3: Pretensioned Strand 1 – Fiber 2 (1 in. = 25.4 mm, 1 kip = 4.448 kN).

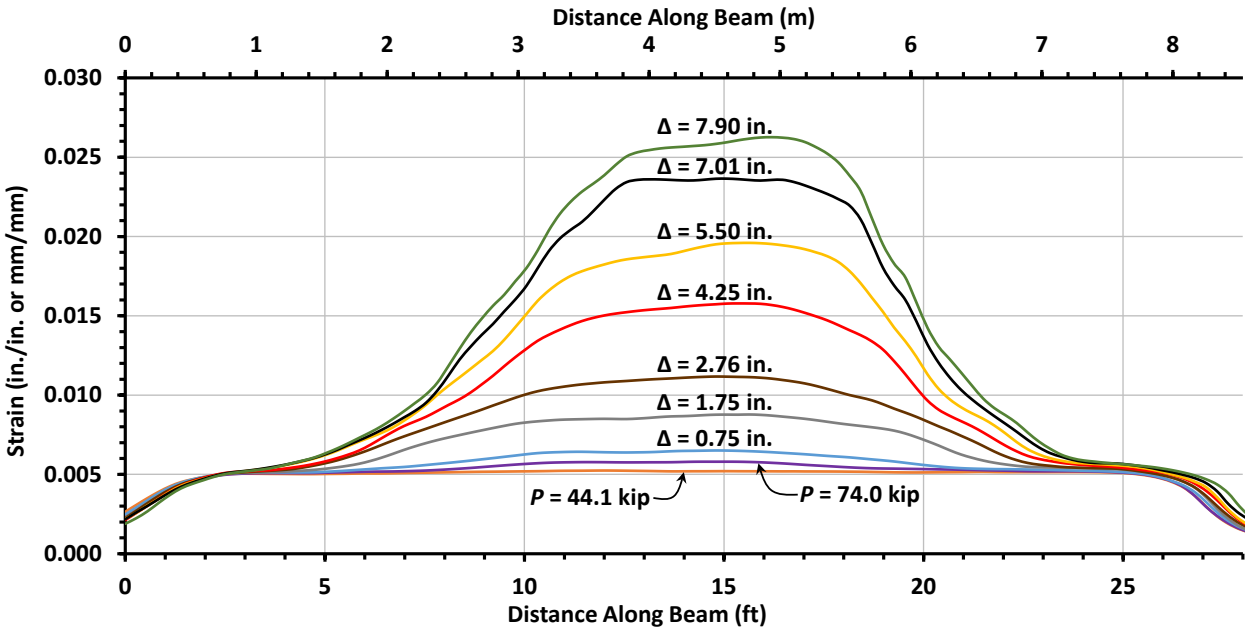

Figure A.4: Pretensioned Strand 2 – Fiber 1 (1 in. = 25.4 mm, 1 kip = 4.448 kN).

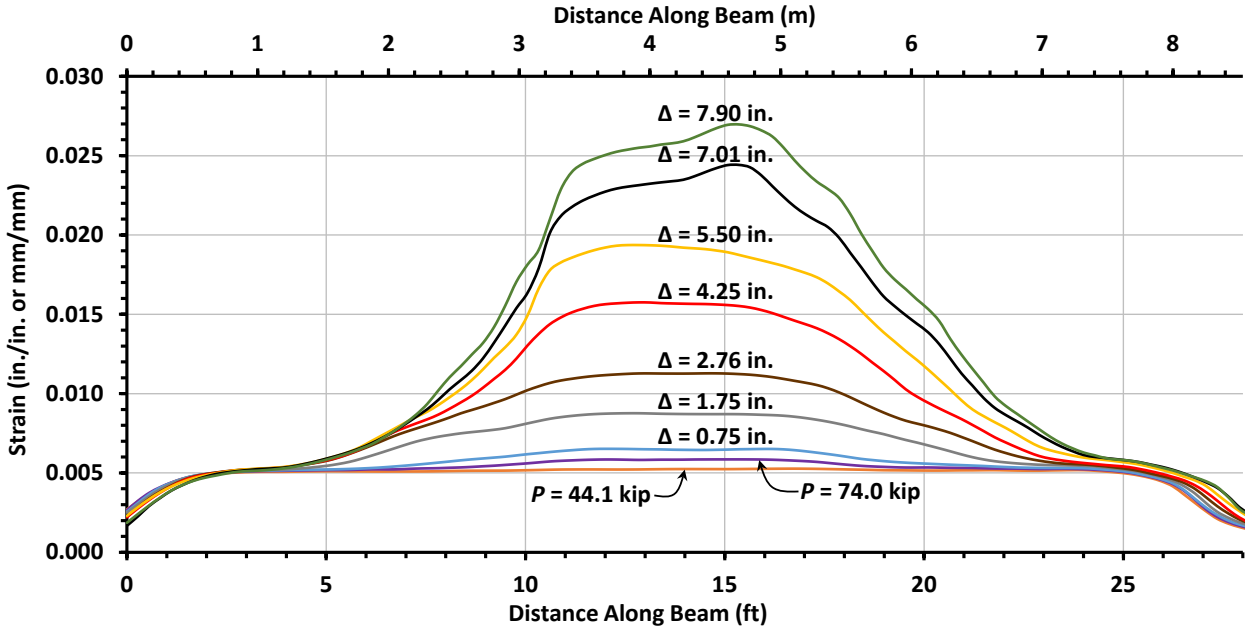

Figure A.5: Pretensioned Strand 2 – Fiber 2 (1 in. = 25.4 mm, 1 kip = 4.448 kN).

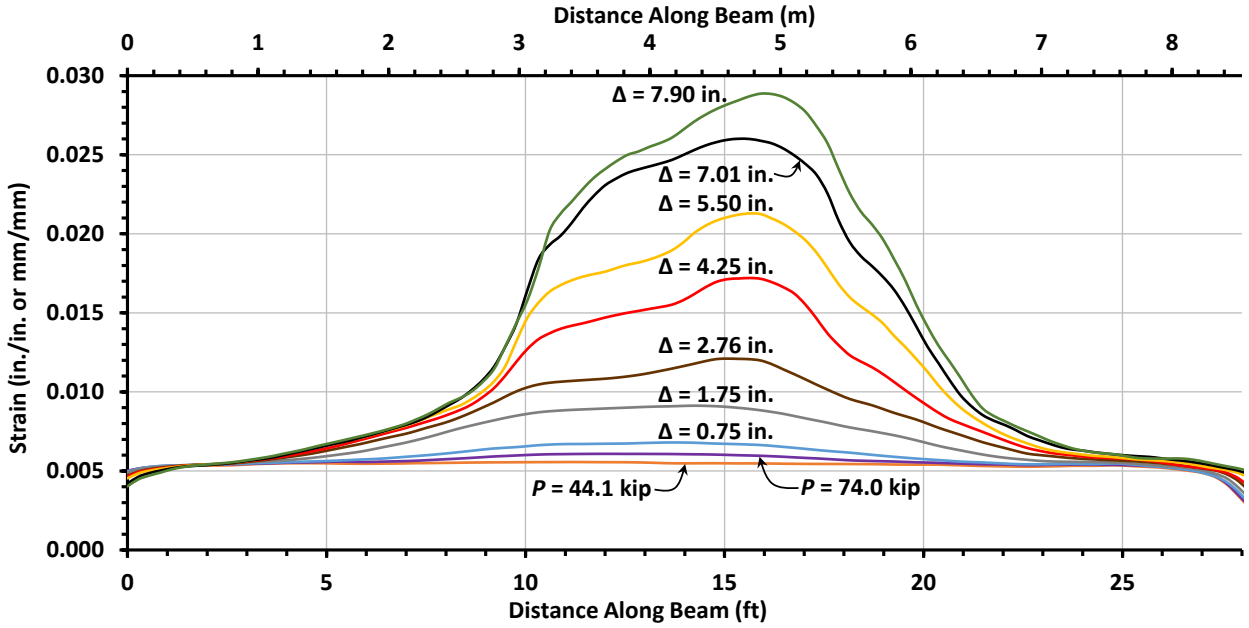

Figure A.6: Post-Tensioned Strand 1 – Fiber 1 (1 in. = 25.4 mm, 1 kip = 4.448 kN).

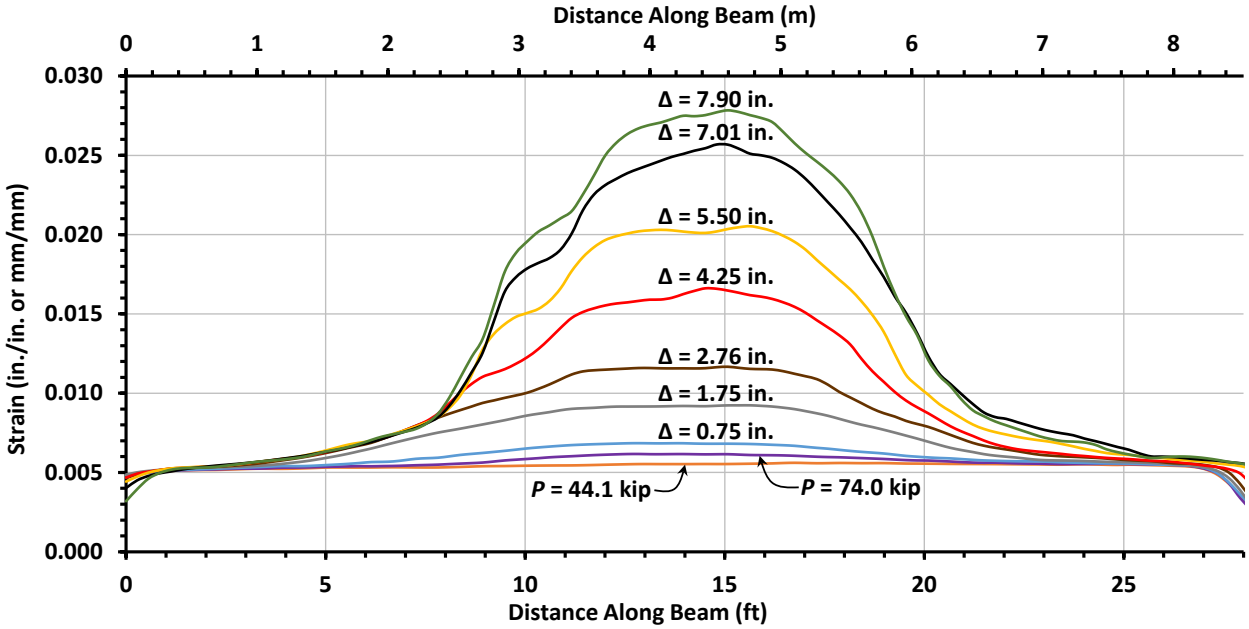

Figure A.7: Post-Tensioned Strand 1 – Fiber 2 (1 in. = 25.4 mm, 1 kip = 4.448 kN).

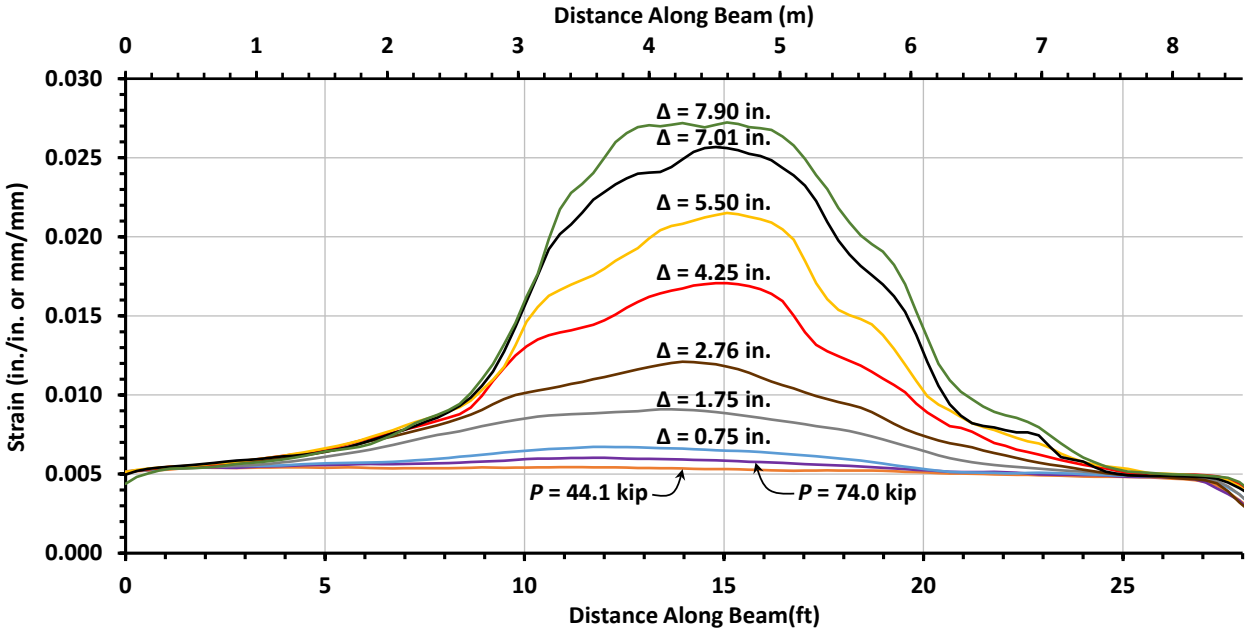

Figure A.8: Post-Tensioned Strand 2 – Fiber 1 (1 in. = 25.4 mm, 1 kip = 4.448 kN).

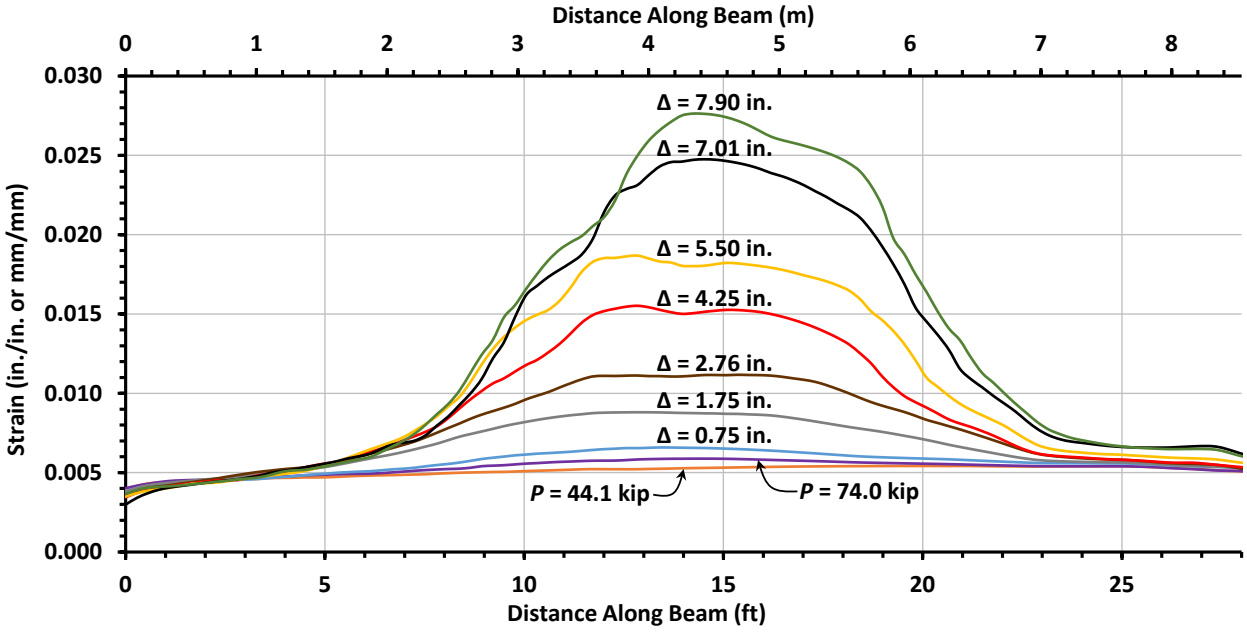

Figure A.9: Post-Tensioned Strand 2 – Fiber 2 (1 in. = 25.4 mm, 1 kip = 4.448 kN).

A.2 Box-Beam Specimen

The box-beam specimen contained two unbonded and two bonded post-tensioned optical fiber sensor-embedded strands. During the load test on the box beam, the optical fibers along the sensor-embedded strands were connected in series using the arrangement illustrated in Figure A.10. The strain data output by the BOTDR module, therefore, show the strain values along the continuous optical fiber extending from the BOTDR module to past the last strand. The measured strains plotted in Figure A.11 to Figure A.18 were extracted directly from these data, with only the correction factors accounting for the effective modulus of elasticity E_p for each fiber applied. The length along the horizonal axis of the strain plots correspond approximately to the 28-ft (8.53-m) length of the beam.

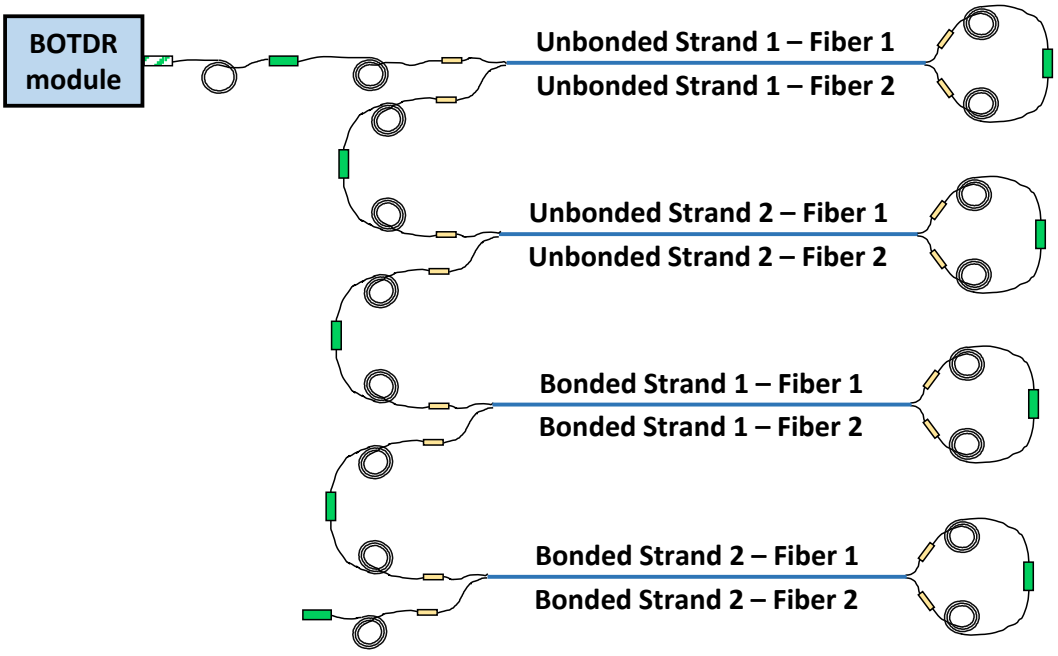

Figure A.10: Optical fiber setup for box-beam specimen.

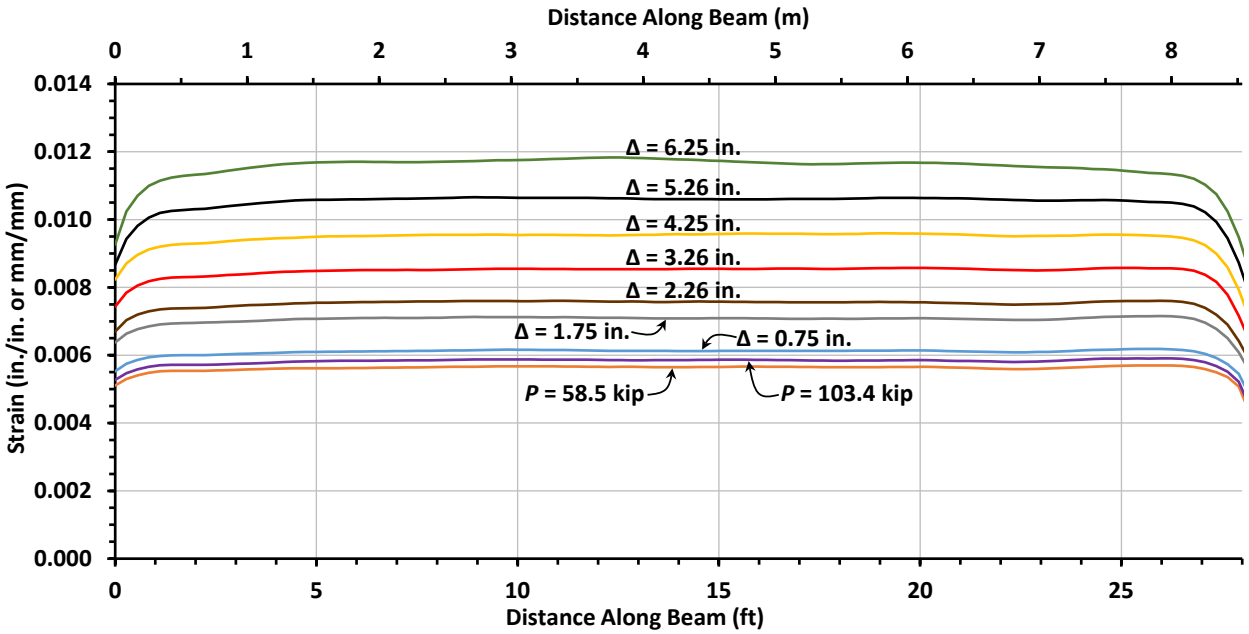

Figure A.11: Unbonded Strand 1 – Fiber 1 (1 in. = 25.4 mm, 1 kip = 4.448 kN).

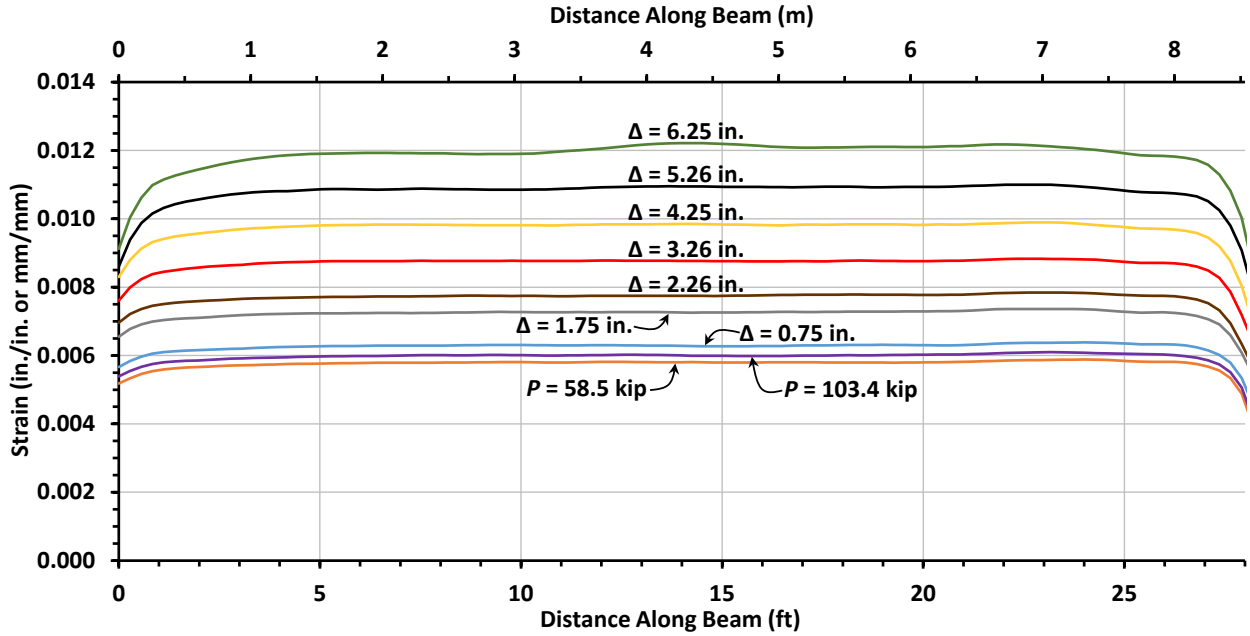

Figure A.12: Unbonded Strand 1 – Fiber 2 (1 in. = 25.4 mm, 1 kip = 4.448 kN).

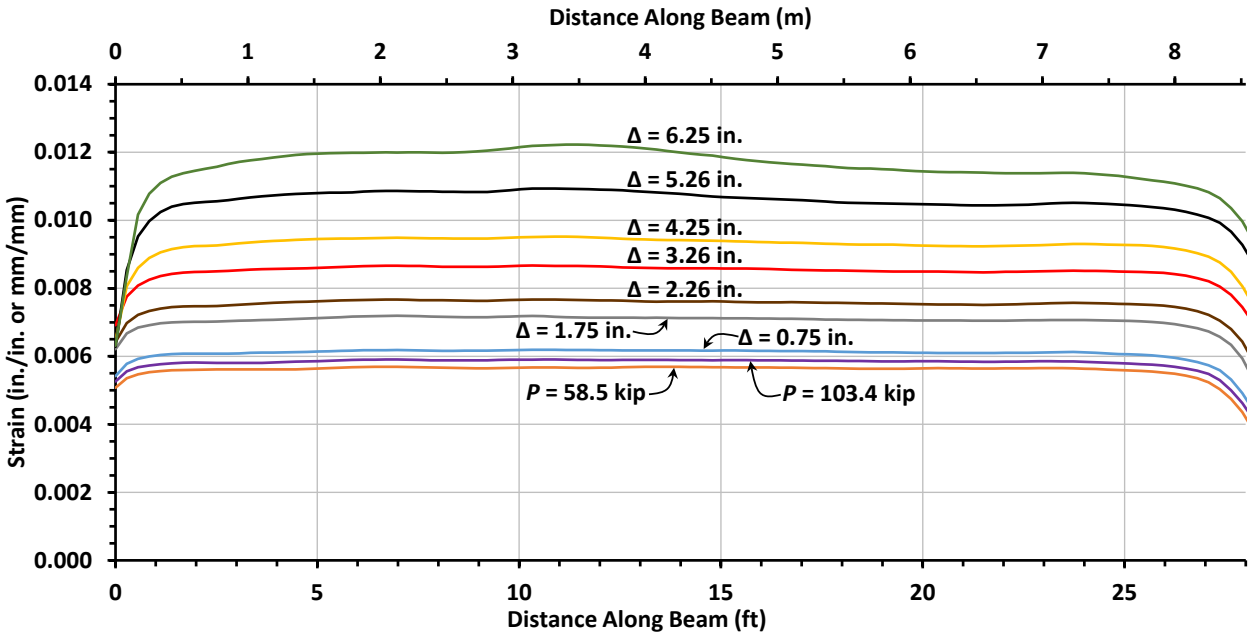

Figure A.13: Unbonded Strand 2 – Fiber 1 (1 in. = 25.4 mm, 1 kip = 4.448 kN).

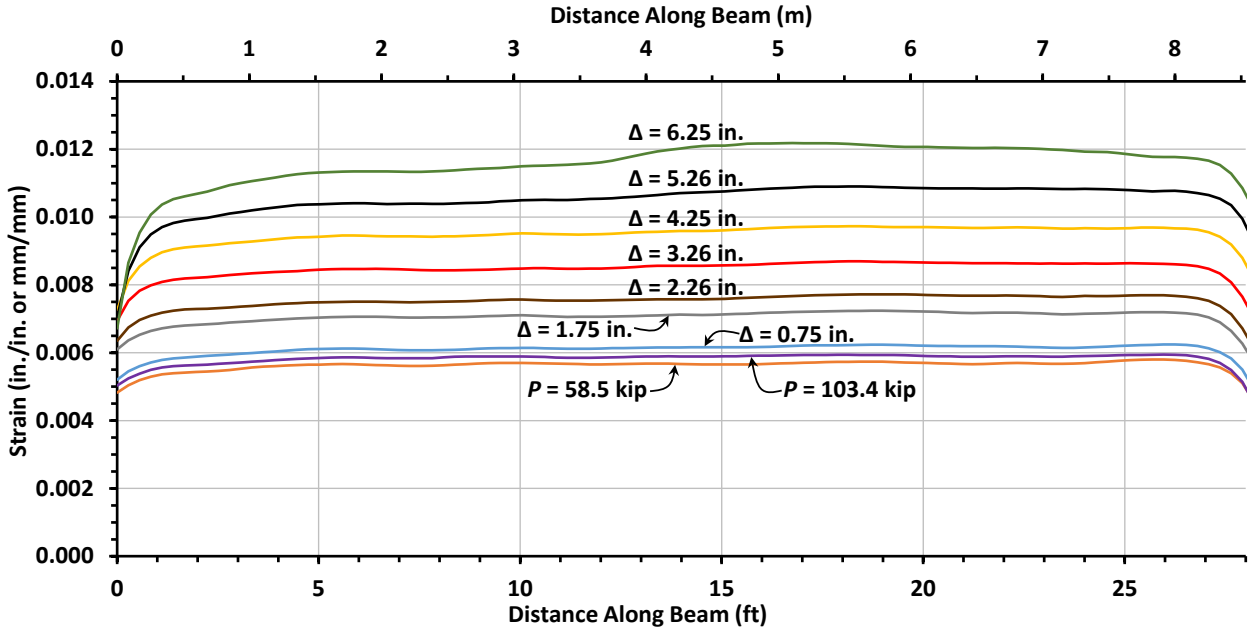

Figure A.14: Unbonded Strand 2 – Fiber 2 (1 in. = 25.4 mm, 1 kip = 4.448 kN).

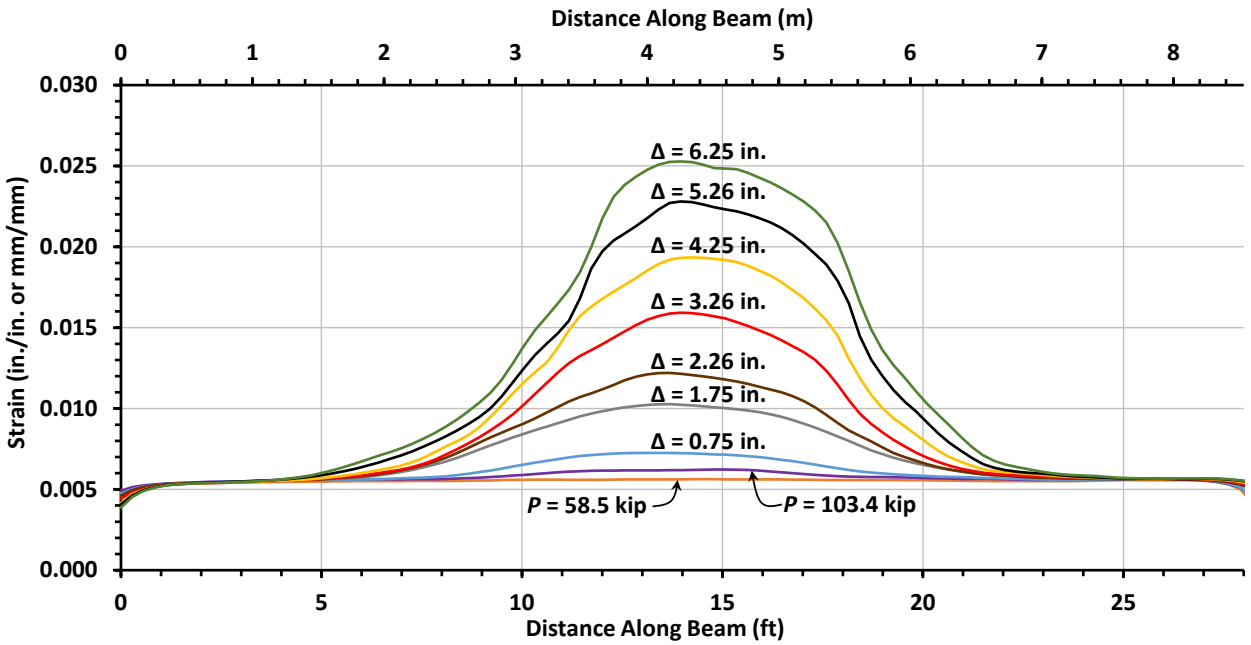

Figure A.15: Bonded Strand 1 – Fiber 1 (1 in. = 25.4 mm, 1 kip = 4.448 kN).

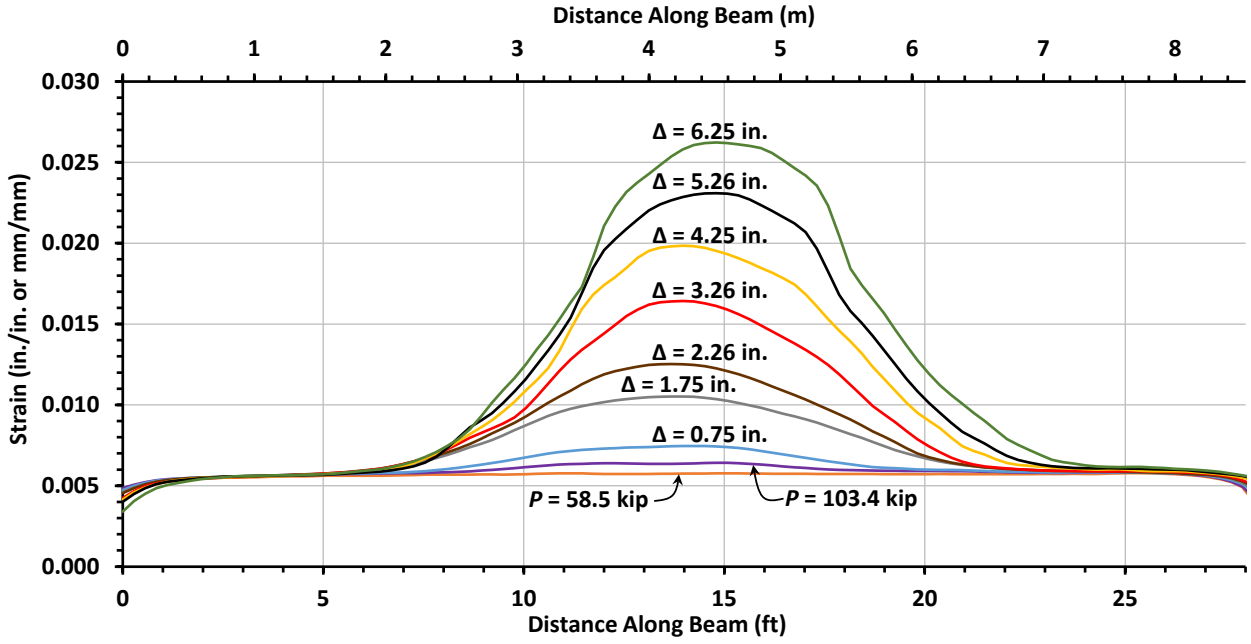

Figure A.16: Bonded Strand 1 – Fiber 2 (1 in. = 25.4 mm, 1 kip = 4.448 kN).

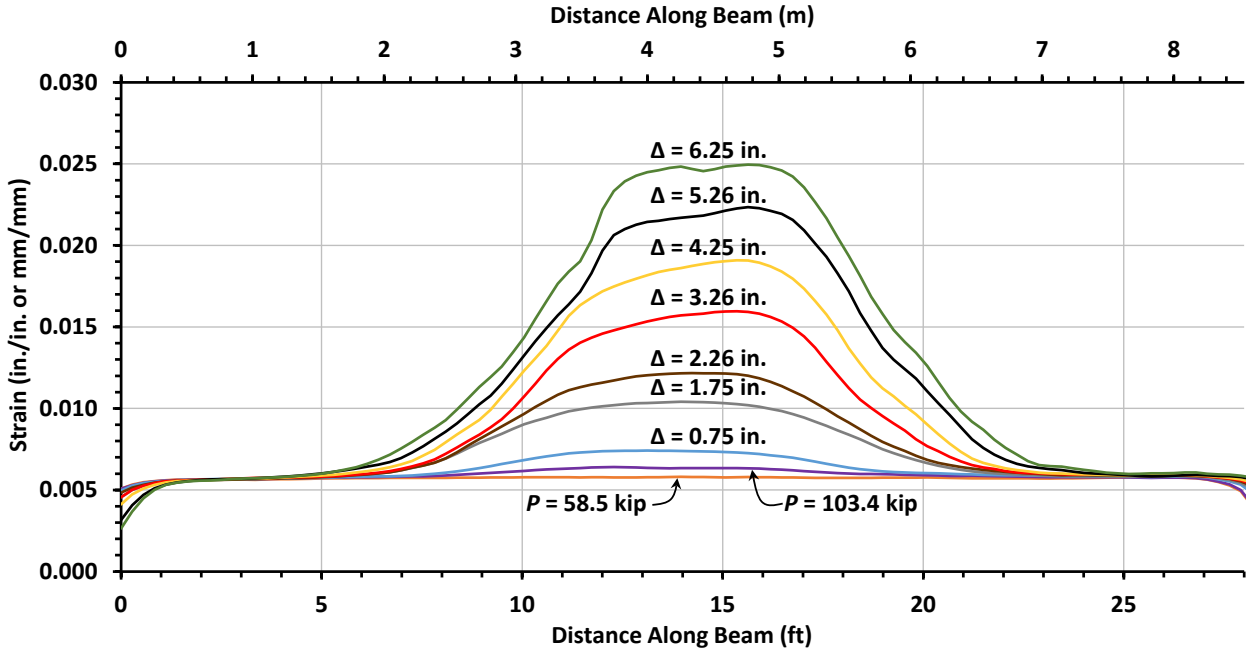

Figure A.17: Bonded Strand 2 – Fiber 1 (1 in. = 25.4 mm, 1 kip = 4.448 kN).

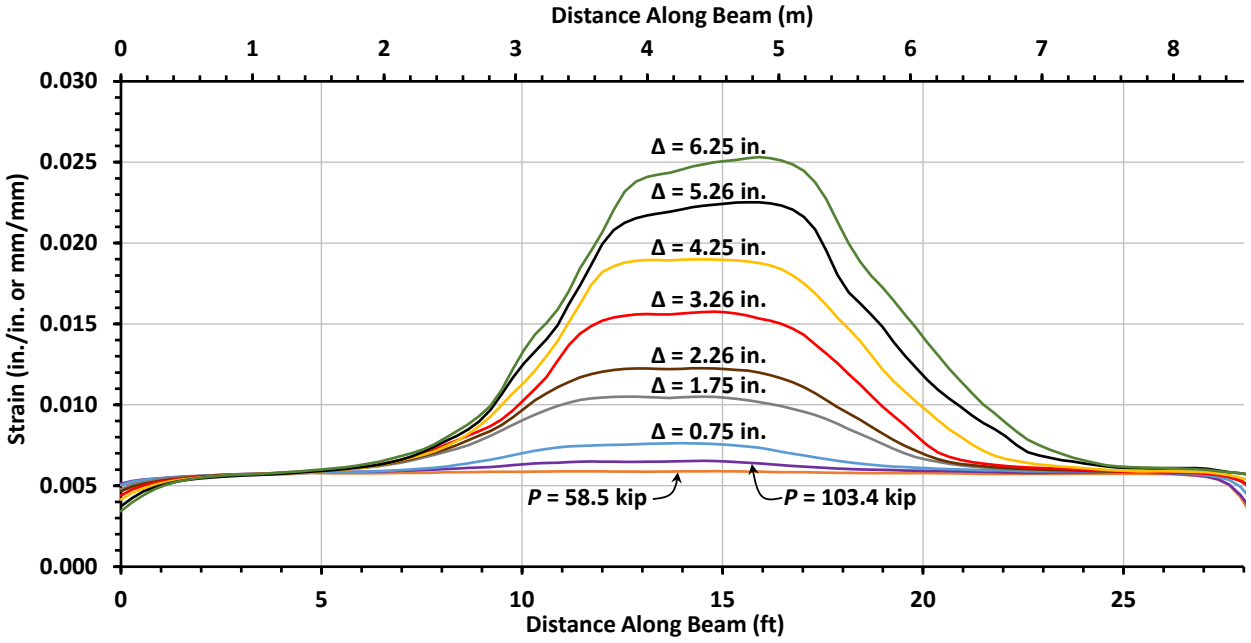

Figure A.18: Bonded Strand 2 – Fiber 2 (1 in. = 25.4 mm, 1 kip = 4.448 kN).

References

ASTM A1061/A1061M - 20a, Standard Test Methods for Testing Multi-Wire Steel Prestressing Strand. (2020). ASTM International. doi:10.1520/A1061_A1061M-20AE01

ASTM A416/A416M - 18, Standard Specification for Low-Relaxation, Seven-Wire Steel Strand for Prestressed Concrete. (2018). ASTM International. doi:10.1520/A0416_A0416M-18

ASTM A615/A615M - 22, Standard Specification for Deformed and Plain Carbon-Steel Bars for Concrete Reinforcement. (2022). ASTM International. doi:10.1520/A0615_A0615M-22

Corning Incorporated. (2015, January). *BOTDR Measurement Techniques and Brillouin Backscatter Characteristics of Corning Single-Mode Optical Fibers, WP4259*. Corning Incorporated. Retrieved May 20, 2024, from https://www.corning.com/media/worldwide/coc/documents/Fiber/white-paper/WP4259.pdf

Feng, C., Kadum, J. E., & Schneider, T. (2019, March). The State-of-the-Art of Brillouin Distributed Fiber Sensing. (S.-K. Liaw, Ed.) *Fiber Optic Sensing - Principle, Measurement and Applications*. doi:10.5772/intechopen.84684

Imai, M., Okubo, K., Sogabe, N., Tobe, H., Oikawa, M., Nakaue, S., & Hayakawa, M. (2019). Stress Distribution Monitoring of Ground Anchor Using Optical Fiber-Embedded Strand. *Proceedings of SPIE 10970, Sensors and Smart Structures Technologies for Civil, Mechanical, and Aerospace Systems 2019*, *109701J.* Denver, Colorado. doi:10.1117/12.2514201

JIS G 3536, Steel Wires and Strands for Prestressed Concrete. (2018). JSA (Japanese Standards Association).

Klar, A., Bennett, P. J., Soga, K., Mair, R. J., Tester, P., Fernie, R., St John, H. D., & Torp-Peterson, G. (2006, July). Distributed Strain Measurement for Pile Foundations. *Geotechnical Engineering, 159*(3), 135-144. doi:10.1680/geng.2006.159.3.135

Klar, A., Goldfeld, Y., & Charas, Z. (2010). Measures for Identifying Cracks within Reinforced Concrete Beams Using BOTDR. *Proceedings of SPIE 7647, Sensors and Smart Structures Technologies for Civil, Mechanical, and Aerospace Systems 2010*, *76472I.* San Diego, California. doi:10.1117/12.848578

Lecoeuche, V. (2023). Temperature and Strain Sensing with a BOTDR: Method for Setting the Calibration Coefficients in the Field. *28th International Conference on Optical Fiber Sensors.* Hamamatsu, Japan: Optica Publishing Group. doi:10.1364/OFS.2023.Th6.96

McKenna, F. (2011, July-Aug.). OpenSees: A Framework for Earthquake Engineering Simulation. *Computing in Science & Engineering, 13*(4), 58-66. doi:10.1109/MCSE.2011.66

Okubo, K., Imai, M., Sogabe, N., Yamanobe, S., Oikawa, M., Nakaue, S., Chikiri, K., Kobayashi, T., & Niwa, J. (2019). Development and Application of the Measuring Method for PC-Tensioning Force by Optical Fibre. *Proceedings of fib Symposium, No. 24, Concrete Innovations in Materials, Design and Structures.* Krakow, Poland.

Popovics, S. (1973, Sept.). A Numerical Approach to the Complete Stress-Strain Curve of Concrete. *Cement and Concrete Research, 3*(5), 583-599. doi:10.1016/0008-8846(73)90096-3

Pugh, J. S., Lowes, L. N., & Lehman, D. E. (2015, Dec.). Nonlinear Line-Element Modeling of Flexural Reinforced Concrete Walls. *Engineering Structures, 104*, 174-192. doi:10.1016/j.engstruct.2015.08.037

Soto, M. A. (2019). Distributed Brillouin Sensing: Time-Domain Techniques. (G.-D. Peng, Ed.) *Handbook of Optical Fibers*, 1663-1753. doi:10.1007/978-981-10-7087-7_7

Sumiden Wire. (2015). *Epoxy Coated Strand: Bonded or Unbonded.* Retrieved December 23, 2023, from Sumiden Wire Products Corporation web site: https://www.sumidenwire.com/products/epoxy-coated-pc-strand

VIAVI. (2019). *Fiber Sensing Module, DTSS Module (Strain & Temperature), DTS Module (Temperature), User Manual, 70DTSS002/UM/01-23/AE Rev 003*. VIAVI, LLC.

VIAVI. (2022). *Data Sheet, VIAVI, T-BERD/MTS-8000 DTSS: Distributed Fiber Optic Solution for Measuring Temperature and Strain Using Single Ended Brillouin OTDR*. VIAVI Solutions Inc. Retrieved December 23, 2023, from https://www.viavisolutions.com/en-us/literature/t-berd-mts-8000-dtss-data-sheets-en.pdf

Williams, C., Khatri, M., Okumus, P., & Holt, R. (2023). Post-tensioning Force Measurement Using Optical Fiber Sensor-Embedded Strand for Prestressed Concrete Structures. In A. Ilki, D. Çavunt, & Y. S. Çavunt (Ed.), *Proceedings of the fib Symposium 2023 - Volume 2, Building for the Future: Durable, Sustainable, Resilient, Lecture Notes in Civil Engineering 350* (pp. 622-633). Springer Nature. doi:10.1007/978-3-031-32511-3_65

Zou, W., Long, X., & Chen, J. (2015, February). Brillouin Scattering in Optical Fibers and Its Application to Distributed Sensors. *Advances in Optical Fibers Technology: Fundamental Optical Phenomena and Applications*, 3-53. doi:10.5772/59145